# Nitrite Reductase Activities of Azurin Variants

A THESIS
SUBMITTED TO THE FACULTY OF THE GRADUATE SCHOOL
OF THE UNIVERSITY OF MINNESOTA
BY

Balabhadra Khatiwada

IN PARTIAL FULFILLMENT OF THE REQUIREMENTS
FOR THE DEGREE OF
MASTER OF SCIENCE

Steven M. Berry

August 2015

**Acknowledgements**

I would like to thank all my family and friends for supporting me throughout my entire education. I would like to pay my especial thanks to my wife Meena Guragain Khatiwada, my parents, Lok Nath & Kala Kumari Khatiwada and my brother Yubaraj Khatiwada for their continuous support and love during all these years. I would like to thank Dr. Steven Berry for giving me a chance to be a part of his research and also for his guidance and mentorship throughout my entire learning experience at UMD. I am also thankful to Dr. Joseph Johnson for many valuable discussions and his suggestions about the research. I would also like to thank my fellow graduate students in lab, specifically: Jacob Strange, Garrett Stoddard and Alexandra Sauer. I am also very grateful to great undergraduate students in our lab; Christine Hedstrom and Tracy Roach.

I would like to dedicate this work to my late grandparents Dhananjaya and Devaka Khatiwada, and my recently deceased uncle Ramesh Pokharel for guiding and encouraging me to be the person I am today.

**Abstract:**

Nitrite reductase (NiR) is an oxidoreductase enzyme that catalyzes the reduction of nitrite ($NO_2^-$) to nitric oxide (NO) in the denitrification stage of the nitrogen cycle. To study the structure and function of this noncoupled dinuclear copper enzyme, functional mimics of NiR were designed by adding a second copper-binding site on the surface of the mononuclear copper protein azurin. The existing copper-binding site in azurin is an electron transfer (T1) site similar to the T1 center of NiR. This T1 copper center was maintained in azurin whereas an additional copper site, a catalytic type 2 (T2) copper site similar to the T2 site of NiR was designed using PCR mutagenesis to create the new variants with both T1 and T2 copper binding sites. The designed T2 copper site in azurin mimics the spectroscopic and functional aspects of native NiR. Four first generation azurin variants namely; NiR3His-Az, NiR-Az, PHM-Az and PHM3His-Az were created. The reactivity, UV-Vis absorption and electron paramagnetic resonance (EPR) spectra of azurin variants showed similarities to that of native NiR. We have further examined the nitrite reduction activity of our mimics using the nitrite reduction assays using Griess assay system and found that the azurin variants were less active than the native NiR. In the attempt to improve the activity of first generation variants, second generation single and double mutant variants were created by adding the mutations to the each 1$^{st}$ generation variants with modified T1 copper center redox potentials. In addition, reduction and re-oxidation rates of the T1 center in the azurin variants were determined and were compared with other variants. This yielded insights into the order of the reaction between the reducing agent, protein, and the substrate in our mimics.

**Table of Contents**

## List of Tables

## List of Figures

# Chapter 1: Introduction

## 1.1 The Nitrogen Cycle

Nitrogen is one of the most important elements in the biology of the earth because of its role constituting the important molecules required for the life in earth. Nitrogen is the critical limiting element for plant growth and is required for the composition of many biologically essential molecules, such as deoxy-ribonucleic acid (DNA), ribonucleic acid (RNA), adenosine triphosphate (ATP) and amino acids, the building blocks of protein. Nitrogen is the fifth most abundant element in the solar system and makes up approximately 79% of the earth's atmosphere, where it is found in the form of nitrogen gas ($N_2$).[1,2,6]

Atmospheric nitrogen is inert; hence plants and humans, like other higher animals, can't synthesize these molecules using nitrogen found in the atmosphere. Atmospheric nitrogen needs to be reduced and form more reactive species, such as ammonium ion ($NH_4^+$) and nitrate ($NO_3^-$), to be usable by plants and ultimately by animals. Plants acquire nitrogen compounds from the soil and water, either deposited by nitrogen fixing microorganisms, or from decomposition of plants, animals and waste. Humans and other higher animals acquire nitrogen compounds from food. These bio-available forms of nitrogen further undergo a series of redox reactions to complete the nitrogen cycle and recycle atmospheric nitrogen (Fig. 1.1). The nitrogen cycle consists of three major processes, namely: nitrogen fixation, nitrification, and denitrification.

Nitrogen fixation is an anaerobic process in the nitrogen cycle where the splitting of inert atmospheric nitrogen molecules and subsequent incorporation of the element into ammonium ion ($NH_4^+$) take place.[1-3] Although $N_2$ can be cleaved by lightning,

biological nitrogen fixation is carried out by microorganisms using the enzyme nitrogenase. Some prokaryotes such as cyanobacteria, bacteria from genus *Azotobacter* and symbiotic bacteria such as bacteria from genus *Rhizobium* and *Bradyrhyzobium* are major, well-known nitrogen fixing species.[1,6]

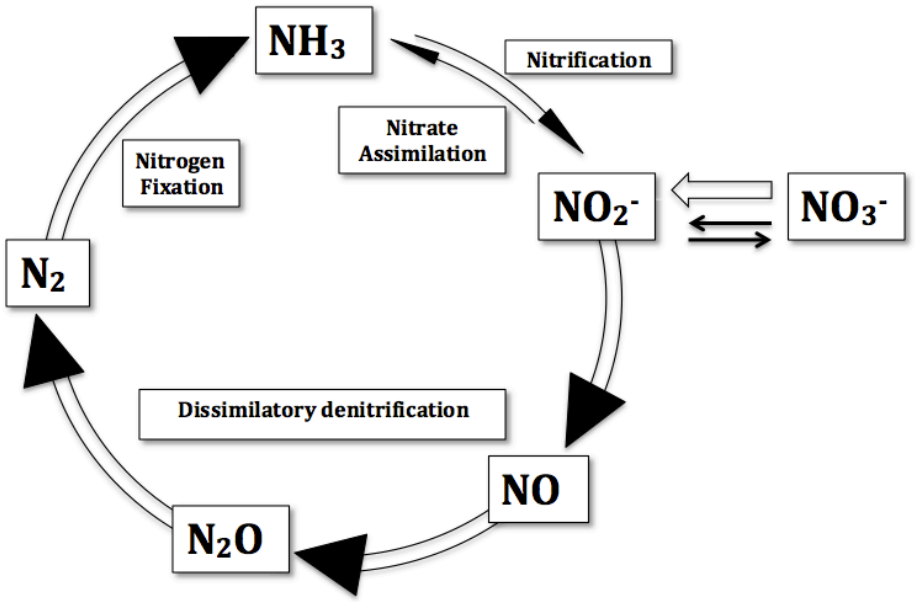


Fig. 1.1: Nitrogen Cycle[3,5]

Nitrification is another process in the nitrogen cycle where the oxidation of ammonia to nitrate ($NO_3^-$) takes place. This oxidation is carried out by nitrifying bacteria and provides $NO_3^-$ in the soil for plant metabolism. In order for $NO_3^-$ to be incorporated into the biomass, reduction to $NH_3$ is necessary.

Denitrification is the third major stage of the nitrogen cycle where the reduction of $NO_3^-$ takes place. Denitrification takes place in two different pathways; assimilatory and dissimilatory denitrification pathways. In assimilatory denitrification, the reduction of nitrate to ammonia, known as ammonification or nitrate assimilation, is carried out by

bacteria such as those of the *Nitrosomonas* family, as well as fungi and plants that use the enzyme nitrate reductase.[3,7-9,11] These enzymes facilitate the reduction of $NO_3^-$ to $NH_3$ via assimilation processes, which involve the intermediate production of nitrite ($NO_2^-$).[5,9,11]

Although nitrogen assimilation is a central pathway within the nitrogen cycle, it is the simpler process that results in ammonia and involves only a few enzymes. Dissimilatory denitrification is the more complex pathway in which the stepwise reduction of nitrate ($NO_3^-$) to $N_2$ occurs. It involves a large number of oxidoreductase enzymes to achieve the series of reductions. The first step of dissimilatory reduction is the nitrate reductase (NAR) catalyzed reduction of $NO_3^-$ to $NO_2^-$, followed by the nitrite reductase (NiR) catalyzed reduction of $NO_2^-$ to nitric oxide (NO), the nitric oxide reductase (NOR) catalyzed reduction of NO to nitrous oxide ($N_2O$) and finally the nitrous oxide reductase (N2OR) catalyzed reduction of $N_2O$ to dinitrogen gas ($N_2$) (Fig. 1.2).

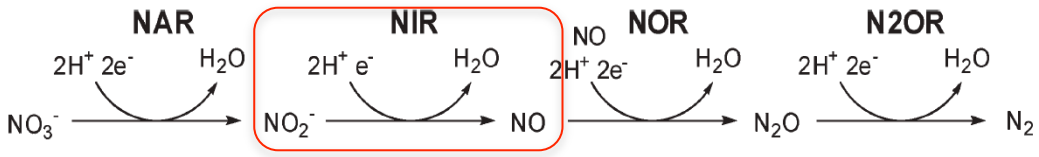


Fig. 1.2: Dissimilatory reduction of nitrite to dinitrogen gas. [9]

Dissimilatory denitrification is believed to be one of the major sources of nitric oxide (NO) and nitrous oxide ($N_2O$) emissions into the atmosphere with a concomitant decrease in soil nitrate concentration.[9-11] A wide range of bacteria and archea can perform denitrification, using a variety of enzymes.

## 1.2 Nitrite Reductase (NiR) in Nitrogen Cycle

The family of the enzymes that catalyzes the reduction of nitrite ($NO_2^-$) to nitric oxide (NO) in the first step of the dissimilatory denitrification pathway are metalloenzymes called nitrite reductases (NiR). These enzymes have metal ion binding active sites that also bind nitrite and in turn form, the reduced nitrogen species NO. Heme (Fe) and copper binding enzymes constitute two well-known classes of nitrite reductases.[7] Heme c and heme d containing NiRs (*cd1*-NiR) are bacterial cytochrome oxidases (cytochrome $_{cd1}$) found mainly in *Pseudomonas aeruginosa.*[9, 12-14] The copper binding nitrite reductases (CuNiR) include coupled copper (Cu-Cu) and non-coupled copper (Type 1 Cu, and Type 2 Cu) binding NiRs. CuNiRs are found in many bacterial species. *Achromobacter cycloclastes*[15,16], *Hyphomicrobium denitrificans*[17], *Alcaligenes xylosoxidans*[18], *Alcaligenes faecalis*[19] *and Rhodobacter sphaeriodes*[20,21] are the species from which CuNiRs are commonly purified.

Three different types of copper containing CuNiRs (or simply NiR), namely classes I, II and III, have been characterized so far. Class I and II NiRs consist of three identical monomeric subunits (homotrimer) with each subunit containing two non-coupled copper centers, namely type 1 (T1) and type 2 (T2) (Fig. 1.3). Class I and II NiRs differ in the properties of T1 site and their color. Class I NiRs are blue, while Class II NiRs are green.[5, 9, 18,19,22] Class I and II NiRs contain one T1 site per monomeric unit,[5,9] whereas class III NiR contains two T1 sites per monomeric unit.[23] Class III NiRs form a hexamer of monomers.

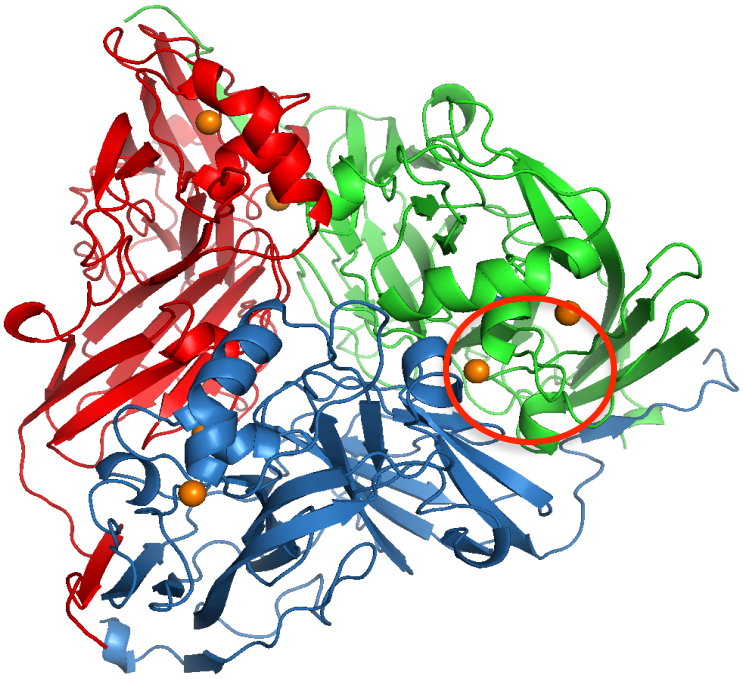

Fig. 1.3: Image of green *Achromobacter cycloclastes* NiR (AcNiR), (PDB ID: 1NIA).[16]

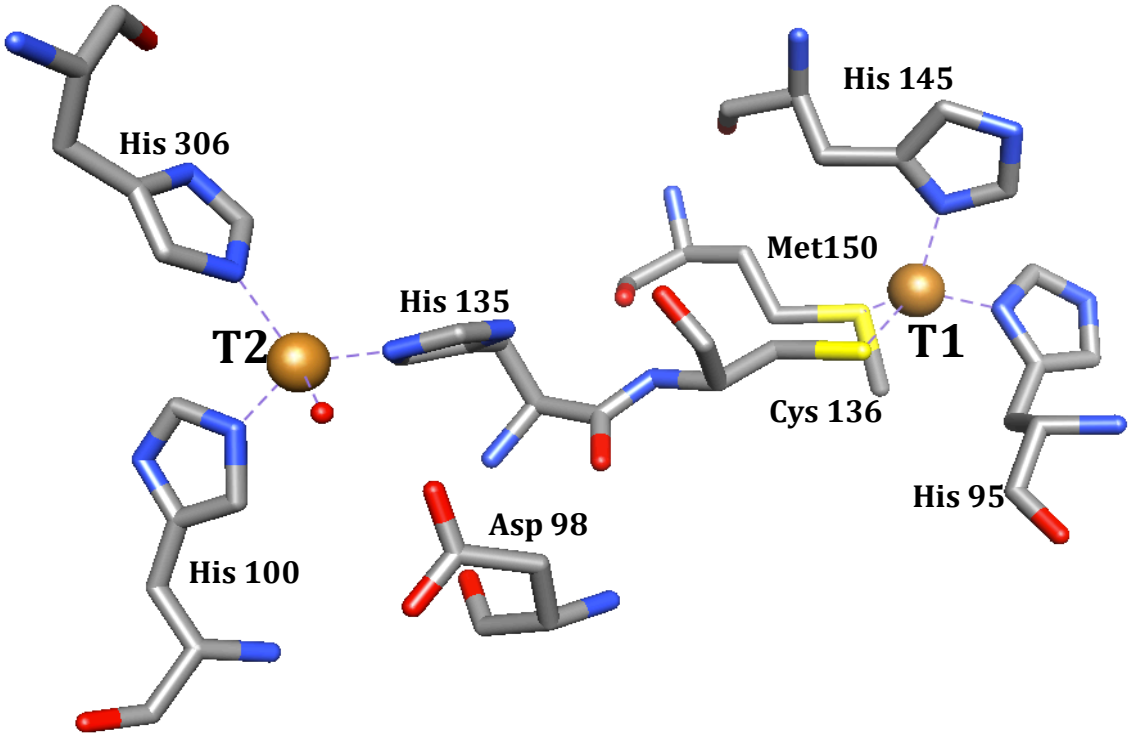


Fig. 1.4: Active site of AcNiR (PDB ID: 1NIA) where T1 is the electron transfer site and T2 is the catalytic site

The T1 and T2 copper centers of class I and II NiRs are ~12.5 Å apart and non-coupled electronically. The T1 copper center of NiR binds a Cu(II) ion and serves as an electron transfer site, whereas the T2 site is the catalytic site where the reduction of $NO_2^-$ to NO takes place. The T1 site receives the electron from other redox proteins, such as azurin and pseudoazurin, and is reduced to Cu(I). It is believed that the electron at the reduced T1 site is transferred to the T2 site, which is used for the nitrite reduction.[5,9,24] The T1 Cu(II) of NiR is coordinated by two histidines (His95 & His145 (numbers from CuNiR of *Achromobacter cycloclastes*)), one cysteine (Cys136) and one axial methionine (Met150) residue (Fig. 1.4).[5,18,19,22-24]

The color of the blue and green NiRs is due to slight differences in the geometry and structural properties of the T1 copper sites and their influence on the ligand to metal charge transfer (LMCT) transition between T1 Cu(II) and $S_{Cys}$.[9,25,26] The T1 copper site gives a ~600 nm absorption band due to the distorted tetrahedral geometry of the T1 center giving rise to a dominant S(Cys) $p\pi \rightarrow$ Cu $3d_{(x^2-y^2)}$ electronic transition. The S(Met) ligand of blue NiR deviates slightly from the axial position of the His-His-Cys plane, whereas that of green NIR is in a tilted position and thus changes the geometry slightly.[5,25,26] The T1 copper site in green NiR has a flattened tetrahedral geometry around the copper ion, giving rise to a dominant S(cys) $p\sigma \rightarrow$ Cu $3d_{(x^2-y^2)}$ transition which gives an increased absorption at 450 nm. [25,26]

T1 and T2 Cu(II) sites are connected by His135 and Cys136 residues, which provide a direct electron transfer pathway from T1 to T2 sites. In addition to the electron transferred from T1 site, the reduction of $NO_2^-$ requires two protons per mole of $NO_2^-$ as shown in the equation below.[24,30,32]

$$NO_2^- + 2H^+ + e^- \rightarrow NO + H_2O$$

The T2 copper has three histidine residues (His100, His135 and His306) coordinated to the copper whereas water or $NO_2^-$ bind as the fourth ligand. His100 and His135 come from same monomeric unit whereas His306 comes from another monomeric unit in the trimer. This coordination of copper to the histidines of different subunits is believed to keep the monomers bound together. In addition to these three histidines, nearby residues Asp98 and His255 are highly conserved residues that are believed to play a major role in nitrite binding and catalysis. Asp98 is believed to provide one of the two protons required for the reduction of $NO_2^-$whereas His255 is believed to help create a binding pocket for $NO_2^-$ in addition to providing the second proton.[5, 24, 28-32, 34]

The mechanism of reduction of $NO_2^-$ by NiR is debated. The first mechanism of NiR was proposed by Averill in 1994 and Suzuki *et al*. proposed an alternative mechanism in 2000. These two mechanisms differ in the modes and order of $NO_2^-$ binding to T2 sites (Fig. 1.5). Averill's mechanism suggests that the electron transfer from T1 to T2 takes place first followed by the binding of $NO_2^-$ to reduced T2 Cu(I). The mechanism suggests that $NO_2^-$ is bound to T2 Cu(I) in $\eta^1$-N(nitrite) fashion. Once the $NO_2^-$ is bound to the Cu(I), two consecutive proton transfers from nearby residues help generate a Cu(I)–$NO^+$ complex, which is in resonance with the corresponding Cu(II)–NO radical form. NO is released as a gas from the unstable Cu(II)-NO radical species. [9, 33]

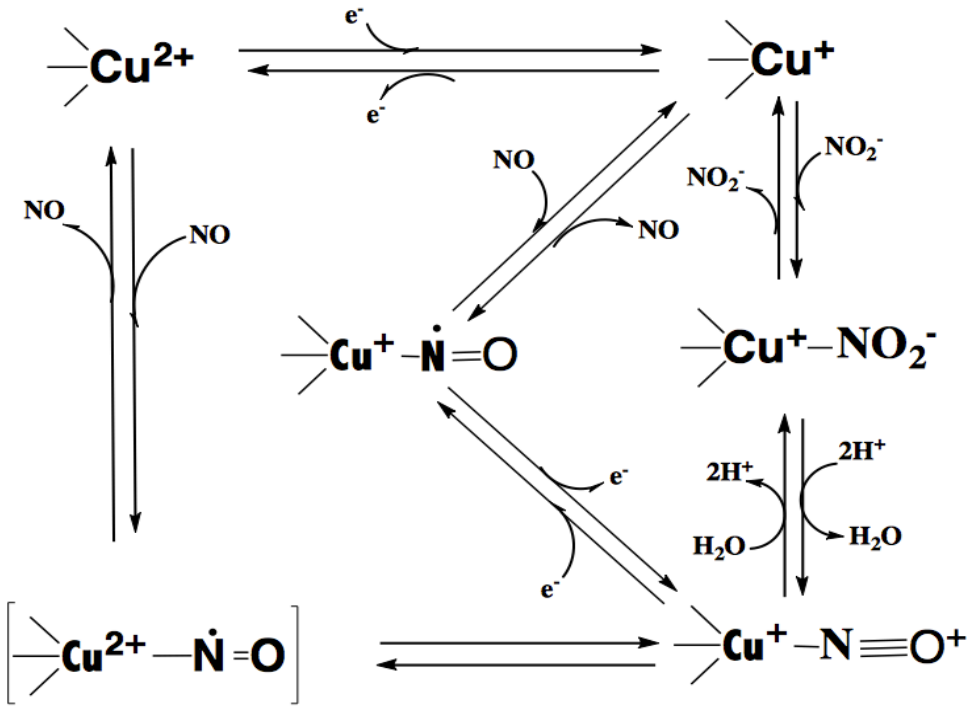


Fig. 1.5: Mechanism of NiR catalyzed reduction of $NO_2^-$ in T2 site adapted from Averill.[33,9]

Suzuki *et al*. used the crystal structure of blue NiR from *Alcalagenes xylosoxidans* (AxNiR) to suggest that the $NO_2^-$ binds to oxidized T2 copper, Cu(II), in a side-on fashion with both oxygens from $NO_2^-$ binding to the copper. A hydrogen from nearby Asp98 residue also helps $NO_2^-$ bind more tightly by hydrogen bonding with the oxygen of $NO_2^-$ (Fig. 1.6). Once $NO_2^-$ binds and forms the hydrogen bond, the reduction potential of the T2 center increases, making the T1 to T2 site electron transfer spontaneous. The presence of the hydrogen bonding allows for the fast formation of an intermediate, HONO, which quickly releases NO and forms the oxidized Cu(II) with water bound to Cu(II). This mode of $NO_2^-$ binding is different from Averill's mechanism which shows the N from $NO_2^-$ binding to the T2 copper.[5,9, 34,35] Suzuki's mechanism is largely supported by the computational studies done by Li *et al*.[35] and the work done by

Hasnain *et al.*[34] but with some differences. Work from Hasnain *et al.* showed $\eta^2$-O,O nitrite-binding mode to Cu(I) with a short Cu–N bond distance which further suggests that the distinct Cu(II)-NO intermediate is formed as opposed to Cu(II)-$NO^+$ as suggested by Suzuki *et al.* [34]

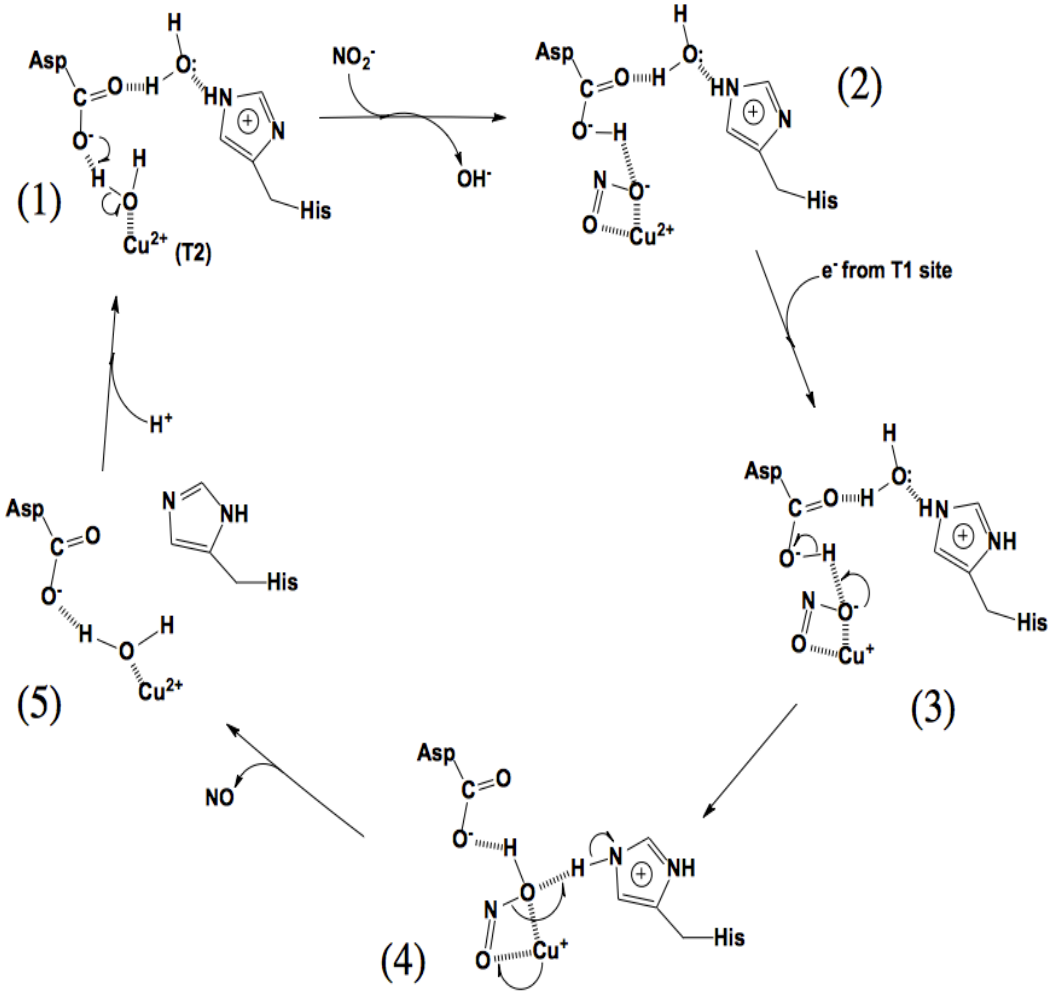


Fig. 1.6: Mechanism of NiR catalyzed reduction of $NO_2^-$ adapted from Suzuki et. al. [5]

As the mechanism of native NiR is debated, a few different ways of studying the mechanism suw used protein engineering to create a functional mimic of native NiR using another electron transfer protein called azurin as a scaffolding.

## 1.3 Azurin as a functional mimic of NiR:

In addition to the study of native system itself,[5,10-32] researchers have used synthetic model complexes,[36,37] computational studies,[34,36] as well as protein engineering using other existing proteins as a model.[44,45,47] Protein engineering is a viable way of studying the native system by using another protein as a scaffolding to model and mimic the functional and/or structural aspects of the native system. We used protein engineering to create a functional mimic of native NiR using another electron transfer protein called azurin as a scaffolding.

Azurin is a small (14 kDa) bacterial protein (Fig. 1.7). It is a mononuclear blue copper protein in the cupredoxin family containing a T1 Cu(II) binding site. Azurin is an oxidoreductase protein purified from *Pseudomonas aeruginosa* (P.a.) and is thought to be the redox partner of native NiR and act as an electron shuttle to its T1 Cu.[5, 39,43] Electron transport proteins play key roles in the electron transport chain, photosynthesis and many other important biological processes. P.a. azurin in particular, has been used extensively for non-native applications, such as a scaffolding to engineer artificial amino acids as well as di-copper sites.[44,45,47] It has also been investigated as an anti-cancer agent due to its cytotoxic properties, blocking breast cancer cell proliferation by inducing apoptosis.[46]

The T1 copper-binding site of P.a. azurin is similar to the T1 site of native NiR. As in native NiR, T1Cu in azurin is ligated by two histidines (His46 & His117) and one cysteine (Cys112) in a trigonal planar geometry. In addition, there are long-range axial interactions with methionine (Met121) and a backbone carbonyl oxygen (Gly45 CO) (Fig. 1.8).[42] *P.a.* azurin has 128 amino acids that fold into the common "cupredoxin" or Greek-key motif, which is eight antiparallel β-strands in a barrel arrangement similar to

native NiR. Azurin is a well-characterized cupredoxin family member. In addition to having preexisting T1 copper center with similar properties to native NiR, it is a small and stable protein that can handle multiple mutations while maintaining its ability to fold into a functional protein, which makes azurin an ideal and robust mimic system to design a second copper-binding site using protein engineering.[40,41.45,46)

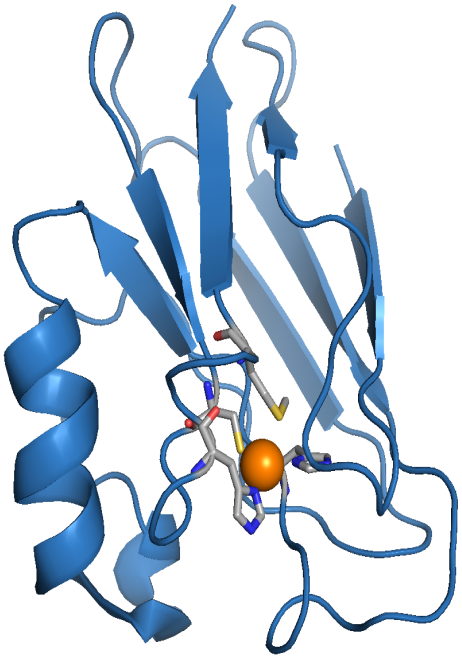

Fig. 1.7: Image of Cu(II) bound P.a Azurin (PDB: 4AZU).(55)

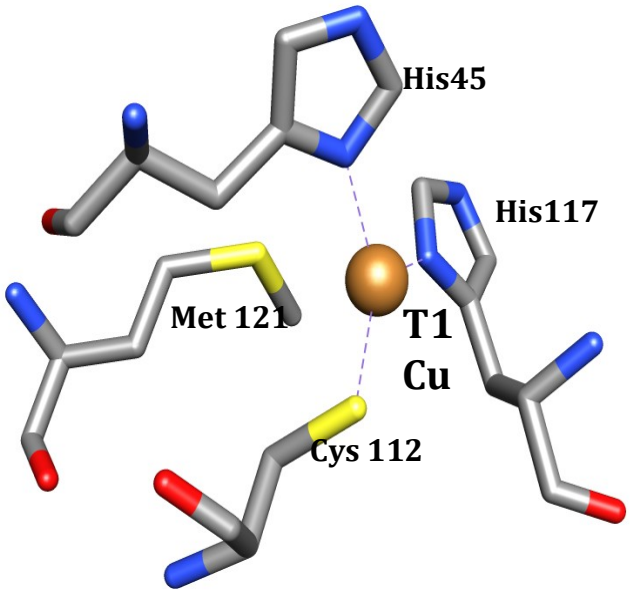


Fig. 1. 8: T1 Cu(II) site of Azurin (PDB: 4AZU).

To mimic the functional and spectroscopic properties of native NiR, we needed to create the T2 binding site similar to that in native NiR. For this purpose, we created mimics by designing the secondary copper-binding site (T2 site) on the surface of azurin, using QuikChange™ mutagenesis (see Section 1.3.1). The new designed T2 site of azurin variants was similar to the T2 site of native NiR. The variants such created were named the "first generation variants". In addition, the electron transfer from T1 to T2 sites in

NiR is believed to take place via a Cys-His direct electron transfer pathway which is not present in our mimics. To address that, a direct electron transfer pathway was provided by inserting an electron transport amino acid residue between T1 and T2 sites (see Section 1.3.2). Next, the reduction potentials of T1 and T2 sites are similar in the native NiR whereas our azurin variants were found to have higher reduction potential of T1 site, which would make the electron transport from T1 to T2 kinetically unfavorable. The reduction potential of T1 site was decreased by mutating certain amino acid residues (see Section 1.3.2). These variants with the direct electron transport pathway between T1 and T2, as well as with the decreased T1 site reduction potential were called "second generation variants". Lastly, our variants lack the amino acid residues that attract $NO_2^-$ or create the $NO_2^-$ binding pocket at T2 site that increases the $NO_2^-$ affinity. We aim to address that by creating the "third generation variants" (not discussed in this Thesis).

**1.3.1 First generation azurin variants to mimic native NiR:**

Four first generation variants were created by incorporating a second copper-binding site into the antiparallel β-strands 5 and 8 on the surface of azurin. These four azurin variants were named NiR-Az, NiR3His-Az, PHM-Az and PHM3His-Az, where Az stands for azurin. All four variants were created by conserving the preexisting T1 Cu site with a T2 Cu binding site incorporated at ~12 Å away from T1 Cu site. This kept the distance between T1 and T2 sites close to that of native NiR (~12.5 Å). The incorporation of the T2 center in azurin was achieved by mutating certain amino acid residues using QuikChange™ mutagenesis. For the NiR-Az variant, three mutations were made: Asp10 was mutated to His (Asn10His), Gln14Asp, and Asn16His (Fig. 1.8). Histidines are well known copper binding amino acids. By incorporating the Asp residue close to new T2

Cu site, it resembled the T2 site of native NiR. Although the NiR-Az variant has a similar T2 Cu site to native NiR, it lacks the third histidine, important for providing the proton required for the reduction of $NO_2^-$. To overcome the issue, NiR3His-Az was prepared by mutating all three residues (Asn10, Gln14, and Asn16) to His residue (Fig. 1.9). One of the His in the T2 site of native NiR comes from a separate monomeric unit which is not available in our small mimic protein.[50]

The PHM-Az variant is named after another copper binding oxidoreductase enzyme peptidylglycine α-hydroxylating monooxygenase (PHM). PHM catalyzes the hydroxylation of the alpha carbon of peptidyglycine and generates the final amidated peptide product. PHM consists of two copper centers namely CuH and CuM sites. The CuM site in PHM is the catalytic site consisting of two histidines and a methionine residues ligated to the copper.[48,49] In our PHM-Az mimic, the designed T2 copper site mimics the CuM site of native PHM. In the CuM site of native PHM, the two His ligands come from one beta-strand whereas the Met ligand is located by itself between the two His ligands on the adjacent strand.[9] PHM-Az was designed by incorporating the mutations Gln8Met, Gln14His, and Asn16His (Fig. 1.11) whereas PHM3His-Az was designed by mutating all three residues in T2 site of PHM-Az to histidines (Fig 1.12).[50] Although the PHM-Az and PHM3His-Az mimics were not designed for nitrite reduction, they resemble the Type 2 site in native NiR and hence were similarly tested for nitrite reduction. Figures 1.9-1.12 show the cartoon images of the first generation azurin variants generated by inserting the theoretical mutations using the software PyMoL.

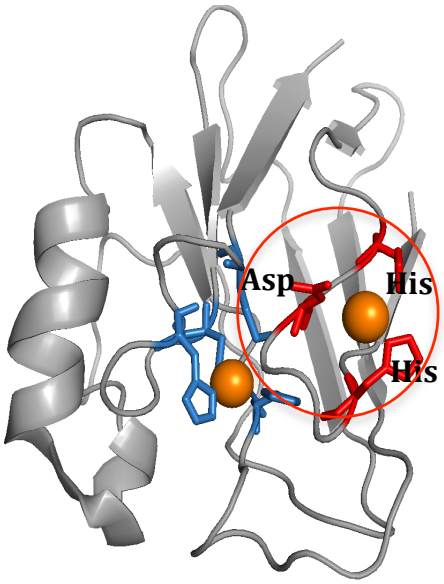


Fig. 1.9: PyMoL generated cartoon image of NiR-Az. The red circle shows the new incorporated T2 site

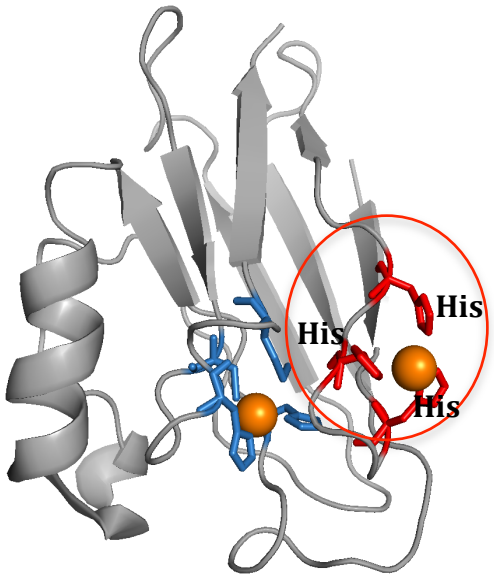


Fig. 1.10: PyMoL generated cartoon image of NiR3His-Az. The red circle shows the new incorporated T2 site

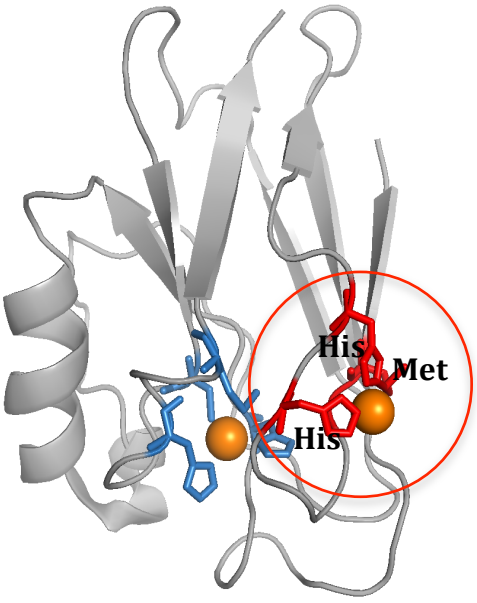


Fig. 1.11: PyMoL generated cartoon image of PHM-Az. The red circle shows the new incorporated T2 site

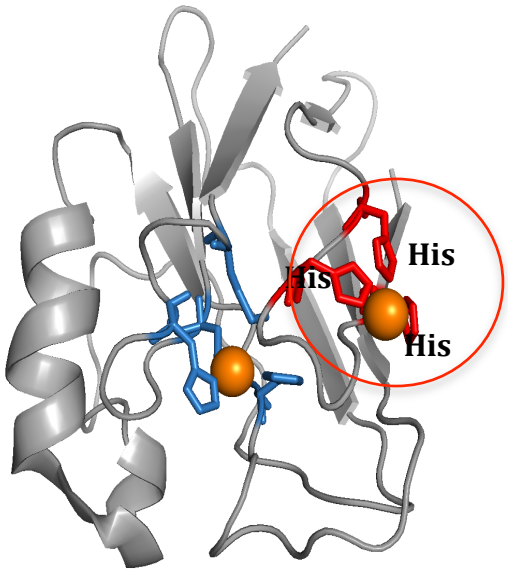


Fig. 1.12: PyMoL generated cartoon image of PHM3His-Az. The red circle shows the new incorporated T2 site

### 1.3.2 Second generation azurin variants:

Once the first generation variants of azurin were created, their nitrite reduction activity was measured. The NiR3His-Az and PHM3His-Az variants (three histidines on T2 center) showed higher nitrite reduction activity than the variants with two histidines in their T2 centers. The first generation azurin variants only incorporated a copper center and did not initially address some aspects of electron transfer chemistry. For example, the designed azurin variants lacked the direct electron transfer pathway of T1 Cu(I)-Cys-His-T2 Cu(II) found in native NiR. The lack of a direct electron transport pathway between the T1 and T2 coppers in our system could slow the electron transfer rates.

A second issue to be addressed was the reduction potential difference between the T1 and T2 centers of the designed azurin variants. The reduction potentials of T1 and T2 Cu centers of native NiR are around 255 ± 3 mV, 244 ± 18 mV respectively.[51] In our lab, the reduction potentials of the azurin mimics were measured to be ~350-360 mV and ~250-270 mV for T1 and T2 centers respectively (Table 1.1).

Table 1.1: Reduction potentials of the 1st and 2nd generation azurin variants:

| Variants | Reduction potentials of T1 site (mV) | Reduction potentials of T2 site (mV) |
|---|---|---|
| *Native *Ax*NiR[51] | 255 ± 3 | 244 ± 18 |
| †NiR3His-Az | 359 ± 5 | 270 ± 5 |
| †PHM3His-Az | 357 ± 5 | 258 ± 5 |
| †NiR-Az | 350 ± 5 | 257 ± 5 |
| †PHM-Az | 353 ± 5 | 251 ± 5 |
| ††NiR3His-Phe15Trp | 359 ± 5 | 270 ± 5 |
| ††NiR3His-Phe114Pro | 269± 8 | 270 ± 5 |
| ††NiR3His-Met121Gln | 269± 8 | 270 ± 5 |

*Reduction potential values from *Alcaligenes xylosoxidans (AxNiR)* at pH 7.0.[51]
†Reduction potential values measured in our lab at pH 5.1.
†† Theoretical reduction potential values based on the values reported previously for the same mutations at pH 7.0.[52]

There is therefore about a 100 mV difference in the reduction potential of T1 and designed T2 center in NiR3His, whereas there is little difference between the native copper centers. The larger difference between the copper centers in azurin could affect the electron transport rate. Therefore, to address these thermodynamic and kinetic issues in electron transport, "second" generation single mutant and double mutant azurin variants were created. Second generation variants include all combinations of the Phe15Trp (F15W), Phe114Pro (F114P), and Met121Gln (M12Q) mutations. The logic behind these mutations will be discussed below. Only these variants of NiR3His-Az will be shown here.

Tryptophan is known to assist in long-range electron transport by electron hopping.[54] The Phe15Trp mutation in the azurin mimics inserts a tryptophan residue between T1 and T2 copper site providing the possibility of a more direct electron transport, which should make the electron transfer between T1 and T2 kinetically favored (Fig. 1.13). Phe114Pro and Met121Gln are mutations near the T1 copper center and known to decrease the reduction potential by about 90 ± 8 mV.[52,53] In the Phe114Pro mutation (Fig. 1.14.), the hydrogen bond between Phe114 and Cys112 is broken which in turn frees up Cys112 to move closer to the T1 copper increasing the electron density near the copper and thus decreasing the reduction potential.[52,53] In the Met121Gln mutation (Fig. 1.15), the carbonyl oxygen from Gln that replaces S from the Met gets closer to the T1 copper and increases the electron density around the T1 center reducing the reduction potential.[52,53] Figures 1.13-1.15 show the cartoon images of the second generation single mutant azurin variants generated by inserting the theoretical mutations using the software PyMoL.

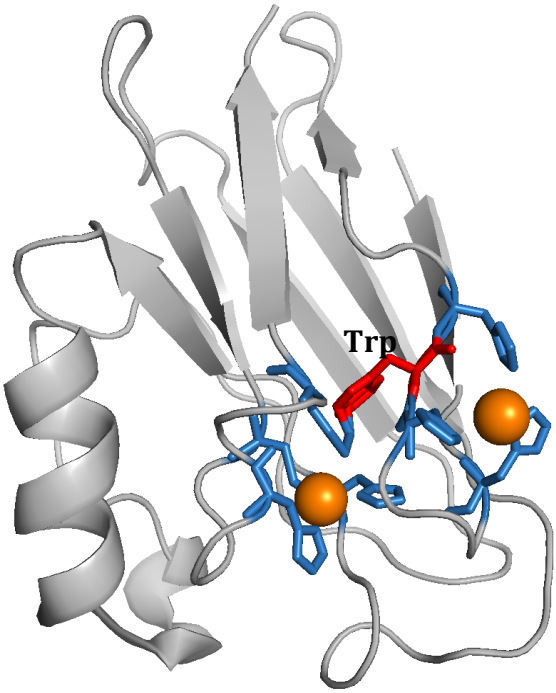


Fig. 1.13: PyMoL generated cartoon image of NiR3His-F15W azurin variant.

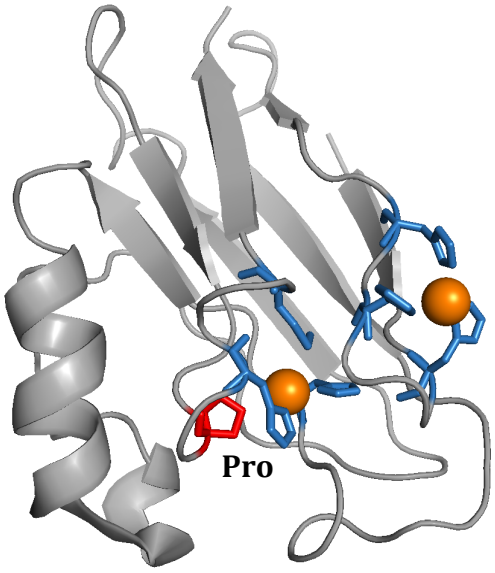


Fig. 1.14: PyMoL generated cartoon image of NiR3His-F114P azurin variant.

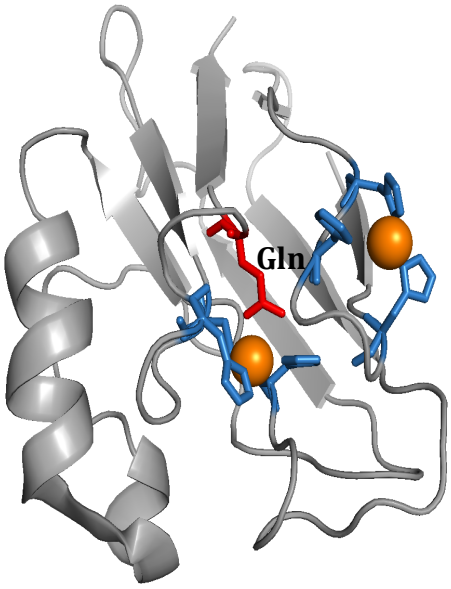


Fig. 1.15: PyMoL generated cartoon image of NiR3His-M121Q azurin variant.

To further explore the activities of these second generation single mutant variants, the mutations were combined by pairing up these three mutations to prepare double mutant azurin variants Phe15Trp/Phe114Pro (Fig. 1.16), Phe15Trp/Met121Gln (Fig. 1.17) and Phe114Pro/Met121Gln (Fig. 1.18) were prepared by adding these mutations to NiR3His azurin and the other azurin mimic proteins. These variants were expected to have increased nitrite reduction activity by providing an electron transfer wire along with the lower reduction potentials. Figures 1.16-1.18 show the cartoon images of the second generation double mutant azurin variants generated by inserting the theoretical mutations using the software PyMoL.

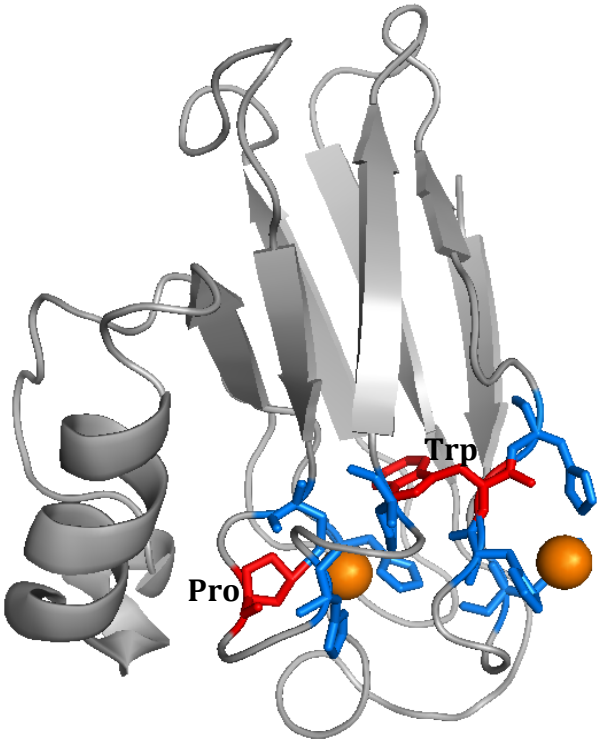


Fig. 1.16: PyMoL generated cartoon image of NiR3His-F15W/F114P azurin variant

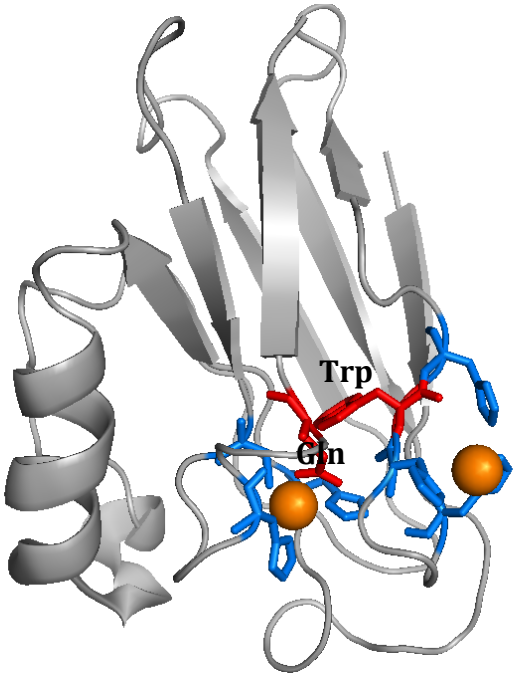


Fig. 1.17: PyMoL generated cartoon image of NiR3His-F15W/M121Q azurin variant

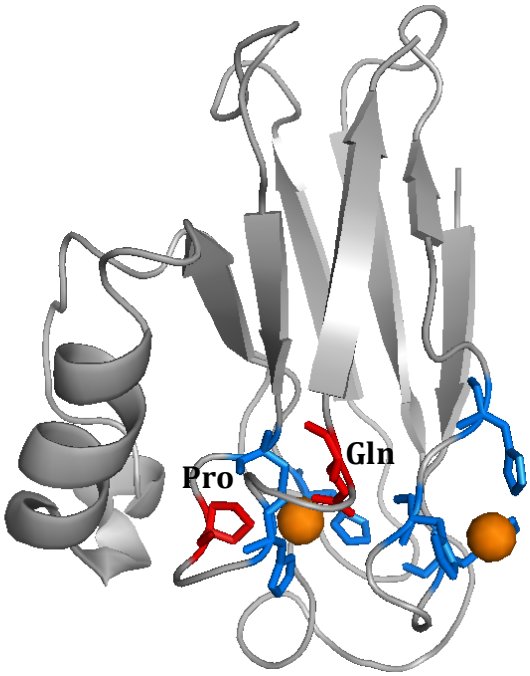


Fig. 1.18: PyMoL generated cartoon image of NiR3His-F114P/M121Q azurin variant

Therefore, 7 variants (one 1st generation, three 2nd generation single mutants and three 2nd generation double mutants) of each NiR-Az, NiR3His-Az, PHM-Az and PHM3His-Az (hence 28 total) variants were created. These variants were characterized using spectroscopic methods, such as EPR and UV-Vis spectroscopy. Their nitrite reduction activities were also measured. In this thesis, the methods for: (i) protein purification, (ii) protein sample preparation for spectroscopic characterization & nitrite reduction activity assays and (iii) nitrite reduction assays of these variants will be discussed in Chapter 2. The latest results on the kinetics of nitrite reduction and discussion of the activity assay will be discussed in Chapter 3. Finally, tangential studies on the metal ion exchange properties of T1 Cu(II) wild type azurin will be discussed in Chapter 4.

## Chapter 2: Materials and Methods and spectroscopy

### 2.1 Azurin Purification:

The 28 azurin variants discussed in Chapter 1 were created by previous students in our lab using Quikchange™ site-directed mutagenesis with previously reported protocols.[1-3] The *Pseudomonas aeruginosa* gene for the production of azurin was coded in a pET9a plasmid and the plasmid was transformed into BL21* *E coli*. The pET9a plasmid also contains a kanamycin resistance gene, hence the BL21* *E. coli* cells were grown on LB-agar plates in the presence of 0.05 g/L kanamycin, which allows the selective growth of the desired cells. Once the *E. coli* cells grew on the LB-kanamycin plates, a sterile culture tube was prepared with ~8 mL of LB broth. To the sterile culture tubes, ~ 2 μL of 0.05 g/L kanamycin stock solution per mL of LB broth was added. The cells were transferred and incubated at 37 °C for ~6 hours. Four liters of Bacto™ tryptone/yeast extract media known as 2xYT was prepared by dissolving 16 g of Bacto™ tryptone, 10 g of yeast extract and 5 g of NaCl per liter of water. All media were sterilized by autoclaving. About 1 mL each of starter culture was transferred into each of five flasks containing 0.8 L 2xYT media. About 200 mg of solid kanamycin sulfate was dissolved in 5 mL of water and 1 mL was added to each flask. The cells were then incubated in a shaker at 30 °C for ~12 hours. After 12 hours of incubation, the gene for the production of azurin was induced for ~3 hours with 3 mM isopropyl-beta-D-thiogalactopyranoside (IPTG). IPTG activates the T7 promoter region of bacteriophage T7 RNA polymerase in the BL21* *E.coli* displacing the repressor on the *lac* operon. When IPTG is added, it results in the overexpression of T7 polymerase, which is able

transcribe the pET9a plasmid DNA into RNA. The RNA for azurin is in turn translated to make azurin protein.

To extract the azurin protein from BL21* *E. coli,* the pellets were isolated from the 2xYT media by centrifuging the cells for ~10 minutes at 7000 rpm at 4°C in an Avanti® J-E centrifuge. The cell pellets were then suspended in the 20% sucrose, 1mM EDTA, 30 mM tris solution at pH 8.0. The cells were lysed using osmotic shock with pure Millipore water and the azurin was extracted. The resulting extracted protein was purified using SP-sepharose cation exchange in 50 mM ammonium acetate buffer at pH 4.10, followed by pH adjustment to 6.35. The protein was concentrated, filtered and further purified with and Q-sepharose anion exchange column chromatography, in 50 mM ammonium acetate buffer at pH 6.35. Typical purification yields were about 30 mg azurin per liter of media. The resulting protein was concentrated using Amicon® Millipore stirred ultrafiltration cells. These cells concentrate the protein using Millipore 10,000 normal molecular weight limit (NMWL) Ultracell® YM filter membrane and gas pressure (nitrogen gas in our lab) to filter the buffers while retaining azurin in the cell.

## 2.2 UV-Vis spectroscopy:

The concentration of expressed azurin variants was determined by slowly titrating the apo-protein with 100 mM $CuSO_4$ until the blue color of azurin, which absorbs at $A_{625\ nm}$, reached a maximum. The molar absorptivity of wild type azurin (5000 $M^{-1}cm^{-1}$) was used to determine the final concentration. Once the concentration of protein was determined, holo-azurin variants were prepared by slowly titrating purified apo-azurin variants with 5 eq. of $CuSO_4$ with stirring on ice (4 °C). The samples were left on ice for ~20 minutes to ensure the complete equilibration of Cu(II) to the T1 and designed T2

copper sites in the protein. As there are only two Cu(II) binding sites, the excess 3 eq. of $CuSO_4$ was removed by running 1 mL aliquots of the samples through the PD-10 size-exclusion desalting column (Sephadex-25 columns from GE Healthcare Life sciences) and collection of the protein fraction. These PD-10 columns were also used to accomplish final buffer exchange to 50 mM ammonium acetate buffer (pH 5.1). The sample stocks such prepared were diluted to ~200 µM and UV-Vis absorption spectra were obtained using a Shimadzu UV2401 PC UV-Vis spectrophotometer (Fig. 2.1).

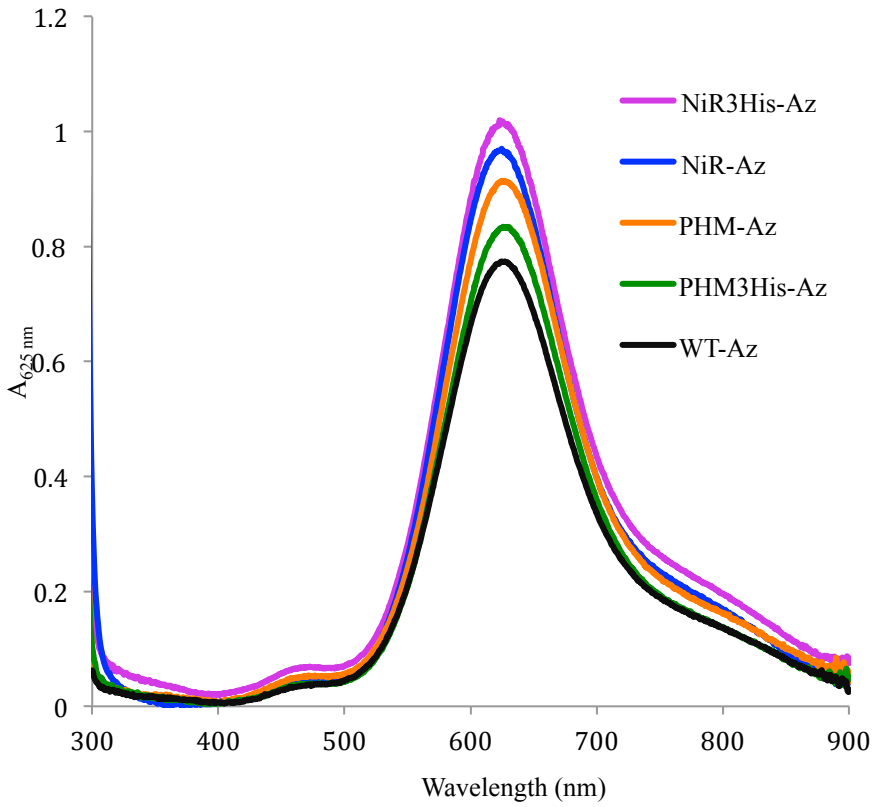


Fig. 2.1: UV-Vis spectra of first generation variants showing Cu(II) bound to T1 site.

The UV-Vis spectra of the first generation azurin variants (Fig. 2.1) show the characteristic blue color, similar to wild type azurin (WT-Az). The absorption band at 625 nm with Cu(II) bound is due to the S(Cys) ligand to metal charge transfer

transition as described in Chapter 1. The UV-Vis spectra of second generation single (Fig. 2.2) as well as the double mutant variants also show the strong absorption band at around 625 nm. The Phe114Pro variants had the absorbance band shifted to 600 nm due to loss of hydrogen bonding of Phe114 residue to Cys112 residue, whereas Met121Gln variants look more greenish in color due to an increase in the absorption band at ~450 nm. This is a result of the change in geometry and loss of axial interaction from Met121 residue. Even with these minor spectroscopic changes, the absorption at ~625 nm confirms that the T1 site of each of the variants bind Cu(II) to T1 site.

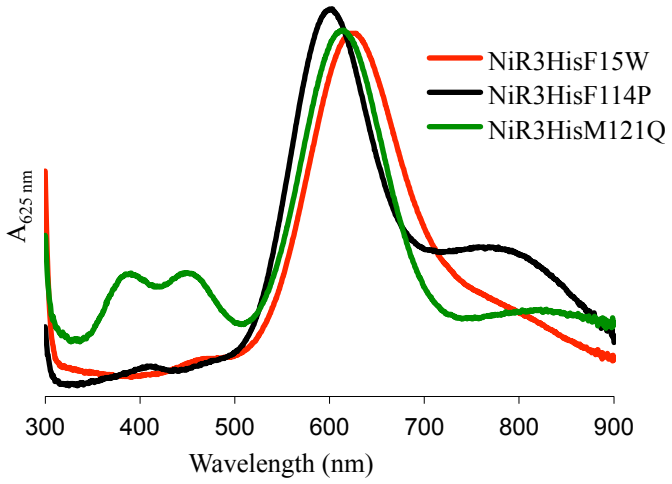


Fig. 2.2: UV-Vis absorption spectra of NiR3His-Az 2nd generation singe mutant variants.

## 2.3 Electron paramagnetic resonance (EPR):

Electron paramagnetic resonance (EPR) spectroscopy is a technique that detects unpaired electrons. Cu(II) has an electron configuration of $[Ar]3d^9$ and has one unpaired electron. Hence it is EPR active. EPR spectroscopy uses microwave energy under an applied magnetic field to split the spin state levels of the unpaired electron into high

and low energy levels.[7] The difference in energy level of the two electron spin states due to the applied magnetic field is reflected in the "*g"* factor. In addition, the magnetic field generated by the spin of copper nucleus gives rise to hyperfine splitting. The energy difference between the hyperfine peaks is given by the hyperfine coupling constant (*"A"* factor).[7] The *"A"* factor depends on the amount of the interaction between the unpaired electron and the nucleus. The number of hyperfine peaks in the EPR spectra are determined by the nuclear spin and the number of nuclei and is given by the equation ***2nI+1,*** where *"n"* is the number of equivalent nuclei, and *"I"* is the nuclear spin. Since the nuclear spin of Cu(II) is *3/2* (*I = 3/2*), the total number of hyperfine peaks seen per Cu(II) nucleus is four.

EPR can be used to characterize the Cu(II) bound azurin variants. Since the electronic environment of T1 and T2 sites are different, they are expected to show different EPR parameters. The *"g"* values are further divided into "$g_x$", "$g_y$" and "$g_z$" which denote the different electronic environments around the copper ion in the x, y, and z directions. EPR spectra of azurin variants show the axial symmetry where "$g_x$" and "$g_y$" are similar or equivalent due to similar ligand environments and are often referred to together as "$g\perp$". The "$g_z$" value for Cu(II) azurin is different due to its unique ligand in the z direction and also called "$g_{//}$". In our azurin variants, four hyperfine peaks are seen in the "$g_{//}$" region. The "$g_{//}$" value is determined by finding the middle of the hyperfine peaks where as the "$A_{//}$" factor denotes the distance between the hyperfine peaks. The Cu(II) atoms bound to azurin give four hyperfine peaks with distinct $A_{//}$ and $g_{//}$ values, which will be presented later in this chapter.

EPR samples were prepared in 50 mM ammonium acetate buffer (pH 5.1). Samples with three different Cu(II) loadings were prepared for EPR spectroscopy using an azurin variant stock with a concentration more than 0.5 mM. The first type of sample had Cu(II) bound to the T1 site and T2 empty (called T1Cu only) to confirm and characterize the copper binding at the T1 site in all the azurin variants. T1Cu only samples were prepared by slowly titrating $CuSO_4$ to the apo azurin variants with stirring on ice. To ensure only the T1 site was populated with Cu(II), only 0.9 eq. of $CuSO_4$ were added. Since, the T1 site has stronger affinity for copper, added copper binds to T1 site first. This sample was used to yield the EPR spectra with T1 Cu(II) signals only.

The second type of EPR sample prepared was T1 with Hg (II) and T2 with Cu(II) (called T2 Cu only). Since Hg (II) is EPR silent, these samples were prepared to obtain EPR spectra of T2 sites with Cu(II) only. T1 site was first populated by adding 1.5 eq of $HgCl_2$ to the protein. The sample was left on ice for ~20 minutes to ensure that all of T1 sites were filled with Hg (II). The protein was then run through PD-10 desalting columns into 50 mM ammonium acetate buffer (pH 5.1) and collected in 300 uL fractions. The fractions containing an $A_{280\ nm}$ peak, indicating protein, were collected and the concentration of the protein was estimated based on the $A_{280\ nm}$ peak using and absorptivity of $E_{280} = 8440\ M^{-1}\ cm^{-1}$. To the resulting sample, 0.5 to 0.75 eq. of $CuSO_4$ were added to bind the T2 center. This way only the T2 site had Cu(II) bound without any free copper, and the T1 had Hg (II).

The third type of EPR sample prepared was azurin variants with both T1 and T2 Cu(II) ions (called T1T2 Cu). T1T2 Cu samples were prepared to obtain EPR spectra with overlapping T1 and T2 signals of the azurin variants. The samples were prepared

by slowly titrating the apo azurin variants with 5 eq. of $CuSO_4$, stirring on ice and left for ~20 minutes to ensure adequate equilibration. The samples were then passed through PD-10 columns into 50 mM ammonium acetate buffer (pH 5.1).

Once the desired copper containing samples were prepared, they were concentrated to ~2 mM using the Millipore 10,000 normal molecular weight limit (NMWL) Ultracell® YM Centricon centrifugal concentrating device. These centrifugal concentrating devices filter the buffers while retaining azurin in the cell. Once concentrated, 150 µL of sample was mixed with glycerol in a 1:1 ratio to yield a 300 µL total volume of ~1 mM azurin variant. The samples were transferred to EPR sample tubes, flash frozen and stored in liquid nitrogen at -196 °C.

EPR spectra were obtained for first generation mutants (NiR-Az, NiR3His-Az, PHM-Az & PHM3His-Az), second generation single mutants (Phe15Trp, Phe114Pro, Met121Gln mutants of 1$^{st}$ generation variants) and second generation double mutant variants (Phe15Trp/Phe114Pro, Phe15Trp/Met121Gln and Phe114Pro/Met121Gln mutants of 1$^{st}$ generation variants) using a Varian E-Line Century Series X-band EPR spectrometer in a liquid nitrogen finger dewar at -196 °C. The microwave frequency was typically 9.27 GHz with a center field of 3000 gauss. A field width of 1600 gauss was scanned over 60 seconds with 2 scans averaged per spectra. A wait time of 10 seconds was set between scans with the modulation amplitude set to 5 Gauss and a time constant of 0.032. Fifteen spectra were obtained for each variant and averaged to get the final spectrum.

The EPR parameters, such as number of hyperfine peaks, their center ("*g"* values)

and the distances between hyperfine peaks ("*A*" values) were obtained using the simulation program Simpow6.[4]

**2.3.1 T1, T2 and T1T2 Cu(II) EPR spectra and simulation of 1st generation azurin variants:**

Figures 2.3, 2.4 and 2.5 show the EPR spectra and simulated spectra of first and generation azurin variants when Cu(II) is bound to T1 site only, T2 site only and both T1 and T2 sites, respectively. All three T1 Cu(II), T2 Cu(II) and T1T2 Cu(II) EPR spectra demonstrate and confirm the copper binding to the respective sites.

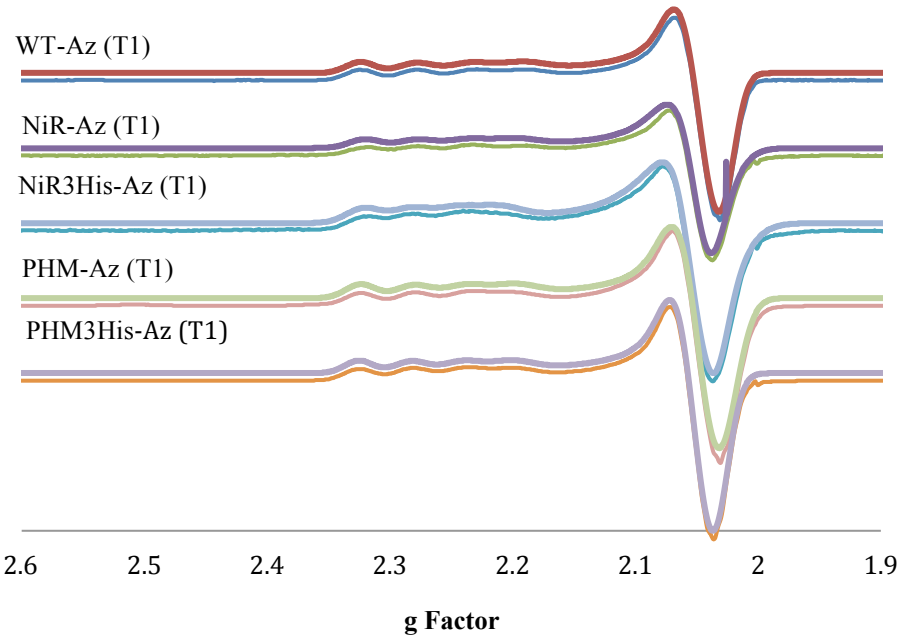


Fig. 2.3: EPR spectra of T1 Cu(II) of first generation variants along with the simulated spectra predicted by simpow6 overlaid on the top.

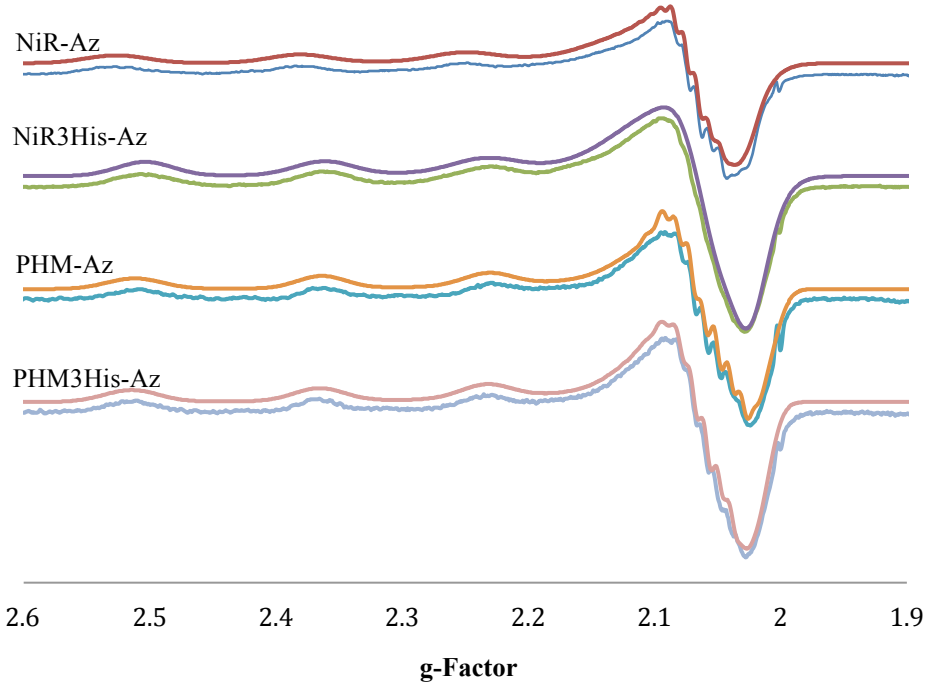


Fig. 2.4: EPR spectra of T2 Cu(II) of first generation variants along with the simulated spectra predicted by simpow6 overlaid on the top.

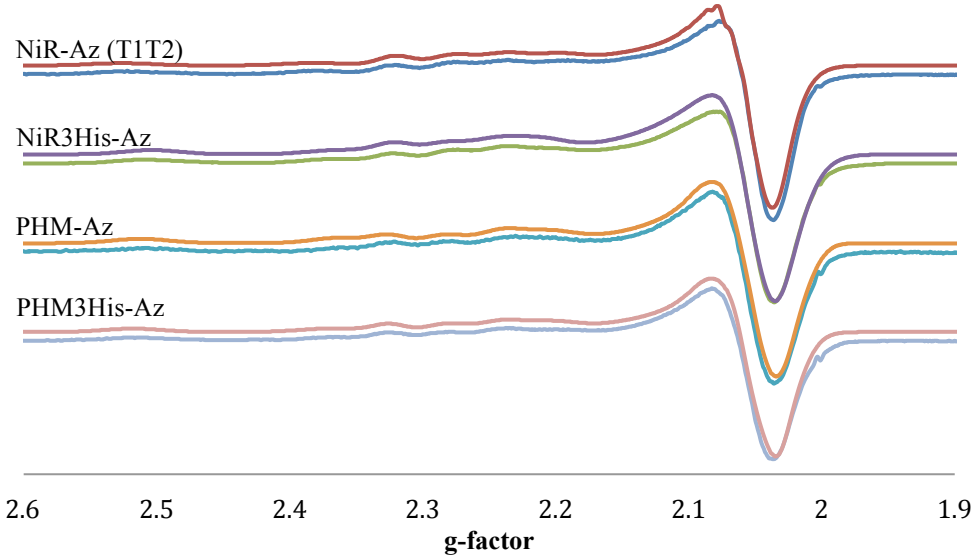


Fig. 2.5: EPR spectra of T1T2 Cu(II) of first generation variants along with the simulated spectra predicted by simpow6 overlaid on the top.

### 2.3.2 T1, T2 and T1T2 Cu(II) spectra and simulation of 2nd generation single mutant azurin variants:

Figures 2.6, 2.7 and 2.8 show the EPR spectra and simulated spectra of second generation single mutant azurin variants when Cu(II) is bound to T1 site only, T2 site only and both T1 and T2 sites, respectively. All three T1 Cu(II), T2 Cu(II) and T1T2 Cu(II) EPR spectra demonstrate and confirm the copper binding to the respective sites.

(*Note: Single letter abbreviation of the amino acids is used for simplicity. Phe15Trp-Az variant is written as F15W, Phe114Pro as F114P and Met121Gln as M121Q)

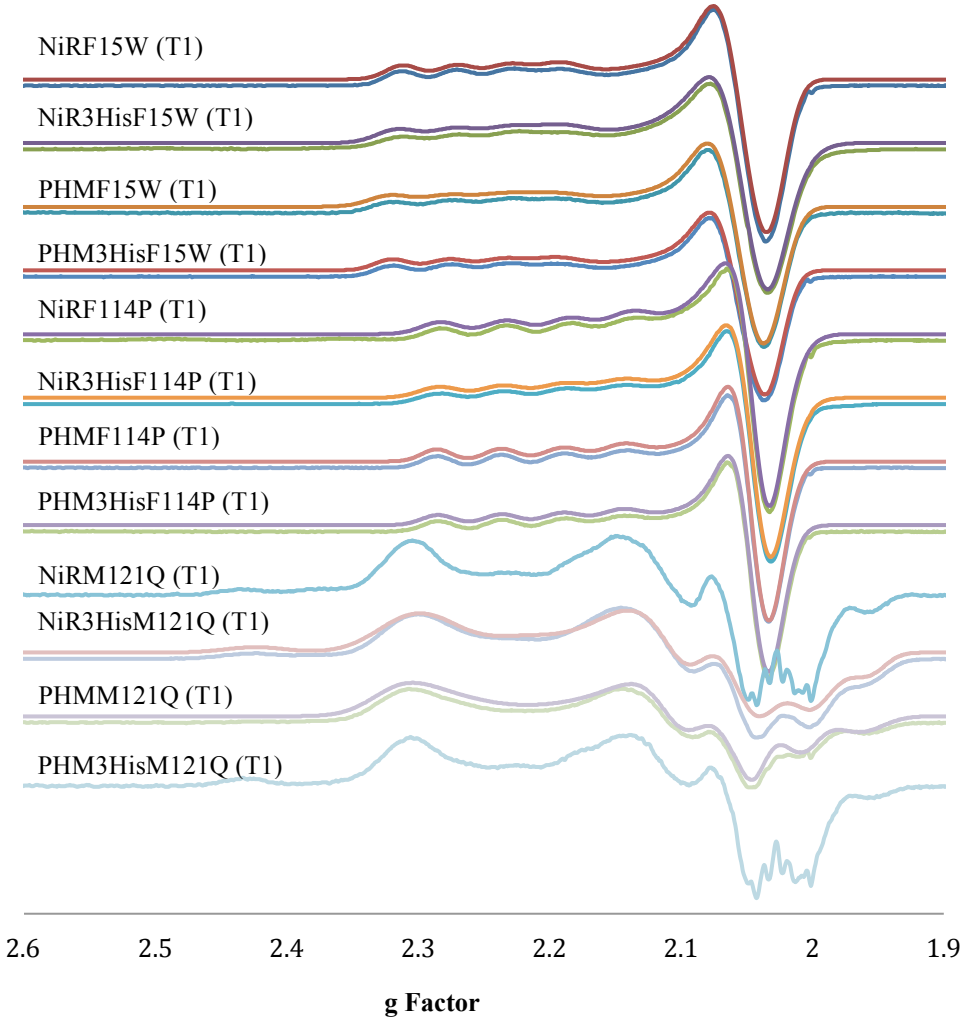


Fig. 2.6: EPR spectra of T1 Cu(II) of second generation single mutant variants along with the simulated spectra predicted by simpow6 overlaid on the top. Simulations of NiRM121Q and PHM3HisM121Q variants are yet to be done.

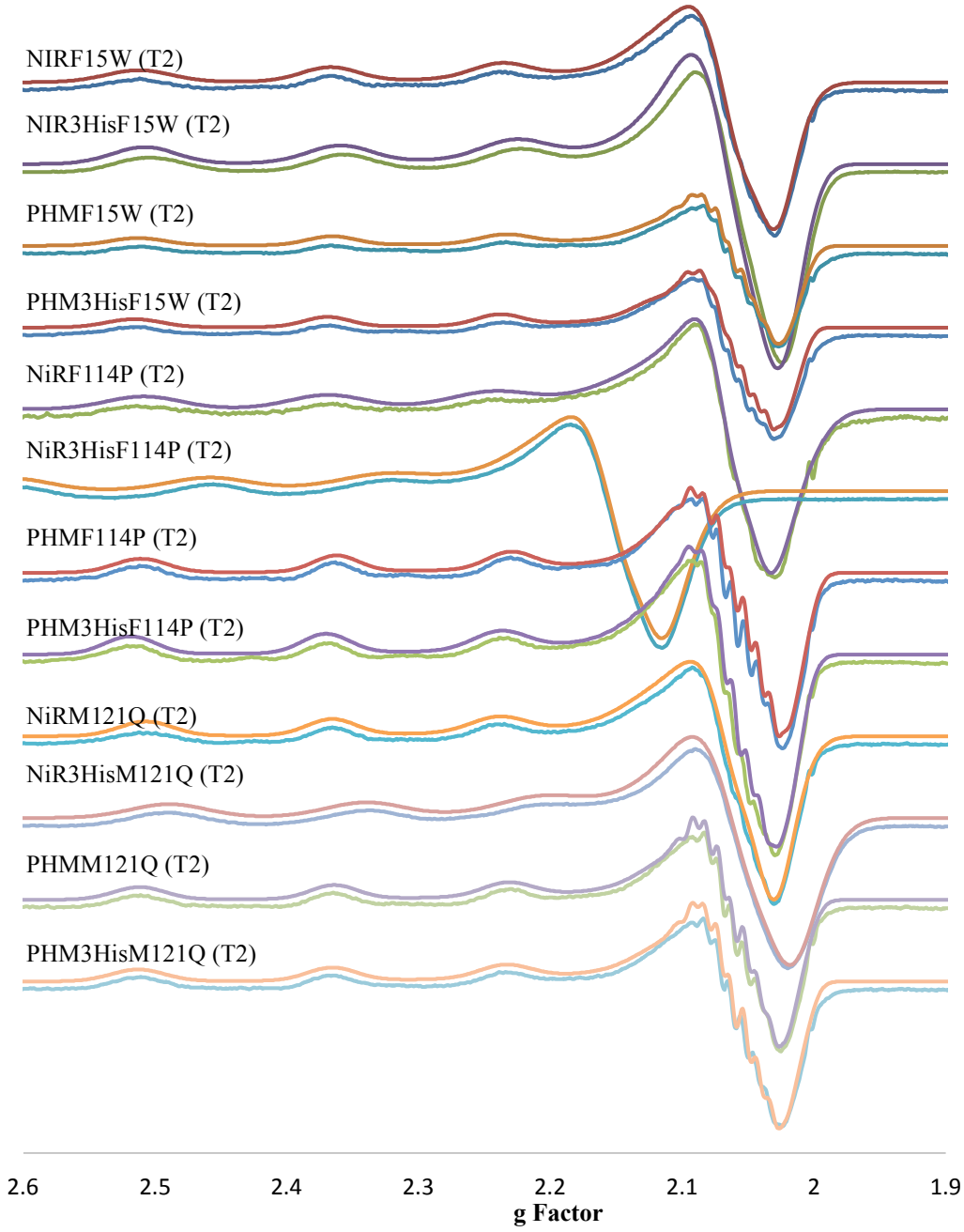


Fig. 2.7: EPR spectra of T2 Cu(II) of second generation single mutant variants along with the simulated spectra predicted by simpow6 overlaid on the top.

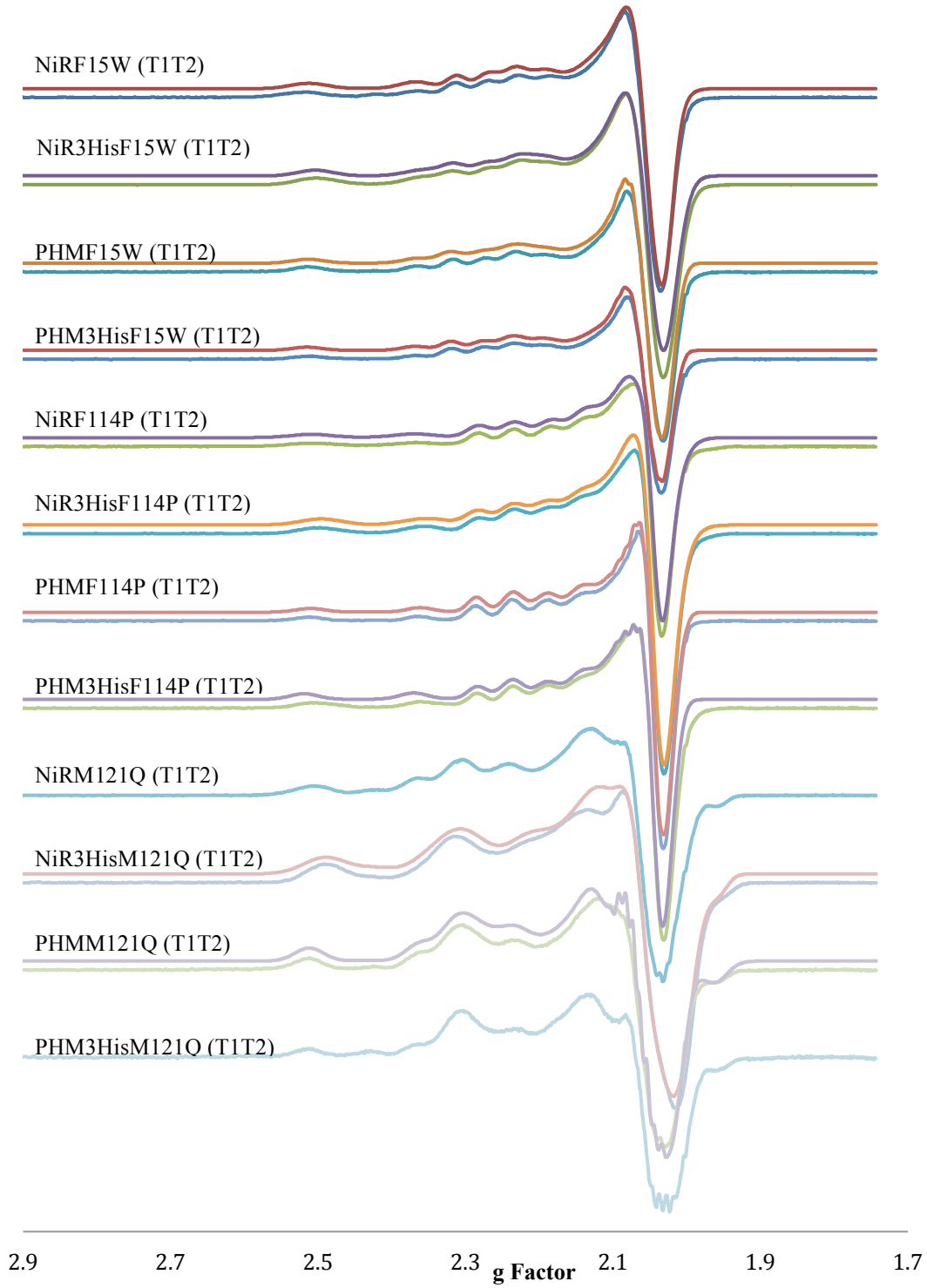


Fig. 2.8: EPR spectra of T1T2 Cu(II) of second generation single mutant variants along with the simulated spectra predicted by simpow6 overlaid on the top. The simulations for NiR-M121Q and PHM3His-M121Q variants are yet to be done.

**2.3.3: T1, T2 and T1T2 Cu(II) EPR spectra and simulation of 2nd generation double mutant azurin variants:**

Figures 2.9, 2.10 and 2.11 show the EPR spectra and simulated spectra of second generation double mutant azurin variants when Cu(II) is bound to T1 site only, T2 site only and both T1 and T2 sites, respectively. All three T1 Cu(II), T2 Cu(II) and T1T2 Cu(II) EPR spectra demonstrate and confirm the copper binding to the respective sites.

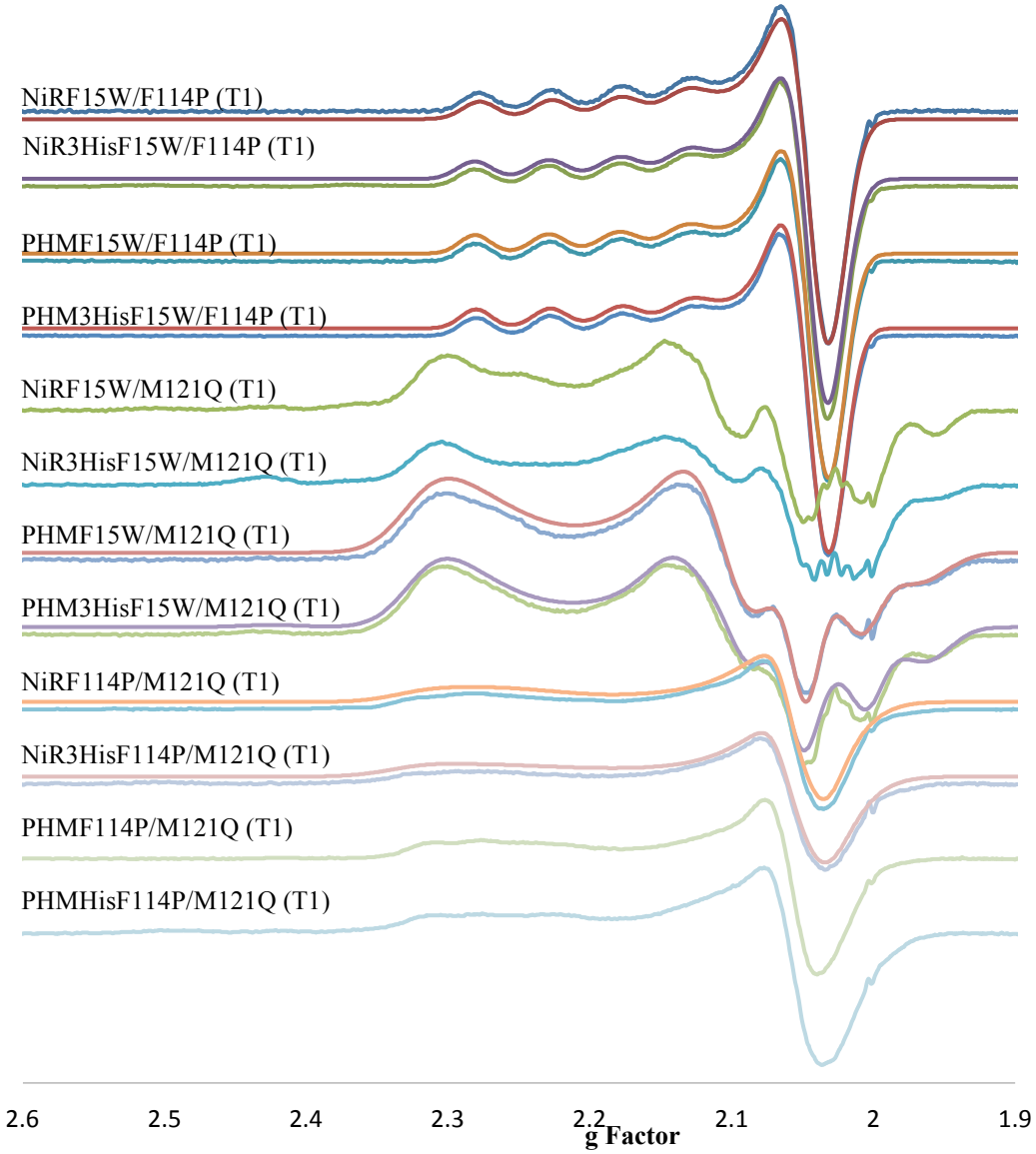


Fig. 2.9: EPR spectra of T1 Cu(II) of 2nd generation double mutant variants along with the simulated spectra predicted by simpow6 overlaid on the top. The simulations for NiR-F15W/M121Q, NiR3His-F15W/M121Q, PHM-F114P/M121Q, and PHM3His-F114P/M121Q variants are yet to be done

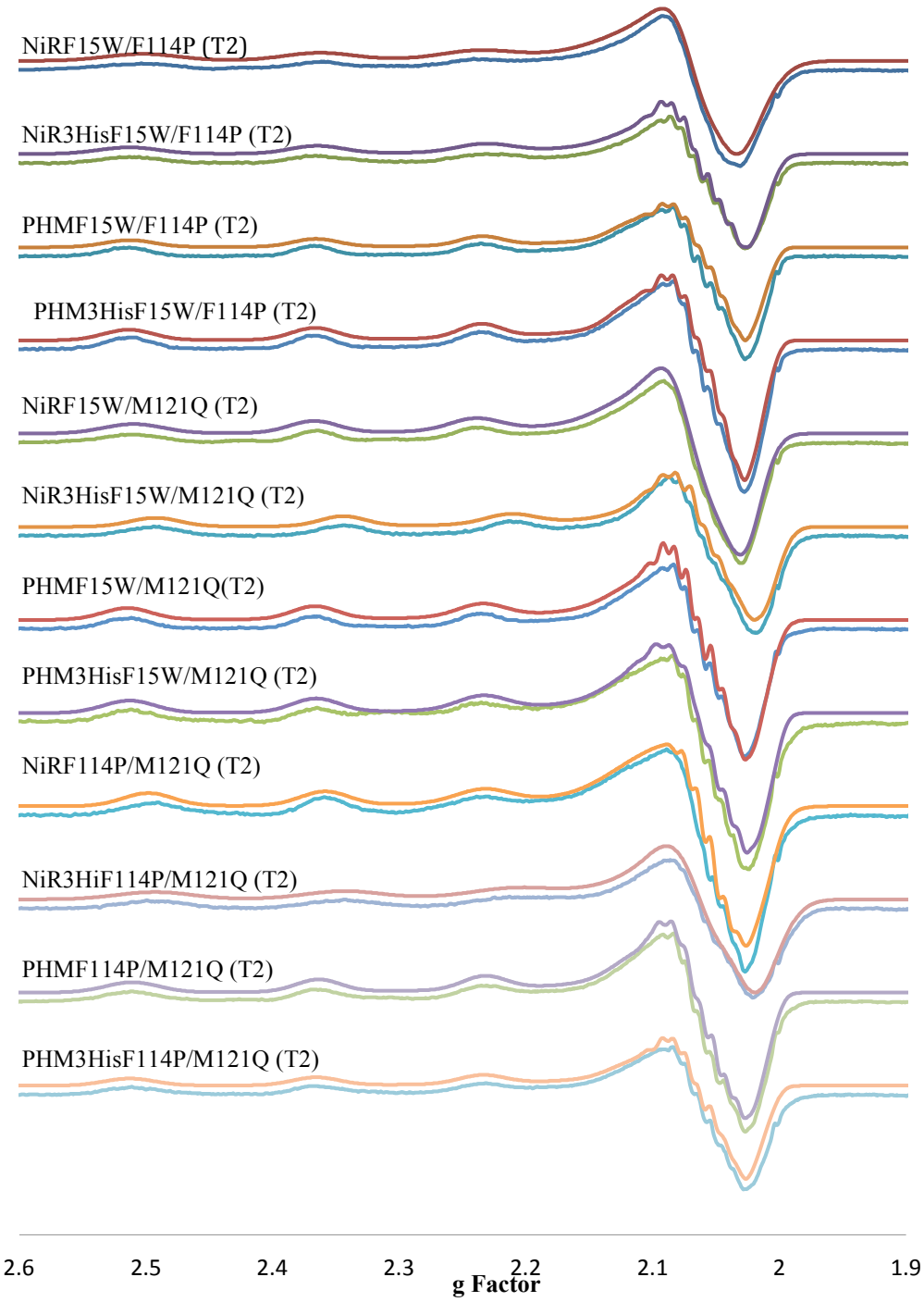


Fig. 2.10: EPR spectra of T2 Cu(II) of 2nd generation double mutant variants along with the simulated spectra predicted by simpow6 overlaid on the top.

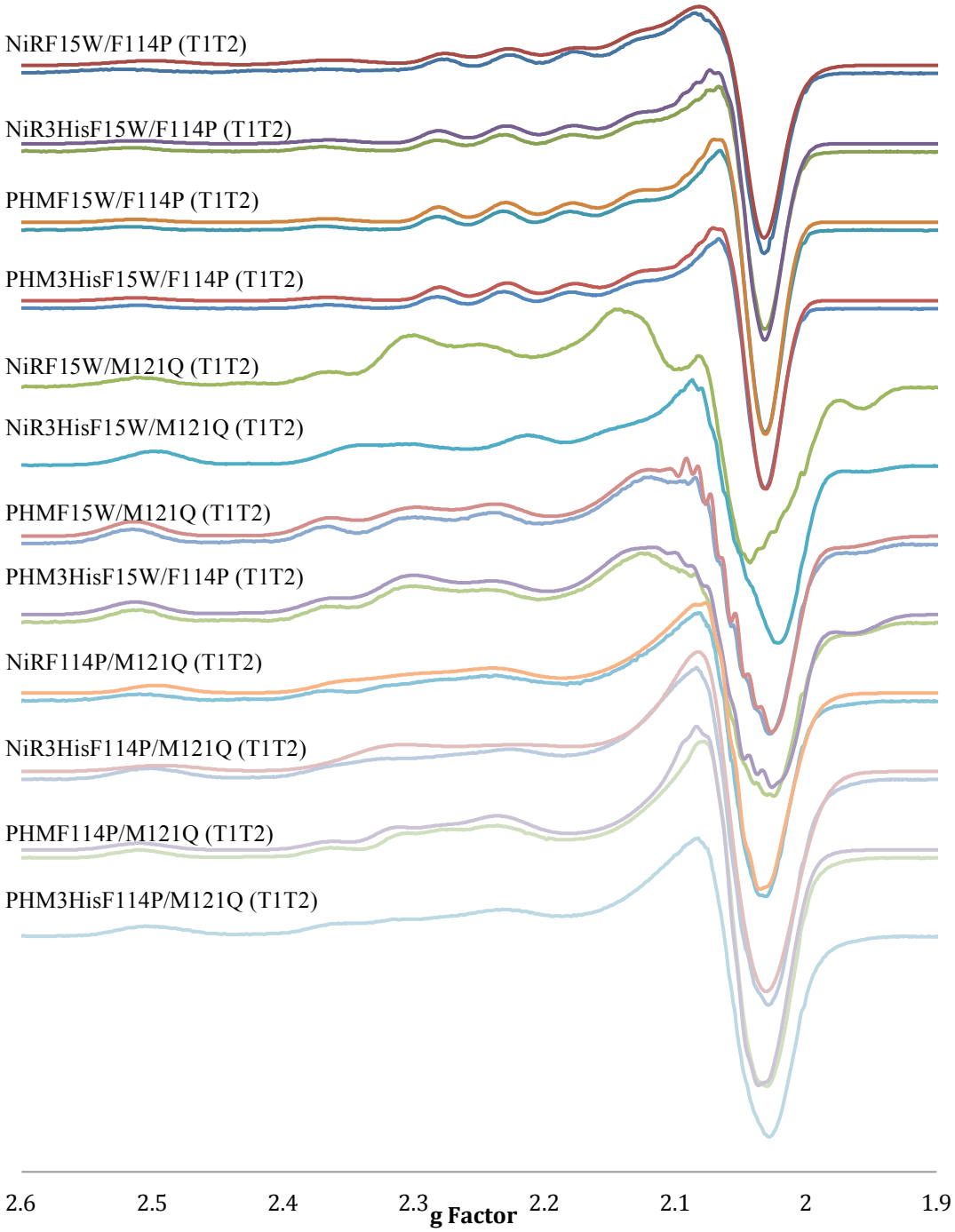


Fig. 2.11: EPR spectra of T1T2 Cu(II) of 2nd generation double mutant variants along with the simulated spectra predicted by simpow6 overlaid on the top. The simulations for NiR-F15W/M121Q, NiR3His-F15W/M121Q, and PHM3His-F114P/M121Q variants are yet to be done.

EPR spectra of each variant confirm the Cu(II) binding to the T1 as well as designed T2 sites. The "*A"* and *"g"* values of these spectra were determined from the simulation program simpow6. These values are summarized in Tables 2.1, 2.2 and 2.3.

Table 2.1: $A_{//}$ & $g_{//}$ values of T1 and T2 Cu(II) of 1st generation variants:

| Variants | T1 | | T2 | |
|---|---|---|---|---|
| | $g_{//}$ | $A_{//}$ (Gauss) | $g_{//}$ | $A_{//}$ (Gauss) |
| WT-Az | 2.26 | 55 | NA | NA |
| NiR-Az | 2.26 | 52 | 2.31 | 159 |
| NiR3His-Az | 2.26 | 47 | 2.29 | 160 |
| PHM-Az | 2.26 | 53 | 2.29 | 165 |
| PHM3His-Az | 2.26 | 53 | 2.30 | 165 |

The T1 site of all of the 1st generation azurin variants are similar to wild type azurin (WT-Az) and exhibit $A_{//}$ values similar to that of WT-Az (~55 Gauss) whereas T2 Cu(II) has higher $A_{//}$ (>150 Gauss) and $g_{//}$ (~2.30) values.

Table 2.2: $A_{//}$ & $g_{//}$ values of T1 and T2 Cu(II) of 2nd generation single mutant variants:

| Variants | T1 | | T2 | |
|---|---|---|---|---|
| | $g_{//}$ | $A_{//}$ (Gauss) | $g_{//}$ | $A_{//}$ (Gauss) |
| NiR-Phe15Trp | 2.25 | 51.53 | 2.30 | 161.5 |
| NiR3His-Phe15Trp | 2.25 | 53.45 | 2.29 | 165.1 |
| PHMPhe15Trp | 2.26 | 52.82 | 2.30 | 163.8 |
| PHM3His-Phe15Trp | 2.26 | 53.40 | 2.30 | 162.7 |
| NiR-Phe114Pro | 2.21 | 64.9 | 2.30 | 154.3 |
| NiR3His-Phe114Pro | 2.21 | 61.9 | 2.29 | 159.7 |
| PHMPhe114Pro | 2.21 | 63.5 | 2.29 | 165.5 |
| PHM3His-Phe114Pro | 2.21 | 62.5 | 2.30 | 164.5 |
| NiR-Met121Gln | - | - | 2.30 | 157.3 |
| NiR3His-Met121Gln | 2.29 | 0 | 2.27 | 168.3 |
| PHM-Met121Gln | 2.29 | 20.7 | 2.30 | 164.8 |
| PHM3His-Met121Gln | - | - | 2.30 | 163.8 |

(Note: The $g_{//}$ and $A_{//}$ values of T1 Cu(II) EPR spectra of NiR-Met121Gln and PHM3His-Met121Gln (shown as dashes in table 2.2) are not yet determined due to difficulty in simulating the spectra.)

Table 2.3: $A_{//}$& $g_{//}$ values of T1 and T2 Cu(II) of 2nd generation double mutant variants:

| Variants | T1 | | T2 | |
|---|---|---|---|---|
| | $g_{//}$ | $A_{//}$ (Gauss) | $g_{//}$ | $A_{//}$ (Gauss) |
| NiR-Phe15Trp/Phe114Pro | 2.20 | 66.2 | 2.30 | 155.8 |
| NiR3His-Phe15Trp/Phe114Pro | 2.20 | 68.0 | 2.30 | 165.1 |
| PHM-Phe15Trp/Phe114Pro | 2.20 | 67.2 | 2.30 | 163.5 |
| PHM3His-Phe15Trp/Phe114Pro | 2.20 | 68.0 | 2.30 | 163.5 |
| NiR-Phe15Trp/Met121Gln | - | - | 2.30 | 160.0 |
| NiR3His-Phe15Trp/Met121Gln | - | - | 2.28 | 167.6 |
| PHM-Phe15Trp/Met121Gln | 2.29 | 20.0 | 2.30 | 164.3 |
| PHM3His-Phe15Trp/Met121Gln | 2.29 | 27.6 | 2.30 | 163.8 |
| NiR-Phe114Pro/Met121Gln | 2.28 | 33.9 | 2.29 | 156.3 |
| NiR3His-Phe114Pro/Met121Gln | 2.28 | 37.8 | 2.28 | 167.8 |
| PHM-Phe114Pro/Met121Gln | 2.27 | 39.3 | 2.30 | 163.9 |
| PHM3His-Phe114Pro/Met121Gln | - | - | 2.30 | 163.8 |

(Note: The $g_{//}$ and $A_{//}$ values of T1 and T2 Cu(II) EPR spectra of NiR-Phe15Trp/Met121Gln, NiR3His-Phe15Trp/Met121Gln and PHM3His-Phe114Pro/Met121Gln variants (shown as dashes in table 2.3) are not yet determined due to difficulty in simulating the spectra)

The 2nd generation variants show some significant differences from the first generation variants. The $g_{//}$ values of the T1 site of Phe114Pro variants are smaller than the 1st generation variants (Table 2.2). On the other hand, the $g_{//}$ values of the T1 site of Met121Gln variants are larger than the 1st generation variants. These results suggest that the change in the atomic environment of T1 center due to Phe114Pro and Met121Gln mutations have a significant effect in the $g_{//}$ and $A_{//}$ parameters. The Met121Gln mutation in particular changes the shape of EPR spectra of the T1 site from axial to more of a rhombic shape. This may be due to the removal of axial interaction of T1 Cu(II) with the Met residue changing the T1 site geometry. The Phe15Trp mutation is between the

T1 and T2 sites and only shows a minimal impact on the $g_{//}$ values of both the T1 and T2 sites.

The $g_{//}$ values of the T2 copper site of our variants are ~2.30 with some variations. This value is comparable to the native NiR from *Alcaligenes xylosoxidans* (AxNiR) whose $g_{//}$ value of T2 site is 2.38. [9] The $A_{//}$ values of our variants are larger by 35 gauss than $A_{//}$ values of AxNiR and are likely due to lack of the third histidine in theT2 sites of our variants.[9]

**2.4 Nitrite reduction Assay with Griess Assay system:**

Once the Cu(II) binding in both T1 and T2 was confirmed, the rate of nitrite reduction was measured using kinetic assays, namely the Griess assay and the reduction/re-oxidation assays. The methods for the Griess assay and the reduction/re-oxidation assay will be discussed in detail in this chapter whereas the results for both of these kinetic assays will be discussed in Chapter 3.

The samples for the Griess assay were prepared using the same technique as preparing UV-Vis samples, by titrating 5 equivalents of $CuSO_4$ into apo protein and removing the excess $CuSO_4$ via PD-10 desalting columns. The buffer was exchanged to 20 mM potassium phosphate buffer at pH 6.35. In the buffer and pH variation study done by previous students in our lab, the assay run with potassium phosphate buffer at pH 6.35 was shown to have the minimum background activity and highest nitrite reduction activity of our NiR3His-Az variant. The concentration of the holo protein was determined again using the $A_{625}$ and the molar absorptivity of azurin (5000 $M^{-1}cm^{-1}$) and the final sample was diluted to 100 μM. The sample was aliquoted out in 260 μL aliquots of 100

μM azurin variants in screw cap vials, flash frozen and stored at -80 °C until they were used.

The activity assays were carried out in the inert, $N_2$ and 5% $H_2$ atmosphere in a glovebox using a Genesys-10S UV-Vis spectrophotometer. The samples were brought into the glovebox, thawed at room temperature, and stirred to allow equilibration in the anaerobic conditions for ~20 minutes. Once the samples were equilibrated, 30 μL of nitrite stock with 10x concentration of the desired nitrite concentration for the assay were added to the azurin variant aliquot (e.g., if 5 mM $NO_2^-$ was desired for the assay, 30 μL of 50 mM $NO_2^-$ was added). The exact amounts and concentrations of the assay conditions are summarized in Table 2.4. The resulting nitrite-azurin variants mixture was stirred for ~5 minutes for complete mixing of nitrite. Since, a constant supply of electrons is required to keep T1 and T2 sites reduced and to perform multiple turnovers of nitrite reduction, excess (10 μL of 1 M or 333 eq.) ascorbic acid was added (the ascorbic acid stock solution pH was also adjusted to 6.35) to the solution in the screw cap vials to reduce the protein and initiate the reaction. The final concentrations of each component in the screw cap vial were as follows: 33 mM ascorbic acid, azurin 86.7 μM and 1 mM, 5 mM, 25 mM, 50 mM, 75 mM, 100 mM or 150 mM $NO_2^-$ concentrations. Time zero was recorded as soon as ascorbic acid was added. The first data point was taken 2 minutes after ascorbic acid addition for all concentrations of $NO_2^-$. After 2 minutes, 20 μL of the reaction mixture was removed from the reaction vial and two serial dilutions in the 20 mM potassium phosphate buffer were performed to get a 500 μL diluted solution of 0.04 mM final nitrite concentration. This diluted solution was vortexed for 5 seconds after each dilution to ensure a well-mixed solution. In our assays, the concentration of

$NO_2^-$ decreased over time due to the reaction. The concentration of $NO_2^-$ was monitored using the Griess assay.

Sulfanilamide (SAN) and N-(1-napthyl)-1-ethylene dihydrochloride (NED) were the key colorimetric reagents used for the Griess assay.[8,10,11] SAN and NED were prepared and were taken into the glovebox at least 20 mins before the assay was started. The concentrations of SAN and NED used were 1% (W/V) and 0.1% (W/V) respectively. 1% SAN was prepared by dissolving 0.5 g of SAN crystals in 50 mL of 3 M HCl whereas 0.1% NED was prepared by dissolving 0.05 g of NED powder in 50 mL water.

To the 500 μL of the diluted assay solution described above, 500 μL of SAN was added and the resulting mixture was thoroughly vortexed for 3 seconds. To the solution, 500 μL of NED was then added as quickly as possible and vortexed for 9 seconds. This yields a pink color with a maximum absorbance at 540 nm.

Upon the addition of SAN to the assay mix containing $NO_2^-$, a reaction between SAN and $NO_2^-$ takes place first. An intermediate diazonium salt is produced with the loss of a water molecule.[11] When NED is added, it reacts with the diazonium salt intermediate and forms an azo compound with pink color that has an maximum absorbance at 540 nm (Fig. 2.12). The addition of NED following SAN has to be done quickly because ascorbic acid causes interference in the pink color formation by reacting with the diazonium salt intermediate. Hence greater sensitivity is achieved when SAN addition is followed by the quick addition of NED.[5,6] It takes about 10 minutes to form the maximum pink color, hence the $A_{540\ nm}$ was measured 10-20 mins after NED addition.

Data points were removed from the NiR assay every 10 minutes for 1 mM and 5 mM nitrite concentrations, every 15 minutes for 25, 50 and 75 mM nitrite

concentrations, and every 20 minutes for 100 and 150 mM nitrite concentrations. The data points were obtained until a ~5% drop in nitrite concentration (5% drop in $A_{540\ nm}$) was achieved. The time required for the 5% drop in nitrite concentration was varied between 40 minutes and 220 minutes depending upon the variants and the nitrite concentration used. The rate of reduction of $NO_2^-$ in AU $min^{-1}$ was determined by finding the slope of the trendline for the 5% drop in nitrite concentration and corrected for dilution by multiplying by the dilution factor. The dilution corrected rates in AU $min^{-1}$ were converted to the mM $NO_2^-$ $min^{-1}$ by dividing the slope in AU by the absorbance of Griess assay complex with unreacted nitrite before the ascorbic acid addition (0.7 AU). These assays were done in triplicate and plotted against the corresponding nitrite concentrations to get the Michaelis-Menten plots.

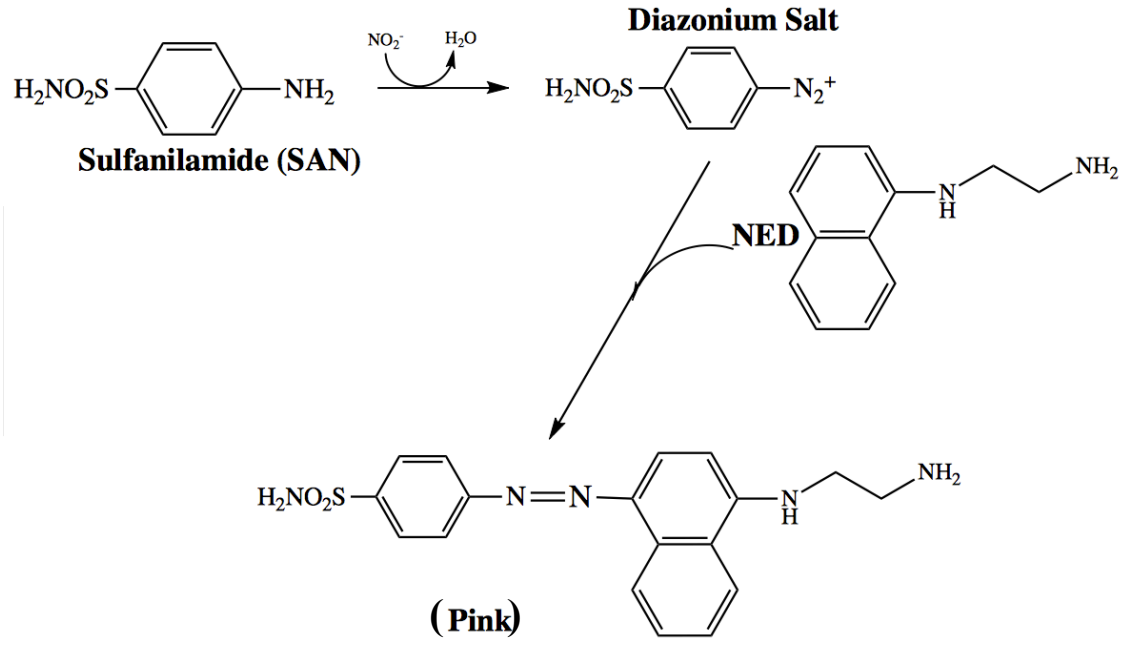


Fig. 2.12: Reactions involved in the Griess Assay.[8,11]

Table 2.4: Nitrite dilutions for the Griess assay:

| **$NO_2^-$ concentration** | **$NO_2^-$ addition & Data Interval** | **Dilutions conditions** |
|---|---|---|
| 1 mM | 30 µL of 10 mM stock added. Data taken every 10 minutes | 20 µL of original assay mix diluted into 480 µL of buffer, then reacted with SAN and NED to make final volume 500 µL. |
| 5 mM | 30 µL of 50 mM stock, Data taken every 10 min | 20 µL of original assay mix diluted into 480 µL of buffer, then reacted with SAN and NED. After 10 minutes, 200 µL of pink assay mix was diluted into 800 µL to make final volume 1 mL. |
| 25 mM | 30 µL of 250 mM stock, Data taken every 15 min | First dilution: 20 µL of original assay mix diluted into 480 µL of buffer. Second dilution: 20 µL of diluted assay mix further diluted into 480 µL of buffer, then reacted with SAN and NED. |
| 50 mM | 30 µL of 500 mM stock, Data taken every 15 min | First dilution: 20 µL of original assay mix diluted into 980 µL of buffer. Second dilution: 20 µL of diluted assay mix further diluted into 480 µL of buffer, then reacted with SAN and NED. |
| 75 mM | 30 µL of 750 mM stock, Data taken every 15 min | First dilution: 20 µL of original assay mix diluted into 980 µL of buffer. Second dilution: 20 µL of diluted assay mix further diluted into 480 µL of buffer, then reacted with SAN and NED. |
| 100 mM | 30 µL of 1 M stock, Data taken every 20 minutes | First dilution: 10 µL of original assay mix diluted into 490 µL of buffer. Second dilution: 10 µL of diluted assay mix further diluted into 490 µL of buffer, then reacted with SAN and NED. |
| 150 mM | 30 µL of 1.5 M stock, Data taken every 20 minutes | First dilution: 10 µL of original assay mix diluted into 490 µL of buffer. Second dilution: 10 µL of diluted assay mix further diluted into 490 µL of buffer, then reacted with SAN and NED. |

**Note:** Potassium phosphate buffer (pH 6.35) was used for all of the assays

- 30 µL of various concentrations $NO_2^-$ stock was added for all concentrations.
- The first data point was taken after 2 minutes of ascorbic acid addition for all concentrations.

## 2.5 T1 Cu(II) Reduction/ re-oxidation Assay:

The reduction and re-oxidation assay is another type of kinetic assay used in our lab to understand the mechanism of nitrite reduction by our variants. The reduction/re-oxidation assay was used to monitor the dependence of nitrite reduction and the electron transfer from T1 to T2 Cu(II) site by monitoring the reduction of T1 copper by ascorbic acid and the subsequent re-oxidation upon the $NO_2^-$ binding to T2 site. We used a Genesys-10S UV-Vis spectrophotometer in the inert atmosphere in glovebox. Using the same method described above for the Griess assay, 0.1 mM protein samples were prepared in potassium phosphate buffer at pH 6.35. The samples were degassed in a 50 mL falcon tube by bubbling with argon gas for 15-20 minutes to reduce oxygen in the sample before bringing the sample into the glove box. The samples were incubated for ~15 minutes in the glovebox with the cap open to let it equilibrate to room temperature and the anaerobic environment. Once the samples were equilibrated, 2 mL aliquots of the protein were used in a 3 mL, flat bottom cuvette for re-oxidation assays to properly house the stir bar for proper mixing. The $A_{625\ nm}$ peak was monitored every 2 seconds during the entire assay.

To monitor the initial reduction rates and the dependence of reduction of T1 Cu(II) on the concentration of reducing agent, various concentrations of ascorbic acid were added to the sample while stirring. Ascorbic acid with the final concentration of 0.05 mM, 0.1 mM, 0.2 mM, 0.5 mM, 0.75 mM and 1 mM (i.e., 0.5-10 eq.) was used. The initial rate of reduction of $A_{625\ nm}$ peak was monitored. These rates were recorded and plotted on y-axis against the ascorbic acid concentration for each mutant, and will be presented and discussed in Chapter 3.2.

For the re-oxidation reactions, only 1-1.5 eq. of ascorbic acid was added to the sample so as to reduce the protein, but not to yield any excess ascorbic acid in solution. Once the protein was fully reduced, an appropriate amount of $NO_2^-$ was added to give a final $NO_2^-$ concentration ranging from 1 mM to 150 mM. Different concentrations of $NO_2^-$ stock were used to keep the added volume of $NO_2^-$ under 60 μL so as to minimize the protein dilution. Upon the addition of $NO_2^-$, the $A_{625\ nm}$ started to increase due to the re-oxidation of T1 site caused by the electron transfer to T2 site, thus reducing $NO_2^-$ in the process. Since only one eq. of ascorbic acid was added, the re-oxidation shows the single turnover of the protein. The rate of re-oxidation was determined by finding the slope of the linear region of re-oxidation curve with the largest slope and an $R^2$ value as close to 1.00 as possible. The slopes were normalized for the concentration of azurin and were plotted against the concentration of $NO_2^-$ to find the rate constant. These experiments were done in triplicate. The re-oxidation reaction results are presented in Chapter 3.2.

## Chapter 3: Enzyme Kinetics

This chapter will include the results and discussion on the kinetics experiments on the nitrite reduction activities of our azurin variants.

### 3.1 Michaelis-Menten enzyme kinetics from the Griess assay:

The azurin variants with T2 Cu(II) were hypothesized to act as an enzyme just like NiR and they were tested for their nitrite reduction activities using the Griess assay as described in Chapter 2. As explained previously, various nitrite concentrations were used as substrate. The Michaelis-Menten enzyme kinetics and its steady-state approximation were used as shown in Equation 3.1. The enzyme concentration [E] remains constant over multiple turnover cycles of the excess substrate, [S] (i.e. nitrite), compared to enzyme concentration [E].[1] When the nitrite is added to the azurin variants, it binds to the open ligand-binding site T2 Cu(II) of azurin variants and forms an enzyme substrate [ES] product. For our azurin variants to perform multiple turnovers, a continuous supply of electrons is necessary for the reduction of T1 and T2 Cu(II) and in turn for the reduction of $NO_2^-$ to NO. Excess (333 equivalents) ascorbic acid was used as the source of electrons for multiple turnovers.

$$[E] + [S] \underset{k_r}{\overset{k_f}{\leftrightarrows}} [ES] \xrightarrow{k_{cat}} E + P \qquad \textbf{(Eq. 3.1)}$$

The production of NO as the product using our azurin variants as enzymes was confirmed earlier in our lab by the colorimetric test involving the formation of an $[Fe(NO)(EDTA)]^{2-}$ complex. The initial rate of nitrite reduction was determined as

described in the Chapter 2 Methods. The rates were plotted against the corresponding nitrite concentrations to get the Michaelis-Menten plots and the Michaelis-Menten parameters such as $V_{max}$, $K_m$ and turnover number.

### 3.1.1 Control with wild type azurin:

We ran control assays to confirm the reduction of nitrite observed by our designed azurin variants was unique. The nitrite reduction assay was attempted at various nitrite concentrations with 86 μM wild type azurin, instead of the designed azurin variants, prepared in the same fashion as the other variants. The pink color, or absorption at 540 nm, formed as a result of the Griess testing of aliquots from the reaction (See Chapter 2) was monitored over time (Figure 3.1).[3,4]

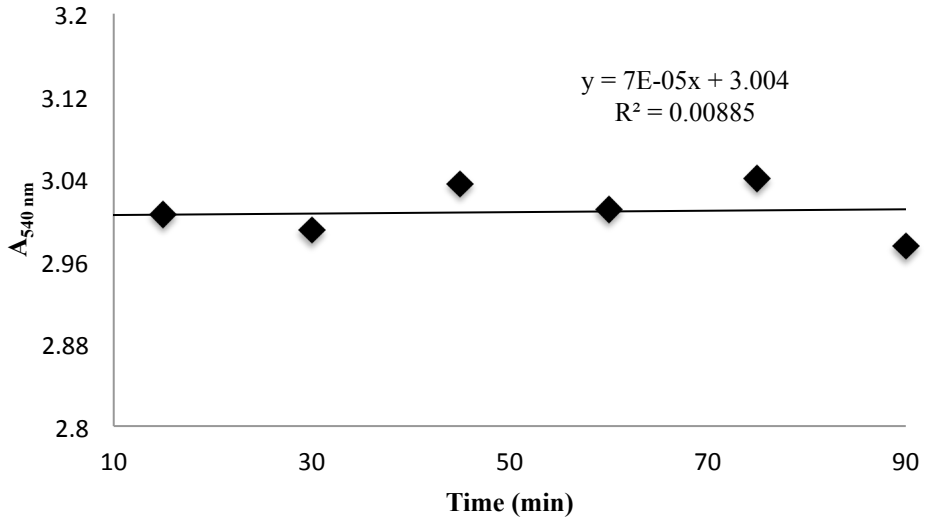


Fig. 3.1: Determination of initial rate of reduction of 5 mM $NO_2^-$ with 33 mM ascorbic acid and 86 μM wild type azurin using Griess assay in 20 mM phosphate buffer at pH 6.35.

The initial rate of reduction of nitrite ($v_o$) was determined by running the Griess assay for 90 minutes and plotting $A_{540}$ versus time to find the slope. The initial reduction

rate was found to be ~$7.5x10^{-5}$ AU $min^{-1}$ (Fig. 3.1) and was therefore considered to be negligible. This might be as expected since wild type azurin doesn't have any solvent exposed nitrite-binding sites. The T1 Cu(II) site has all four ligand-binding sites occupied by amino acid residues. This control assay confirmed that wild type azurin shows minimal nitrite reduction activity, and also that there is negligible direct reaction between nitrite and ascorbic acid. We concluded therefore that any nitrite reduction seen with the azurin variants is a result of their improved catalytic abilities. The initial reduction rates ($v_o$) of azurin were corrected for $NO_2^-$ concentrations (See Chapter 2.4) and were plotted against the corresponding concentration of $NO_2^-$ to get the Michaelis-Menten plot (Fig. 3.2).

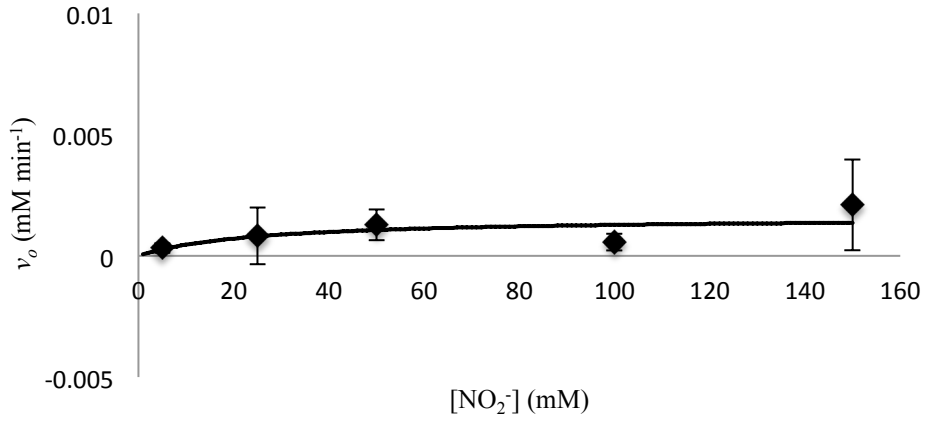


Fig. 3.2: Michaelis-Menten plots for the reduction of $NO_2^-$ by 86 μM wild type azurin in 20 mM potassium phosphate buffer at pH 6.35.

The nitrite reduction activity of wild type azurin remained minimal for all attempted nitrite concentrations, which suggested that that the Type 1 copper site in wild type azurin is not significantly involved in the reduction of nitrite under these conditions.

### 3.1.2 Michaelis-Menten kinetics of the first generation variants:

Assays were also run to determine the Michaelis-Menten kinetics for the first generation variants (NiR-Az, NiR3His-Az, PHM-Az and PHM3His-Az). The initial rate of reduction ($v_o$) was determined by running the assay until a 5% drop in the concentration of $NO_2^-$ was observed by the Griess assay. An example of the initial rate of 1 mM nitrite reduction with NiR3His azurin is shown in Fig. 3.3.

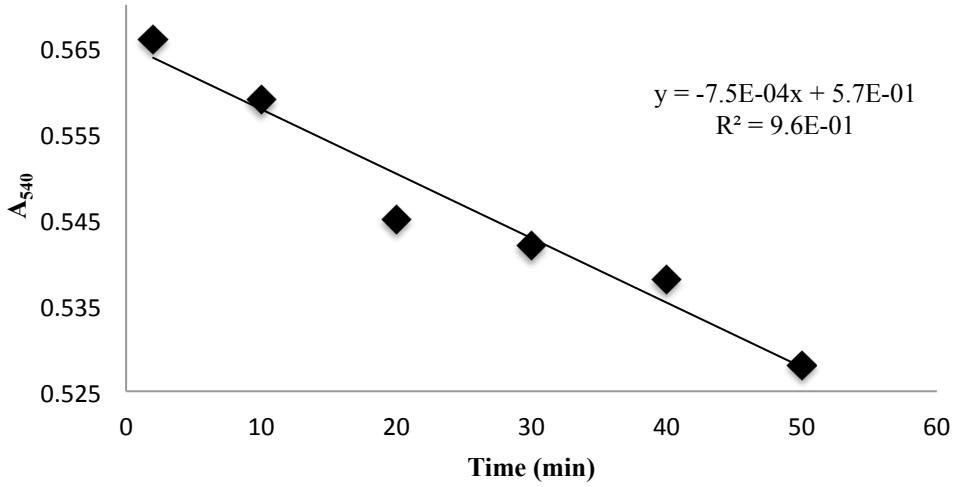


Fig. 3.3: Determination of initial rate of reduction of 1 mM $NO_2^-$ with 33 mM ascorbic acid for 86 µM NiR3His-Az using Griess assay in 20 mM phosphate buffer at pH 6.35.

The initial reduction of $NO_2^-$ shows a linear trend for first 5% drop in the concentration of $NO_2^-$. For 1 mM $NO_2^-$, the slope was found to be $7.5 \times 10^{-4}$ AU $min^{-1}$, which corresponds to $1.10 \times 10^{-3}$ mM nitrite/min. The individual assays for the first generation variants were run at nitrite concentrations of 1 mM, 5 mM, 25 mM, 50 mM, 75 mM, 100 mM and 150 mM. The assay for each concentration was repeated in triplicate, and the average and standard deviation was calculated. These rates were then plotted versus the corresponding nitrite concentrations for the Michaelis-Menten plots shown in Figures 3.4(a)-3.4(d).

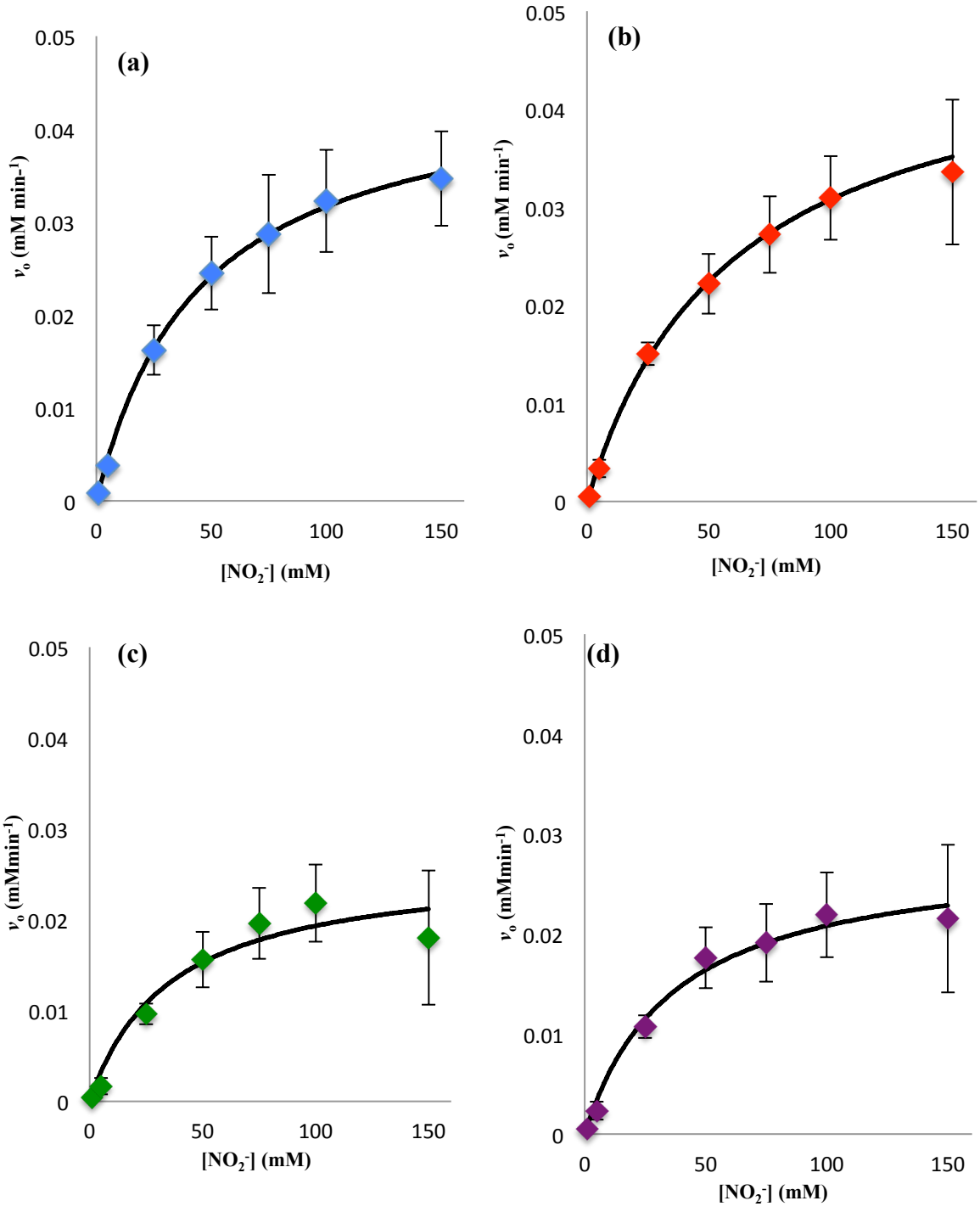


Fig. 3.4: Michaelis-Menten plots for (a) NiR3His-Az, (b) PHM3His-Az, (c) NiR-Az and (d) PHM-Az in 20 mM phosphate buffer at pH 6.35.

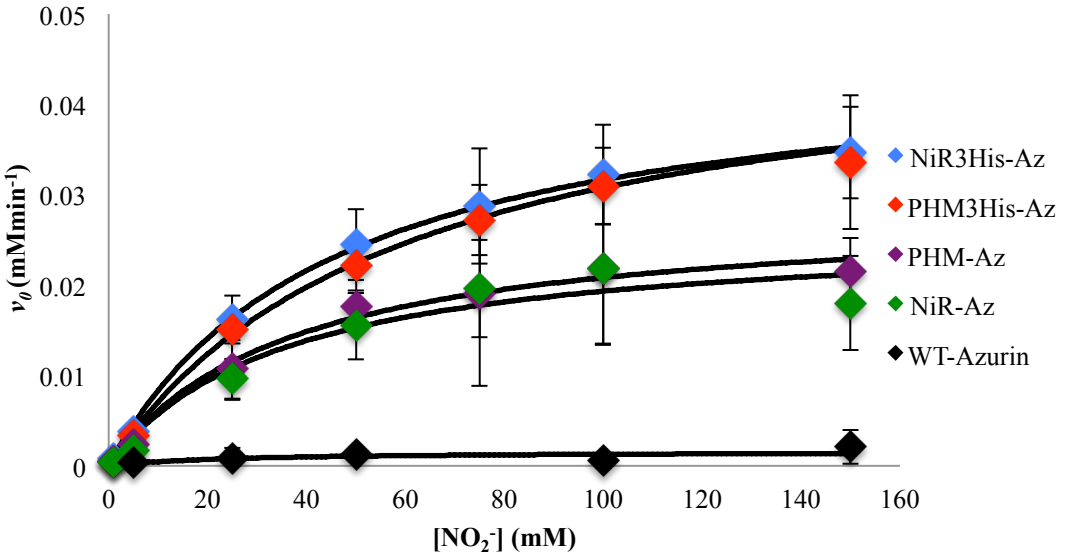


Fig. 3.5: Compilation of Michaelis-Menten plots for first generation azurin variants in 20 mM phosphate buffer at pH 6.35.

The azurin variants show significant nitrite reduction activity compared to wild type azurin, which showed no nitrite reduction. Among the first generation azurin variants, PHM3His-Az and NiR3His-Az had the highest turnover numbers of $9.7 \times 10^{-3} \pm 1.1 \times 10^{-3}$ mM $NO_2^-$ $s^{-1}$ $mM^{-1}$-Az and $9.2 \times 10^{-3} \pm 1.1 \times 10^{-3}$ mM $NO_2^-$ $s^{-1}$ $mM^{-1}$-Az, respectively. NiR-Az and PHM-Az had the lowest turnover numbers with $5.6 \times 10^{-3} \pm 1.4 \times 10^{-3}$ mM $NO_2^-$ $s^{-1}$ $mM^{-1}$-Az and $6.4 \times 10^{-3} \pm 1.1 \times 10^{-3}$ mM $NO_2^-$ $s^{-1}$ $mM^{-1}$-Az, respectively. The $K_m$, $V_{max}$ and the turnover number were found using the Sigma Plot 12.5 Enzyme kinetics tool package and are shown in Table 3.1. NiR3His-Az and PHM3His-Az have the highest turnover numbers indicating the two variants are most efficient at catalyzing nitrite reduction. These quantifiable numbers are consistent with the qualitative plots shown in the compilation Fig. 3.5.

The reason for the varied activities in these four variants is unclear. But we know that both PHM-Az and NiR-Az variants lack the third histidine on designed T2 site, whereas NiR3His-Az and PHM3His-Az have three histidines, similar to the native

NiR. The higher $V_{max}$ and turnover numbers of NiR3His-Az and PHM3His-Az may reflect the importance of the third histidine. It is assumed that three histidines in the T2 site bind the copper(II) ion better. The histidines could also play an important role in providing the proton necessary for the reduction of $NO_2^-$, hence having the third histidine is advantageous in our variants as well.

Table 3.1: $K_m$,$V_{max}$ & turnover numbers of 1st generation variants compared to nativeNiR.

| **Variants** | ***$K_m$*** **(mM)** | ***$V_{max}$*** **(mM $min^{-1}$)** | **Turnover Number (mM $NO_2^-$ $s^{-1}$ $mM^{-1}$-Az)** |
|---|---|---|---|
| Native AfNiR | $53x10^{-3}$±$5.0x10^{-3}$ | NA | $1.0x10^{3}$ ± $3.3x10^{1}$ (2) |
| NiR3His-Az | 33 ± 11 | $48x10^{-3}$ ± $6.0x10^{-3}$ | $9.2x10^{-3}$ ± $1.1x10^{-3}$ |
| PHM3His-Az | 46 ± 17 | $51x10^{-3}$ ± $5.9x10^{-3}$ | $9.7x10^{-3}$ ± $1.1x10^{-3}$ |
| NiR-Az | 36 ± 10 | $29x10^{-3}$ ± $7.5x10^{-3}$ | $5.6x10^{-3}$ ± $1.4x10^{-3}$ |
| PHM-Az | 55 ± 26 | $33x10^{-3}$ ± $5.6x10^{-3}$ | $6.4x10^{-3}$ ± $1.1x10^{-3}$ |

All of these values were compared to the values of native NiR from *Alcaligenes faecalis* (AfNiR).(2) As explained in Chapter 1, 1st generation variants lack either the 3rd His or the Asp residue, found near the T2 site of native NiR as well as having ~100 mV difference in the reduction potential of T1 and T2. In addition, they also lack the direct electron transfer pathway between T1 and T2 sites. It was found that the $K_m$ values of our variants were $6.2x10^2$ -$1.0x10^3$ times bigger than the $K_m$ values of native AfNiR showing weaker $NO_2^-$ affinities of our variants. The turnover numbers of our azurin variants were about $1.1x10^5$ -$1.8x10^5$ times smaller than the native AfNiR. The next goal was to test the activity of the second generation single and double mutant variants to see if the added mutations (described in Chapter 1) improved the activity.

### 3.1.3 Michaelis-Menten kinetics of the NiR3His-Az 2nd generation single mutant variants:

To characterize the second generation single and double mutant variants, we analyzed the activities of variants of one of the most active first generation variant

NiR3His-Az. As explained previously in Chapter 1, Phe15Trp variants have the Phe15 residue mutated to Trp, which is expected to facilitate the electron transfer between T1 and T2 sites by providing a direct electron transfer pathway. Similarly, Phe114Pro and Met121Gln mutations are expected to increase the electron transfer between T1 and T2 by reducing the reduction potential of T1 site. All of these variants were hypothesized to have improved nitrite reductase activity over the first generation variants. The Michaelis-Menten kinetics and corresponding parameters were determined using the Griess assay. The Michaelis-Menten plots for the second generation single mutant variants of NiR3His-Az are shown in Figures 3.6(a) - 3.6(d) and compiled in Figure 3.7.

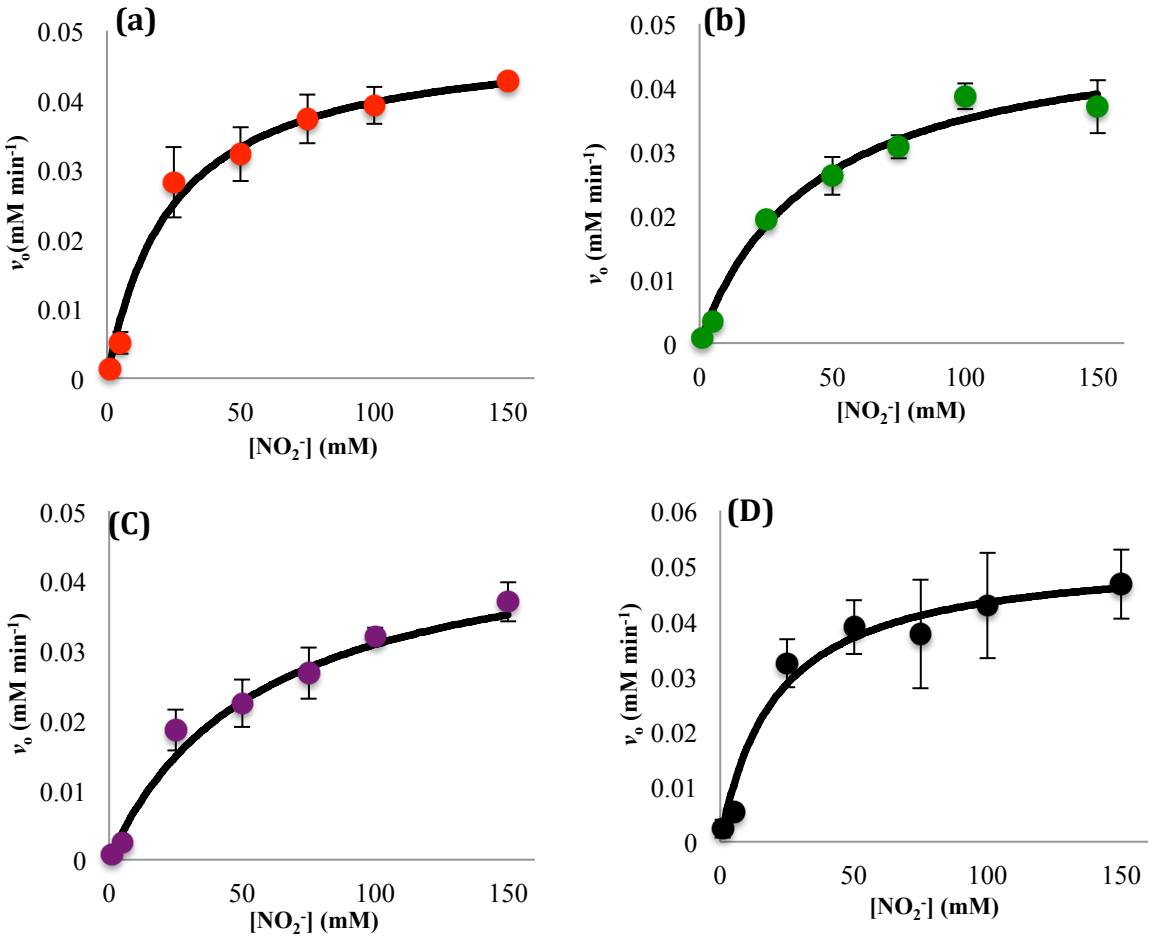


Fig. 3.6: Michaelis-Menten plots for NiR3His-Az second generation single mutant variants (a) NiR3His-F15W (b) NiR3His-F114P (c) NiR3His-M121Q and (d) NiR3His-M121L variants in 20 mM phosphate buffer at pH 6.35.

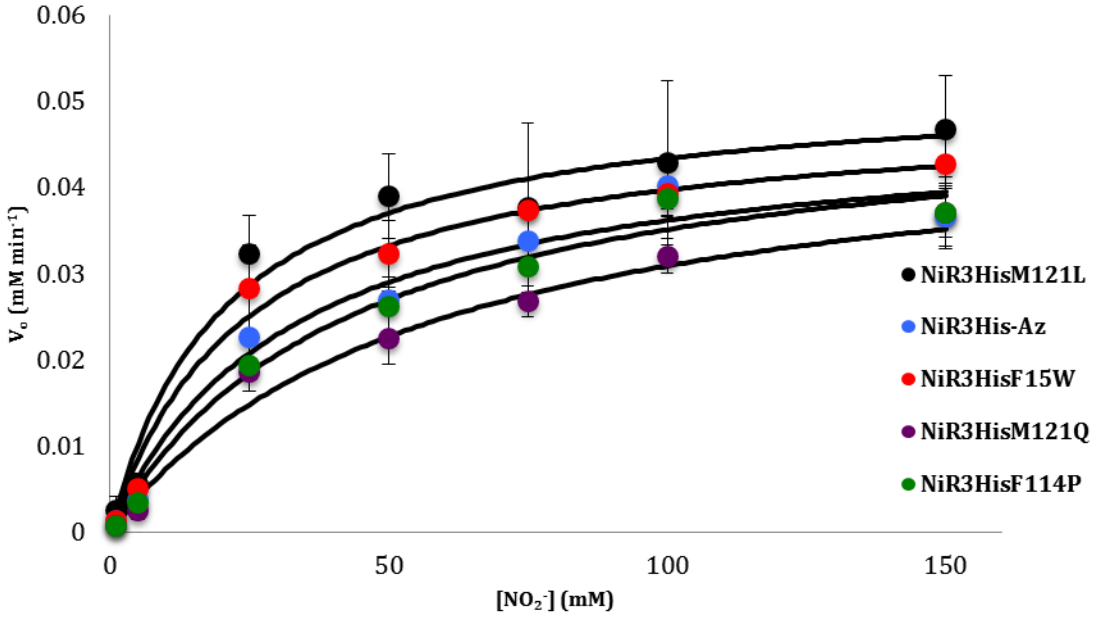


Fig. 3.7: Compilation of Michaelis-Menten plots for NiR3His-Az second generation single mutant variants in 20 mM phosphate buffer at pH 6.35.

The $K_m$, $V_{max}$ and the turnover numbers of second generation single mutant variants of NiR3His-Az were determined in the same way as in the first generation variants and are shown in Table 3.2.

Table 3.2: $K_m$, $V_{max}$ and turnover numbers of 2nd generation single mutant variants of NiR3His-Az.

| **Variants** | **$K_m$ (mM)** | **$V_{max}$ (mM min$^{-1}$)** | **Turnover Number (mM $NO_2^-$ $s^{-1}$ $mM^{-1}$Az)** |
|---|---|---|---|
| NiR3His-Az | 33 ± 11 | 48x10$^{-3}$ ± 6.0 x10$^{-3}$ | 9.1x10$^{-3}$ ± 1.1 x10$^{-3}$ |
| NiR3His-Phe15Trp | 43 ± 14 | 65x10$^{-3}$ ± 8.7x10$^{-3}$ | 13x10$^{-3}$ ± 1.7 x10$^{-3}$ |
| NiR3His-Phe114Pro | 43 ± 14 | 55x10$^{-3}$ ± 6.4x10$^{-3}$ | 11x10$^{-3}$ ± 1.2 x10$^{-3}$ |
| NiR3His-Met121Gln | 59 ± 19 | 50x10$^{-3}$ ± 7.0 x10$^{-3}$ | 9.7x10$^{-3}$ ± 1.3 x10$^{-3}$ |
| NiR3His-Met121Leu | 23 ± 06 | 53 x10$^{-3}$ ± 19x10$^{-3}$ | 10x10$^{-3}$ ± 1.7 x10$^{-3}$ |
| NiR3His-Az with T1Hg(II), T2Cu(II) | 27± 07 | 47 x10$^{-3}$ ± 7.0x10$^{-3}$ | 9.1x10$^{-3}$ ± 1.3 x10$^{-3}$ |

The turnover numbers of NiR3His-Phe15Trp and NiR3His-Phe114Pro are 13x10$^{-3}$ ± 1.7 x10$^{-3}$ mM $NO_2^-$ $s^{-1}$ $mM^{-1}$-Az and 11x10$^{-3}$ ± 1.2 x10$^{-3}$mM $NO_2^-$ $s^{-1}$ $mM^{-1}$-Az,

respectively, whereas the NiR3His-Met121Gln has the turnover number ($9.7 \times 10^{-3} \pm 1.3 \times 10^{-3}$ mM $NO_2^-$ $s^{-1}$ $mM^{-1}$-Az) close to that of NiR3His-Az. These numbers are ~$6.5 \times 10^4$ times smaller than the native AfNiR showing a perhaps slightly higher turnover number than that of NiR3His-Az (first generation), but this improvement was within the error.

As a comparison, a new variant, NiR3His-Met121Leu (NiR3HisM121L) was tested where the Met121 residue was mutated to Leu. The Met121Leu mutation is known to increase the reduction potential of the T1 site.[5] Met121Leu was expected to function in the opposite way as the Met121Gln and Phe114Pro mutations and was hypothesized to have lower nitrite reduction activity due to a decreased thermodynamic favorability of electron transfer to the T2 site. The $K_m$ of the NiR3His-Met121Leu variant was 22.95 mM, which is the smallest of all of the first and second generation variants whereas the turnover number of NiR3HisM121Leu variants ($10 \times 10^{-3} \pm 1.7 \times 10^{-3}$ $NO_2^-$ $s^{-1}$ $mM^{-1}$-Az) was about the same as the NiR3His-Az. The $K_m$, $V_{max}$ and turnover numbers of these variants are presented in Table 3.2. The same activity of NiR3His-Az and the second generation variants including NiR3His-Met121Leu variant indicates that the electron transfer on the second generation variants is not very significant in influencing the rate of nitrite reduction.

Similarly, the second generation single mutant variants of NiR-Az (not NiR3His-Az) were also tested for their nitrite reduction activities and the results show that these variants also showed nitrite reduction activities. The Michaelis-Menten plots for the NiR-Az second generation single mutant variants are compiled in Fig. 3.8, whereas the $K_m$, $V_{max}$ and turnover numbers are presented in Table 3.3.

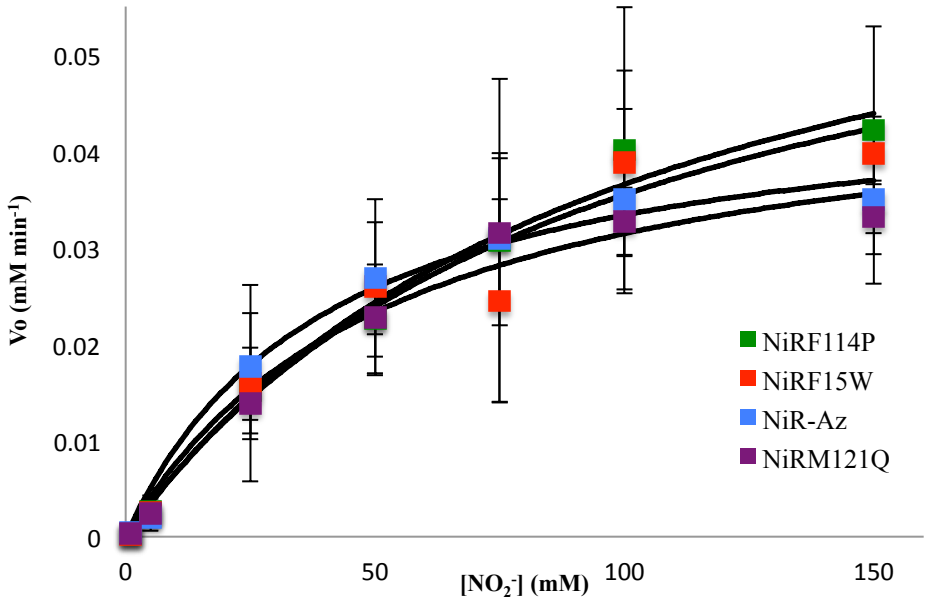


Fig. 3.8: Compilation of Michaelis-Menten plots for NiR-Az second generation single mutant variants in 20 mM phosphate buffer pH at 6.35.

Preliminary results of the second generation single mutant variants of NiR-Az variants show comparatively worse $K_m$ values than the NiR-Az but show higher turnover numbers. NiR-Phe15Trp ($13x10^{-3} \pm 2.3x10^{-3}$ mM $NO_2^-$ $s^{-1}$ $mM^{-1}$-Az), NiR-Phe114Pro ($14x10^{-3} \pm 2.8x10^{-3}$ mM $NO_2^-$ $s^{-1}$ $mM^{-1}$-Az) and NiR-Met121Gln ($9.2x10^{-3} \pm 2.7x10^{-3}$ mM $NO_2^-$ $s^{-1}$ $mM^{-1}$-Az) show an approximately 2 fold increase in the turnover number, hence the improved activity. However, the errors on the $K_m$ and turnover numbers of NiR-Az second generation variants are significant. More trials of NiR-Az second generation single mutant variants need to be done to statistically confirm any improvement on activity.

Table 3.3: $K_m$, $V_{max}$ and turnover numbers of second generation single mutant variants of NiR-Az.

| **Variants** | $K_m$ **(mM)** | $V_{max}$ **(mM min$^{-1}$)** | **Turnover Number (mM $NO_2^-$ s$^{-1}$ mM$^{-1}$Az)** |
|---|---|---|---|
| NiR-Az | 36 ± 1 | $29\times10^{-3} \pm 4.0\times10^{-3}$ | $5.6\times10^{-3} \pm 0.7\times10^{-3}$ |
| NiR-Phe15Trp | 95 ± 19 | $69\times10^{-3} \pm 21\times10^{-3}$ | $13\times10^{-3} \pm 2.3\times10^{-3}$ |
| NiR-Phe114Pro | 100 ± 20 | $73\times10^{-3} \pm 8.5\times10^{-3}$ | $14\times10^{-3} \pm 2.8\times10^{-3}$ |
| NiR-Met121Gln | 54 ± 12 | $48\times10^{-3} \pm 2.8\times10^{-3}$ | $9.2\times10^{-3} \pm 2.7\times10^{-3}$ |

The data suggest neither changing the reduction potential nor providing a direct electron transfer pathway between T1 and T2 in second generation variants has a significant effect on the rate of nitrite reduction activity. This suggests that the T1 and T2 copper centers work independently of each other or the reduction of the T1 and T2 centers is not the rate determining step on the nitrite reduction. To test this hypothesis, $NO_2^-$ reduction assays were run on the 86 µM NiR3His-Az sample prepared in phosphate buffer at pH 6.35 with Hg(II) in the T1 center and Cu(II) in the T2 center. The Michaelis-Menten plot for the sample such prepared is shown in Figure 3.9.

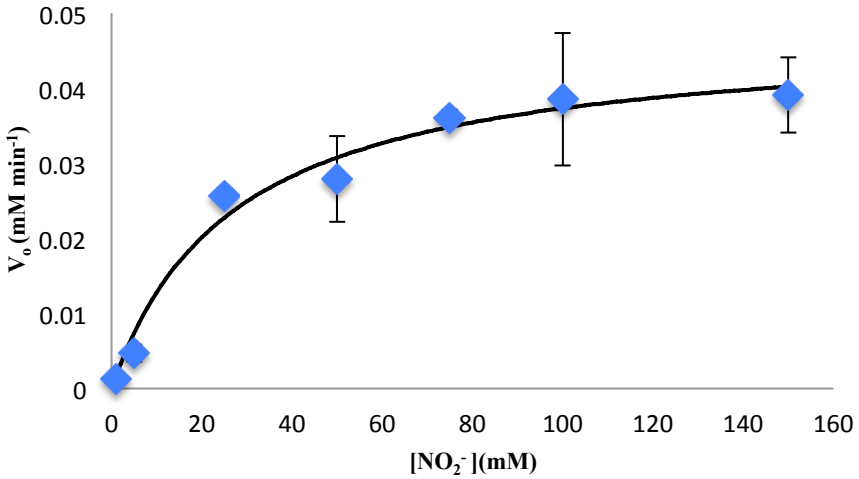


Fig. 3.9: Michaelis-Menten plot of NiR3His-Az variant with T1 Hg(II) and T2 Cu(II) in 20 mM phosphate buffer at pH 6.35

The $K_m$ (27 mM) and turnover number ($9.1x10^{-3}$ mM $NO_2^-$ $s^{-1}$ $mM^{-1}$-Az) of the T1 Hg(II) T2 Cu(II) sample were comparable to that of NiR3His-Az with Cu(II) on both T1 and T2 sites, indicating that the variants with T2-Cu(II) only have about the same activity, and thus suggest that the transfer of electrons from the T1 to T2 center is not the rate limiting step in the activity of our variants. Another possible explanation for no improvement on the second generation variants could be negligible electron transfer between T1 and T2 sites. The NiR3His-Met121Leu variant that was hypothesized to show lower $NO_2^-$ reduction activity due to thermodynamically unfavored electron transfer shows about the same activity as NiR3His-Az and other NiR3His-Az second generation single mutant variants indicating the rate of electron transfer may not have rate determining step on the $NO_2^-$ reduction.

To further explore the effect of the rate of electron transfer rates in the $NO_2^-$ reduction, and hopefully improve the rate of nitrite reduction, the second generation double mutant variants were created by pairing up the mutations explained above to make double mutants.

### 3.1.4 Michaelis-Menten kinetics of the NiR3His-Az second generation double mutant variants:

The second generation double mutant variants were Phe15Trp/Phe114Pro, Phe15Trp/Met121Gln and Phe114Pro/Met121Gln variants of 1st generation variants. The Phe15Trp/Phe114Pro and Phe15Trp/Met121Gln variants are intended to decrease the electron potential of the T1 site as well as provide the electron transfer wire between T1 and T2 sites. Phe114Pro/Met121Gln variants were meant to lower the reduction potential

of the T1 site by twice the amount of each mutation alone. The Michaelis-Menten plots of the second generation double mutant variants are shown in Figures 3.10-3.11.

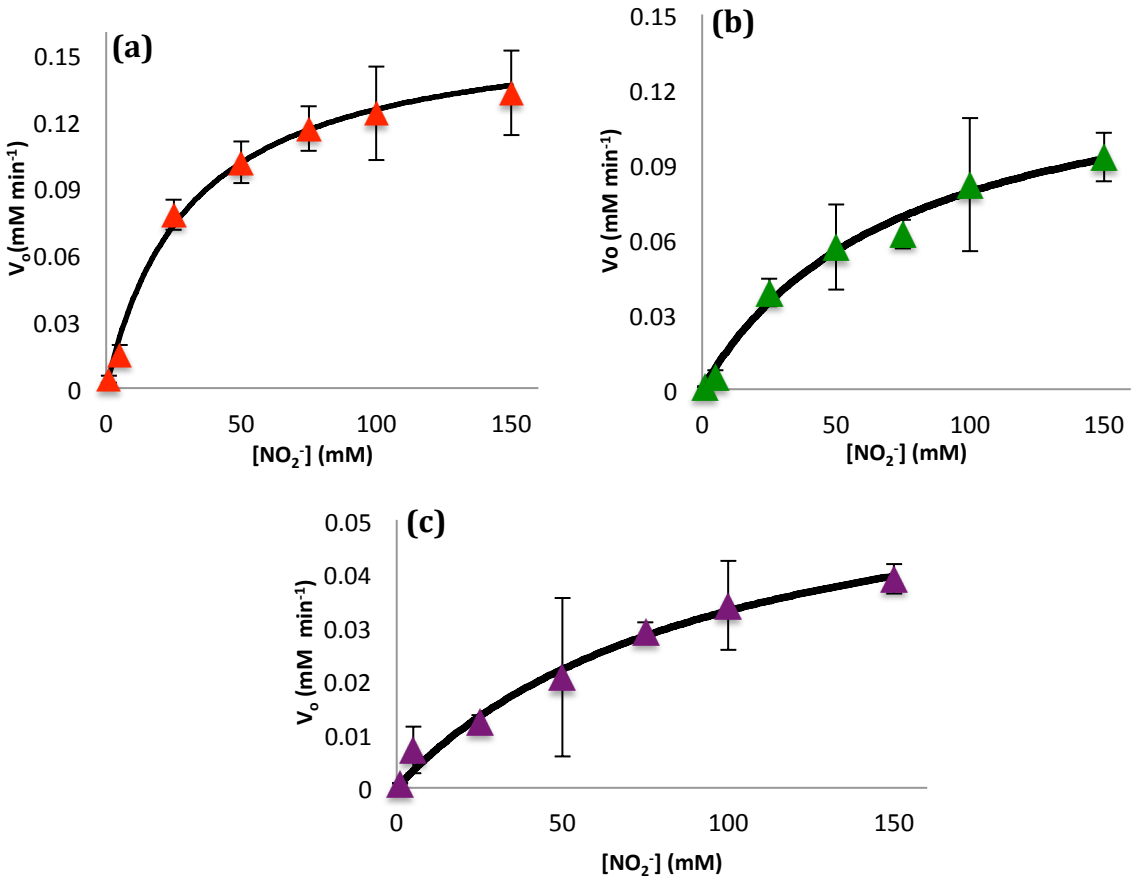


Fig. 3.10: Michaelis-Menten plots for NiR3His second generation double mutant variants (a) NiR3HisF15W/F114P (b) NiR3HisF15W/M121Q (c) NiR3HisF114P/M121Q in 20 mM phosphate buffer at pH 6.35.

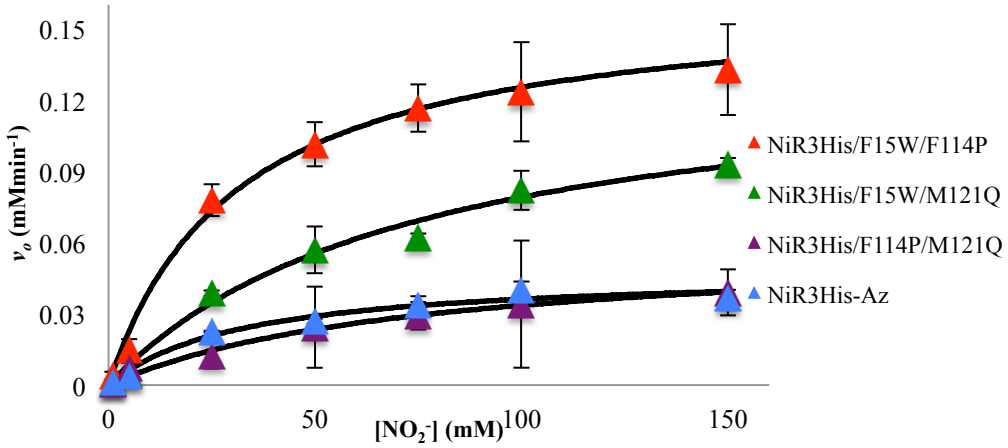


Fig 3.11 Compilation of Michaelis-Menten plots for NiR3His-Az and its second generation double mutant variants in 20 mM phosphate buffer at pH 6.35.

The Phe15Trp/Phe114Pro variant of NiR3His-Az was the most active among the second generation double mutant variants with lowest $K_m$ (31 ± 12 mM) and highest turnover number ($31x10^{-3}$ ± $4.8x10^{-3}$ mM $NO_2^-$ $s^{-1}$ $mM^{-1}$-Az), which is ~3 times faster than the NiR3His-Az and its second generation single mutant variants. NiR3His-Phe15Trp/Met121Gln also had high activity, with a turnover number of $26x10^{-3}$ ± $7.3x10^{-3}$ mM $NO_2^-$ $s^{-1}$ $mM^{-1}$-Az, which is more than 2.5 times faster than NiR3His-Az and its second generation variants while NiR3His-Phe114Pro/Met121Gln variant didn't show much improvement in the activity ($11x10^{-3}$ ± $1.8x10^{-3}$ mM $NO_2^-$ $s^{-1}$ $mM^{-1}$-Az) as it has about the same turnover number as the single mutant variants of NiR3His-Az.

The results show that the nitrite reduction activity of the second generation double mutant variants of NiR3His-Az improved significantly from the first and second generation single mutant variants but are still ~$3x10^4$ to $9x10^4$ times slower than the native AfNiR. The $K_m$, $V_{max}$ and the turnover number values are summarized in Table 3.4.

Table 3.4: $K_m$, $V_{max}$ and turnover numbers of second generation double mutant variants of NiR3His-Az.

| **Variants** | ***$K_m$*** **(mM)** | ***$V_{max}$*** **(mM min-1)** | **Turnover number (mM $NO_2^-$ $s^{-1}$ $mM^{-1}$-Az)** |
|---|---|---|---|
| NiR3His-Az | 36 ± 6.0 | $48x10^{-3}$ ± $4.1x10^{-3}$ | $9.2\ x10^{-3}$ ± $1.1x10^{-3}$ |
| NiR3HisF15W/F114P | 31 ± 12 | $160\ x10^{-3}$ ± $43x10^{-3}$ | $31x10^{-3}$ ± $4.8x10^{-3}$ |
| NiR3HisF15W/M121Q | 74 ± 37 | $140x10^{-3}$ ± $66x10^{-3}$ | $26x10^{-3}$ ± $7.3x10^{-3}$ |
| NiR3HisF114P/M121Q | 76 ± 19 | $59x10^{-3}$ ± $16x10^{-3}$ | $11x10^{-3}$ ± $1.8x10^{-3}$ |

The results suggest that the introduction of electron transfer pathway coupled with lowering the reduction potential of T1 site have a significant effect on the activity of azurin variants. While Phe15Trp variants on the second variants showed just a hint of improvement, the improvement was not significant. Adding Phe114Pro and Met121Gln

mutations on top of the Phe15Trp mutation increase the activity of our variants while decreasing the reduction potential of T1 site by two folds the single mutation don't show much improvement on the turnover numbers of first generation NiR3His-Az.

The nitrite reduction activities of second generation single and double mutant variants of other first generation variants (NiR-Az, PHM-Az and PHM3His-Az) are being measured in our lab.

## 3.2 Single turnover kinetics of first generation azurin variants using reduction/re-oxidation assays:

### 3.2.1 Multiple turnovers:

Improvement in the activity of second generation double mutant variants suggest the T1 copper electron transfer site has an effects on the reaction at T2 catalytic site. However, the NiR3His-Az sample with T1 Hg(II) and T2 Cu(II)-only shows nitrite reduction almost as fast as NiR3His-Az with both T1 and T2 Cu(II). This led us to question the role of the T1 copper site in our mimics, and its effect on the nitrite reduction rates. Since the ascorbic acid can likely provide electrons directly to the T2 site in addition to T1 site, any electrons the T2 site gains from ascorbic acid alone could reduce the $NO_2^-$. To probe the relative roles of the T1 and T2 Cu(II) sites, we performed single turnover reactions. As explained previously, the T1 copper site has an intense blue color that disappears when T1 Cu(II) is reduced to Cu(I) upon addition of 1 eq. of ascorbic acid. The blue color can be regenerated when the T1 copper is oxidized to Cu(II) with an oxidizing agent, such as nitrite in our experiments. This spectroscopic signature of the T1 Cu(II) site was used to monitor a single turnover reaction of our variants. It was hypothesized that if electron transfer occurred between the T1 and T2 sites, the blue

color of the T1 site would reappear following the addition of $NO_2^-$ to the reduced protein.

First, we tested the stability of our azurin mimics by repeating a single turnover experiment multiple times. In the experiment, 100 μM NiR3His-Az sample was prepared in 20 mM potassium phosphate buffer at pH 6.35, degassed with argon gas and taken into the glovebox following the procedure explained in Chapter 2. When the sample was equilibrated, 10 mM $NO_2^-$ was added to the 2 mL aliquot of the NiR3His-Az sample while stirring with the magnetic stir bar. The absorbance at 625 nm was at a maximum and did not change with the addition of $NO_2^-$, indicating no reaction with the blue colored, oxidized form of the enzyme. Then, 2 eq. of ascorbic acid was added to reduce the protein. The $A_{625\ nm}$ decreased, and with monitoring every 2 s, was observed to return quickly, indicating re-oxidation by the presence of $NO_2^-$. Upon recovery of $A_{625\ nm}$, 2 more equivalents of ascorbic acid were added and the $A_{625\ nm}$ peak was further monitored. This process was repeated multiple times over a 10 hour period (Fig. 3.12).

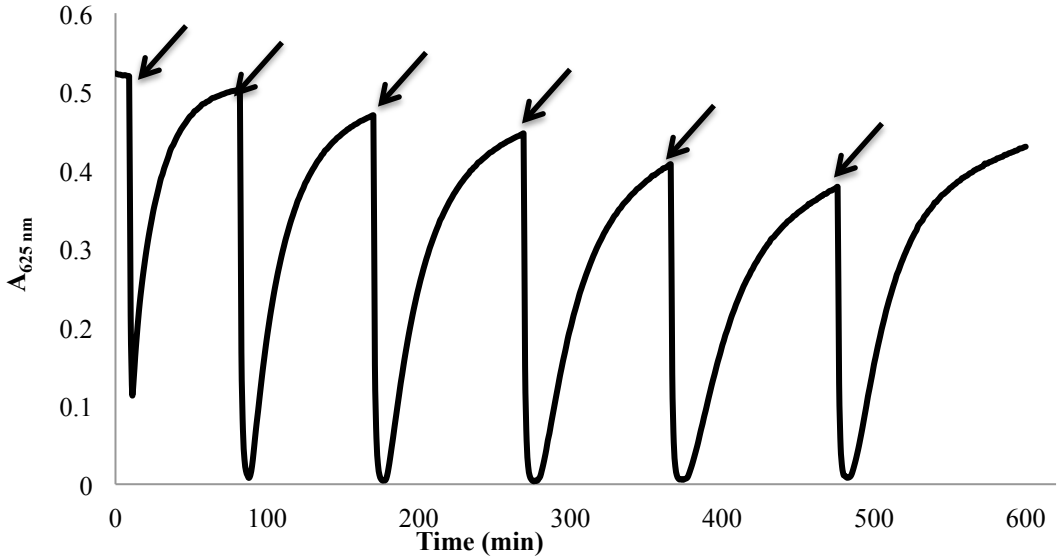


Fig. 3.12: Multiple turnovers of reduction of T1 Cu(II) to Cu(I) with 2 eq. ascorbic acid and re-oxidation back to Cu(II) in the presence of $NO_2^-$ by 100 μM NiR3His-Az. The arrows show the point where 2 eq. ascorbic acid was added.

The multiple turnover cycles and the full recovery of T1 Cu(II), confirms the catalytic nature of our azurin variants. This experiment also demonstrated the robust nature of the NiR-mimic catalysts. There was minimal change in recovery of blue color upon subsequent turnovers, as well as a full recovery of the azurin solution's blue color. This indicated that the protein was not readily denatured under these conditions and that it was capable of catalyzing multiple turnovers.

### 3.2.2 Rates of reduction of first generation variants:

To study the reduction behavior of the azurin variants, and the dependence of reduction rates with the concentration of ascorbic acid was monitored. The loss of blue color, or $A_{625\ nm}$, of azurin variants upon addition of varying ascorbic acid concentrations was monitored with time. The reduction of NiR3His-Az with 0.5 mM ascorbic acid is shown in Figure 3.13a, and the first order fit to the reduction, with respect to azurin, is shown in Figure 3.13b as a representative example of all azurin variants.

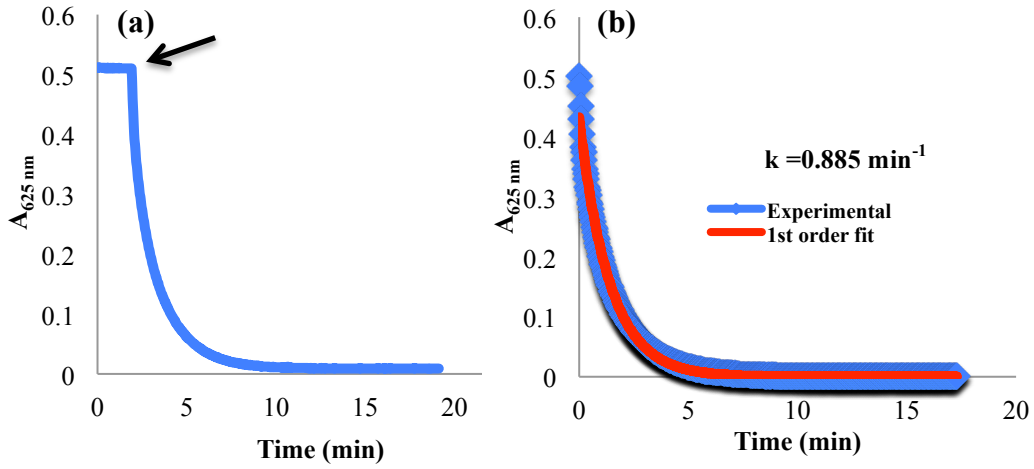


Fig. 3.13: (a) Curve showing the reduction of 100 µM NiR3His-Az variant with 0.5 mM ascorbic acid. Arrow indicates the point where ascorbic acid was added (b) Determination of first order rate constant for the reduction of 100 µM NiR3His-Az with 0.5 mM ascorbic acid (blue) with 1st order fit curve in red.

The reduction by the reaction of ascorbic acid with azurin was found to be the first order with respect to azurin, because, with excess ascorbic acid and limiting azurin concentrations, the reduction curves were best fit with a first order exponential function (Figure 3.13b and Eq. 3.4). This first order equation was derived from the chemical reaction (Eq. 3.2) and its corresponding rate law (Eq. 3.3a). Under excess ascorbate and limiting azurin concentration conditions, it can be assumed that the ascorbate concentration is essentially constant and therefore a new rate constant k' (Eq. 3.3c) is defined. The resulting rate law (Eq. 3.3b) can be integrated to give the exponential function (Eq. 3.4):

$$\mathbf{Az\ (T1Cu^{2+}) + \tfrac{1}{2}\ Asc \rightarrow\ Az\ (T1Cu^{+}) + \tfrac{1}{2}\ Asc^{+}} \qquad \mathbf{(Eq.\ 3.2)}$$

$$\mathbf{Rate = k[Az][Asc]^{1/2}} \qquad \mathbf{(Eq\ 3.3a)}$$

$$\mathbf{= k'[Az]} \qquad \mathbf{(Eq.\ 3.3b)}$$

Where,

$$\mathbf{k' = k[Asc]^{1/2}} \qquad \mathbf{(Eq.\ 3.3c)}$$

$$\mathbf{[Az] = [Az]_o * e^{-k't}} \qquad \mathbf{(Eq.\ 3.4)}$$

The resulting rate constants (k') derived from the fits of Eq. 3.4 to the reduction curves (Fig 3.13b) were used to find the order of reaction with respect to ascorbic acid. The (k')'s were plotted against the square root of the ascorbic acid concentrations ranging from 0.1 mM to 1 mM according to Eq. 3.3c and shown in Fig. 3.14. A linear fit of the (k')'s with square root of ascorbic acid concentration confirmed the half-order reaction of azurin with respect to ascorbic acid. The rate constant k, (in Eq. 3.3a and 3.3c) for the

overall reaction of first generation azurin variants with ascorbic acid was determined by finding the slope of the linear fit (Fig. 3. 14). The rate of the reaction between the azurin and the ascorbic acid was thus shown to be 1st order rate with respect to the azurin and the half-order with respect to the ascorbic acid.

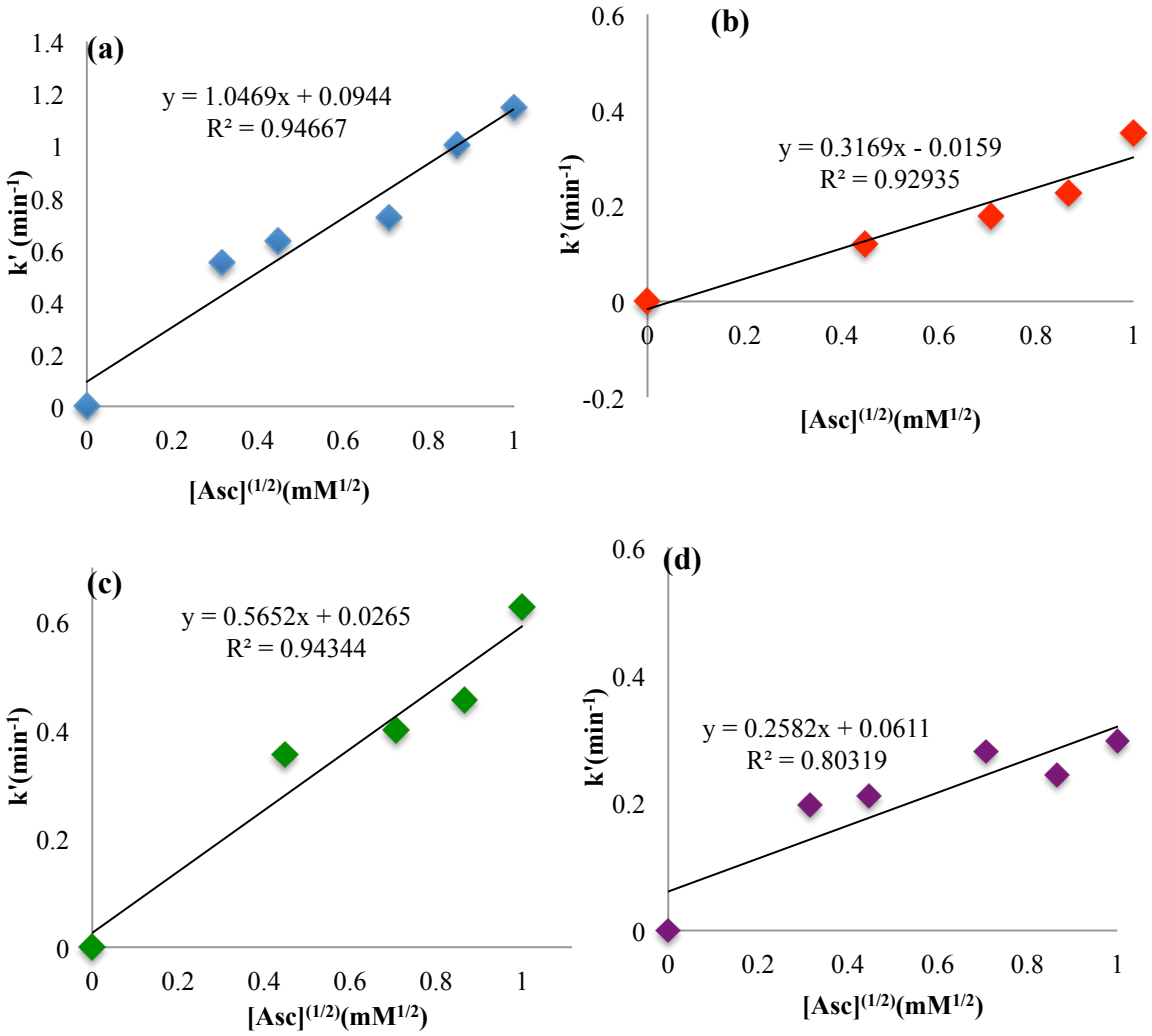


Fig. 3.14: Plots showing half-order reaction with respect to ascorbic acid for reduction of first generation variants. (a) NiR3His-Az (b) PHM3His-Az (c) NiR-Az (d) PHM-Az.

The overall rate constant (k) for the reaction of azurin with ascorbic acid was found to be highest for NiR3His-Az ($105\times10^{-2} \pm 6.7\times10^{-2}$ $min^{-1}mM^{-1/2}$-Az) followed by NiR-Az ($56\times10^{-2} \pm 3.6\times10^{-2}$ $min^{-1}mM^{-1/2}$-Az), whereas the rate constants, k, for PHM-

Az ($26x10^{-2}$ ± $3.6x10^{-2}$ $min^{-1}mM^{-1/2}$-Az) and PHM3His-Az ($32x10^{-2}$ ± $2.2x10^{-2}$ $min^{-1}mM^{-1/2}$-Az) were about the same. These rate constants for the reduction with ascorbic acid for the first generation variants are listed in Table 3.5 along with the absolute rates of reduction (see below) with 0.5 mM ascorbic acid.

Table 3.5: The absolute rates of reduction with 0.5 mM ascorbic acid and the rate constant, k, of ascorbic acid reduction for the first generation variants.

| **Variants** | **Absolute rates of reduction with 0.5 mM ascorbic acid (mM-Az $min^{-1}$)** | **Rate constant, k, for the reduction by ascorbic acid ($min^{-1}$ $mM^{-1/2}$-Asc)** |
|---|---|---|
| Wild Type-Az | $1.7x10^{-2}$ | $26x10^{-2}$ ± $2.1x10^{-2}$ |
| NiR3His-Az | $8.3x10^{-2}$ | $105x10^{-2}$ ± $6.7x10^{-2}$ |
| PHM3His-Az | $2.1x10^{-2}$ | $32x10^{-2}$ ± $2.2x10^{-2}$ |
| NiR-Az | $4.2x10^{-2}$ | $56x10^{-2}$ ± $3.6x10^{-2}$ |
| PHM-Az | $2.4x10^{-2}$ | $26x10^{-2}$ ± $3.6x10^{-2}$ |

To compare the absolute rates of reduction of the first generation variants, the reaction rate was determined by using the experimentally derived k values in Table 3.5, and plugging them into equation 3.3c (or actually the respective best-fit line equations in Figure 3.14), following by equation 3.3b, with an azurin concentration of 0.1 mM (100 μM). The absolute reduction rates of 100 μM of first generation variants with 0.5 mM ascorbic acid, in 20 mM potassium phosphate buffer at pH 6.35, are compared and summarized in Table 3.5.

All of the reduction rates for the variants with a surface T1 copper site are faster than WT azurin ($1.7x10^{-2}$ mM-Az $min^{-1}$, See chapter 4 for details). However, there is some variation among the variants themselves. The rate of reduction of NiR3His-Az with 0.5 mM ascorbic acid was $8.3x10^{-2}$ mM-Az $min^{-1}$ and was faster than the rest of the first generation variants. The initial rates of reduction by 0.5 mM ascorbic acid was found to be slower, but about the same for PHM3His-Az ($2.1x10^{-2}$ mM-Az $min^{-1}$) and PHM-Az

($2.4x10^{-2}$ mM-Az $min^{-1}$). The reduction rate for NiR-Az ($4.2x10^{-2}$ mM-Az $min^{-1}$) was intermediate between the other variants. The T1 sites of azurin are conserved in all of these variants. So, the varied rates of reduction for these 1st generation variants must be due to differences in reactivity of the T2 copper center and indicate that it possibly has a role in the reduction. Additionally, for the nitrite reduction assay using the Griess assay, the reduction of the azurin variants with ascorbic acid for done with 33 mM ascorbic acid. The estimated absolute reduction rate of NiR3His-Az using the linear fit from Figure 3.14(a) for the Griess assay (33 mM ascorbic acid), was $6.1x10^{-2}$. In our lab, it has been observed that the reduction rate of azurin remains constant for more than 10 mM ascorbic acid, hence using excess (33 mM) ascorbic acid is indeed a pseudo-first order.

In addition to the reduction rates of T1 site, reduction with 1 equivalent of ascorbic acid and the subsequent recovery of blue color (re-oxidation of T1 site) with the addition of $NO_2^-$ was monitored and the rate of re-oxidation were determined (see the next Section 3.2.3). The absolute rates of reduction with ascorbic acid, presented above, were more than 48 times faster than the re-oxidation rates of T1 Cu(I) to Cu(II) for our variants (see next Section 3.2.3, and Section 3.2.4 below) suggesting that the reduction of T1 site is not rate limiting step.

**3.2.3 Single turnover re-oxidation of first generation azurin variants:**

To further study the T1 copper site and to confirm the re-oxidation seen in Figure 3.12 was indeed due to the presence of $NO_2^-$ and not due to any other oxidizing agents, the NiR3His-Az was reduced first with 1 eq. of ascorbic acid. Since each ascorbic acid molecule provides two electrons, addition of 1 eq. of ascorbic acid was required to

reduce both the T1 and T2 copper sites in 1 eq. of azurin variant. Once the protein was reduced and remained stably reduced in the glovebox for ~15 minutes, the substrate $NO_2^-$ was added in concentrations ranging from 1-150 mM. With the addition of $NO_2^-$, the $A_{625\ nm}$ peak immediately began recovering (Fig. 3.15). Griess test of the reaction confirmed that nitrite was being consumed as the azurin re-oxidized.

The recovery of $A_{625\ nm}$ peak upon the addition of $NO_2^-$ demonstrated that the re-oxidation of T1 Cu(I) to the Cu(II) state is correlated with the reduction of $NO_2^-$ on the T2 center, since WT azurin with T1 copper alone did not re-oxidize or react with nitrite under these conditions. This lent support for the possibility of electron transfer between the T1 and T2 centers, since the rates of re-oxidation of the T1 copper center are comparable to the rates of nitrite reduction by the Griess assays (see below).

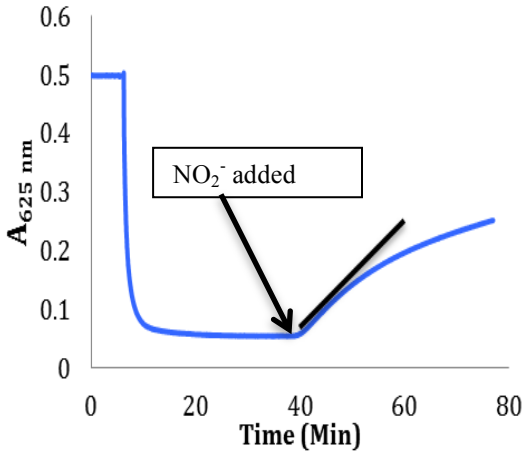


Fig. 3.15: Single turnover of reduction of T1 Cu(II) of NiR3His-Az with 1 eq. of ascorbic acid and re-oxidation with 5 mM $NO_2^-$ added at 40th minute.

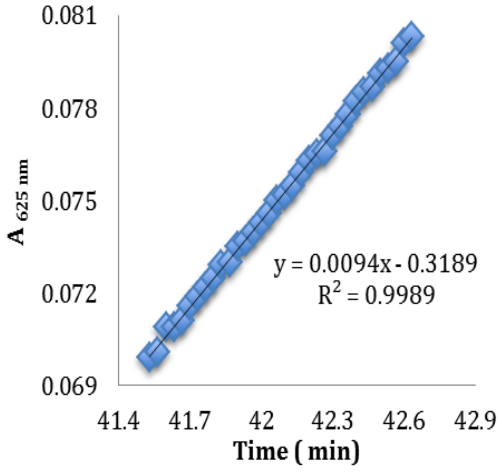


Fig. 3.16: Determination of re-oxidation rate of T1 Cu(I) to Cu(II) of NiR3His-Az with 5 mM $NO_2^-$ by finding the slope of the most linear part.

These re-oxidation assays were repeated for various nitrite concentrations with all of azurin variants. The re-oxidation curves were fit to a first-order exponential function (not shown here), demonstrating the reaction between the azurin variant and nitrite was

first order with respect to azurin. The rates of re-oxidation were determined, however, by measuring the initial slope of the linear part of the re-oxidation curve, typically the first 1-3 minutes (Fig. 3.16). These rates were plotted versus the corresponding nitrite concentrations to find the pseudo-1$^{st}$ order of the reaction between the $NO_2^-$ and the azurin variants and the corresponding rate constant (Fig 3.17). The order of the reaction between the azurin variant and nitrite, as well as the rate constant, were found for each of the first generation variants (NiR3His-Az, PHM3His-Az, NiR-Az and PHM-Az) as shown in Figures 3.17.

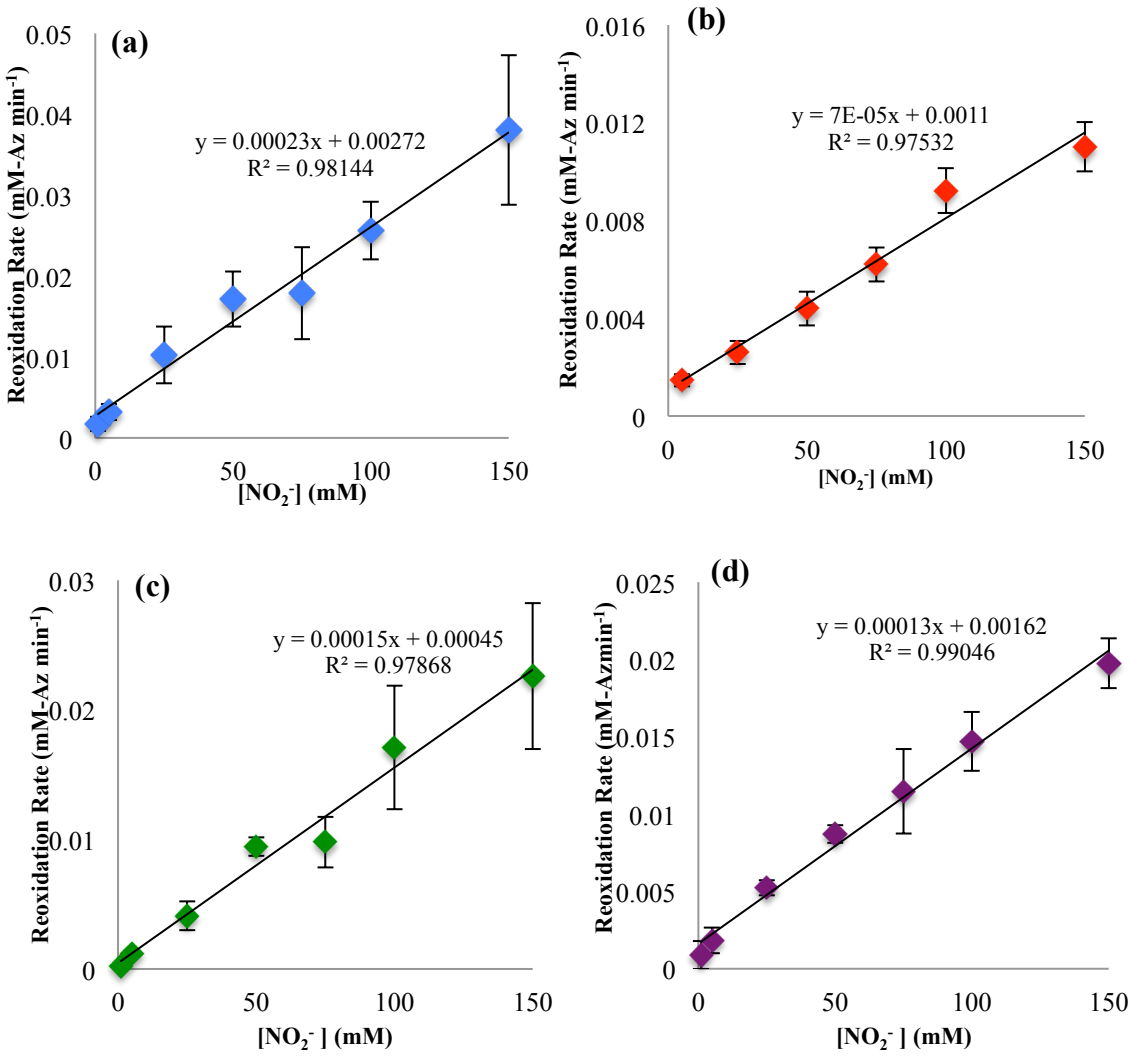


Fig. 3.17: pseudo-first order plots for T1 Cu(II) re-oxidation of first generation azurin variants (a) NiR3His-Az (b) PHM3His-Az (c) NiR-Az and (d) PHM-Az.

The order of the reaction was found to be the first order with respect to nitrite. The pseudo-first order rate constants for re-oxidation were determined and are summarized in Table 3.6.

Table 3.6: The rate constant of azurin variant T1 Cu(I) re-oxidation with $NO_2^-$ for the first generation variants.

| **Variants** | **pseudo-first order re-oxidation rate constant (mM-Az $min^{-1}$ $mM^{-1}$-$NO_2^-$ )** |
|---|---|
| NiR3His-Az | $23x10^{-5} \pm 6.8x10^{-5}$ |
| PHM3His-Az | $7x10^{-5} \pm 1.4x10^{-5}$ |
| NiR-Az | $15x10^{-5} \pm 3.9x10^{-5}$ |
| PHM-Az | $13x10^{-5} \pm 1.7x10^{-5}$ |

The reduction and re-oxidation of wild-type azurin was also attempted in the same way as the first generation variants. Wild type azurin was reduced completely with 0.5 eq. ascorbic acid at a slower rate ($1.7x10^{-2}$ mM-Az $min^{-1}$ for the reduction with 0.5 mM ascorbic acid in 20 mM phosphate buffer at pH 6.35) than the other variants. The re-oxidation of wild type azurin T1 Cu(I) to Cu(II) with $NO_2^-$ however was not seen (Figure not shown) as it lacks the T2 site. This result further suggests that $NO_2^-$ indeed interacts with the T2 site and uses the electron transferred from T1 to T2 site to be reduced to NO gas.

Among the first generation variants, NiR3His-Az ($23x10^{-5} \pm 6.8x10^{-5}$ mM-Az $min^{-1}mM^{-1}$-$NO_2^-$) had the highest pseudo-1$^{st}$ order rate constant for re-oxidation followed by NiR-Az ($15x10^{-5} \pm 3.9x10^{-5}$ mM-Az $min^{-1}$ $mM^{-1}$-$NO_2^-$), PHM-Az ($13x10^{-5} \pm 1.7x10^{-5}$ mM-Az $min^{-1}$ $mM^{-1}$-$NO_2^-$) and PHM3His-Az ($7x10^{-5} \pm 1.4x10^{-5}$ mM-Az $min^{-1}$ $mM^{-1}$-$NO_2^-$ ) indicating that NiR3His-Az has the highest dependence on increasing $NO_2^-$ concentration on the re-oxidation rates among the first generation variants, followed by

NiR-Az and PHM-Az whereas the PHM3His-Az shows the lowest dependence of increasing $NO_2^-$ concentration on the re-oxidation rates.

The absolute rates of re-oxidation (not the rate constant) of first generation variants were also compared to the initial nitrite reduction rates used for Michaelis-Menten kinetics, determined by Griess assay, and will be discussed below (see next Section 3.2.4).

**3.2.4 Rates of reduction and re-oxidation of the first generation variants, compared to Michaelis-Menten rates:**

First of all, the rate of reduction of the T1 Cu(II) to Cu(I) with 1 mM ascorbic acid in potassium phosphate buffer at pH 6.35 for NiR3His-Az variant was $120x10^{-3}$ mM-Az $min^{-1}$ about 73 times faster than the rate of re-oxidation with 1 mM $NO_2^-$ ($1.7x10^{-3}$ mM-Az $min^{-1}$). The rate of reduction with 1 mM ascorbic acid was at least 48 fold (for PHM-Az) faster than the re-oxidation rates with 1 mM $NO_2^-$ for all of the first generation variants. This suggested that the rate-limiting step is not the reduction of the enzyme, but rather the reaction with and reduction of nitrite.

If the reaction of nitrite with the azurin variants was rate limiting, then the rates of reduction of nitrite and the rates of re-oxidation of the azurin variants could be similar. We compared the absolute rates and found those rates obtained from the nitrite reduction assay using the Griess test to indeed be comparable to the rates found with the azurin variant re-oxidation assays with nitrite. For example, the initial rates of re-oxidation for NiR3His-Az (Fig. 3.17a) were $31x10^{-4} \pm 0.77x10^{-4}$ mM-Az $min^{-1}$ for 5 mM $NO_2^-$ and 100 μM NiR3His-Az and are similar to the rates from the nitrite reduction assay using Griess test (Fig 3.4a) ($38 x10^{-4} \pm 5.3x10^{-4}$ mM $min^{-1}$ for 5 mM $NO_2^-$ and 86 μM NiR3His-Az).

Similar to NiR3His-Az, the NiR-Az and PHM-Az variants also showed similar Griess assay rates and re-oxidation rates. For example, the Griess assay rates for 5 mM $NO_2^-$ for NiR-Az (Fig. 3.4c) was $16x10^{-4} \pm 6.7x10^{-4}$ mM-$NO_2^-$ $min^{-1}$ and the re-oxidation rate for same nitrite concentration (Fig. 3.17c) was $11x10^{-4} \pm 2.4x10^{-4}$ mM-Az $min^{-1}$ whereas the Griess assay rates for 5 mM $NO_2^-$ for PHM-Az (Fig 3.4d) was $23x10^{-4} \pm 6.6x10^{-4}$ mM-$NO_2^-$ $min^{-1}$ whereas the re-oxidation rate for same nitrite concentration (Fig 3.17d) was $18x10^{-4} \pm 8.3x10^{-4}$ mM-Az $min^{-1}$. The Griess assay and the re-oxidation rates were comparable to each other within the errors. The similarity between the Griess assay rates and the re-oxidation assay rates was consistent for all of the 1st generation variants except for the PHM3His-Az variant. The PHM3His-Az showed smaller re-oxidation rates than the Griess assay rates. For example, the Griess assay rate for 5 mM $NO_2^-$ for PHM3His-Az (Fig. 3.4b) was $33x10^{-4} \pm 8.9x10^{-4}$ mM-$NO_2^-$ $min^{-1}$ whereas the re-oxidation rate for the same nitrite concentration (Fig. 3.17b) was $14\ x10^{-4} \pm 3.5x10^{-4}$ mM-Az $min^{-1}$; about 2 times smaller than the Griess assay rate.

The relative rates of the 4 first generation variants were mostly consistent between the Griess assays and the re-oxidation assays. Based on Griess assay results, the nitrite reduction rates for NiR3His-Az and PHM3His-Az variants were similar and faster than those of NiR-Az and PHM-Az (Table 3.1). The same trend is seen in the re-oxidation rates, with the exception that PHM3His-Az has a smaller rate. A possible explanation could be that the rate of electron transfer from T1 to T2 copper sites in PHM3His-Az variant is slower than the other variants causing the slow re-oxidation of T1 Cu(I) to Cu(II).

The absolute nitrite reduction rates obtained from the Griess assays compared to the re-oxidation rates are comparable at low nitrite concentrations, but they deviate at high substrate concentrations. The re-oxidation rates show a linear relationship with the increasing $NO_2^-$ concentrations whereas the rates of $NO_2^-$ reduction with Griess assay are asymptotic and level off at the higher $NO_2^-$ concentrations. This difference in the trend is well known because the Michealis-Menten kinetics were obtained under conditions of multiple turnovers of $NO_2^-$ in the presence of excess ascorbic acid with only catalytic amounts of the azurin variants. The $NO_2^-$ reduction rates therefore level off at increasing substrate ($NO_2^-$) concentration approaching the maximum velocity ($V_{max}$), due to the catalytic behavior of the azurin variants that follow the Michaelis-Menten kinetics. On the other hand, the re-oxidation of azurin is a non-catalytic process with a single turnover of reduction of $NO_2^-$ by the reduced azurin variants The rate is determined by finding the initial slope and single turnover curve hence shows a linear relationship with increasing $NO_2^-$ concentration due to the reaction between nitrite and azurin variants.

The similarity between the nitrite reduction rates obtained by the Griess assay and the re-oxidation rates suggest the rate of electron transfer from T1 to nitrite is comparable to the rate of reduction of $NO_2^-$ at T2 site. This supports the hypothesis that electrons are transferred from the T1 to the T2 copper sites during catalysis.

## 3.3 Rates of reduction and re-oxidation of NiR3His-Az second generation variants:

### 3.3.1 Rates of reduction of second generation single mutant variants:

The orders of reaction and the rate constant (k) for the reduction of NiR3His-Az second generation single mutant variants with various concentrations of ascorbic acid was determined in the same way as the first generation variants as explained in Section

3.2.2. The order of reduction of second generation single mutant variants was found to be first-order with respect to azurin (fits not shown) and half-order with respect to ascorbic acid (Fig. 3.18), which is same as the first generation variants. The overall rate constants (k) for the reduction of NiR3His-Az second generation single mutant variants was determined by plotting the rate constants (k') from the first order fit against the square root of corresponding ascorbic acid concentrations (Fig. 3.18). These NiR3His-Az 2nd generation single mutant variants reduction rate constants are summarized in Table 3.7 along with their absolute rates of reduction, as calculated in Section 3.2.2.

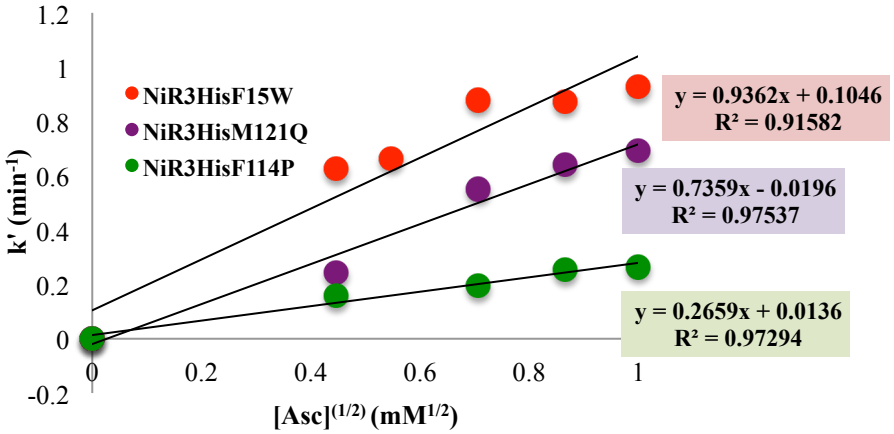


Fig. 3.18: Plots showing half order reaction with respect to ascorbic acid for reduction of NiR3His-Az second generation single mutant variants.

Table 3.7: The absolute rates of reduction and the rate constants (k) of ascorbic acid reduction for the NiR3His-Az second generation single mutant variants.

| Variants | Absolute rate of reduction with 0.5 mM ascorbic acid (mM-Az $min^{-1}$) | Rate constant, k, for the reduction by ascorbic acid ($min^{-1}$ $mM^{-1/2}$-Asc) |
|---|---|---|
| NiR3His-Az | $8.3x10^{-2}$ | $105\ x10^{-2} \pm 6.7\ x10^{-2}$ |
| NiR3His-Phe15Trp | $8.6x10^{-2}$ | $93x10^{-2} \pm 6.9x10^{-2}$ |
| NiR3His-Phe114Pro | $2.0x10^{-2}$ | $28\ x10^{-2} \pm 1.2x10^{-2}$ |
| NiR3His-Met121Gln | $4.8x10^{-2}$ | $71x10^{-2} \pm 1.9\ x10^{-2}$ |
| NiR3His-Met121Leu | $207x10^{-2}$ | 28 *± 1.6 |

*The rate constant for the reduction of NiR3His-Met121Leu was determined by using the (k') for 0.025 mM to 0.125 mM ascorbic acid concentration only, as the reduction is faster than we can accurately detect at higher concentrations.

The rate constants for the reduction (k) were similar but slightly lower than that of the parent NiR3His-Azurin. The rate constant was highest for NiR3His-Met121Leu (27 $min^{-1}$ $mM^{-1/2}$-Asc) NiR3His-Phe15Trp ($93x10^{-2} \pm 6.9x10^{-2}$ $min^{-1}$ $mM^{-1/2}$-Asc), followed by NiR3His-Met121Gln ($71x10^{-2} \pm 1.9\ x10^{-2}$ $min^{-1}$ $mM^{-1/2}$-Asc) whereas NiR3His-Phe114Pro ($28\ x10^{-2} \pm 1.2x10^{-2}$ $min^{-1}$ $mM^{-1/2}$-Asc) had the lowest reduction rate constant among the NiR3His-Az 2nd generation single mutant variants.

The second generation mutations were originally hypothesized to have faster nitrite reduction kinetics, but this was not observed from the Griess assay results. The second generation single mutant variants were therefore studied in reduction assays with various ascorbic acid concentrations to compare the relative rate reduction between these mutants. The absolute rates of reduction upon the addition of 0.5 mM ascorbic acid to the 100 μM NiR3His-Phe15Trp, NiR3His-Phe114Pro, NiR3His-Met121Gln and NiR3His-Met121Leu (Figures not shown) variants, in the potassium phosphate buffer at pH 6.35, were determined in the same way as in Section 3.2.2. These absolute reduction rates were compared between the second generation single mutant variants of NiR3His-Az and summarized above in Table 3.7.

Among the second generation single mutant variants of NiR3His-Az, the NiR3His-Met121Leu variant had the fastest reduction followed by NiR3His-Phe15Trp and NiR3His-Met121Gln, whereas NiR3His-Phe114Pro had the slowest reduction rates (Table 3.7). The initial reduction rate of NiR3His Phe15Trp was about the same as the parent NiR3His-Az whereas the rate of reduction of the NiR3His-Met121Gln and NiR3His-Phe114Pro variants were slower than the NiR3His-Az variant in the potassium phosphate buffer at pH 6.35. The reduction of the NiR3His-Met121Leu variant with

the ascorbic acid however had a faster reduction. The absolute reduction rate of 100 μM NiR3His-Met121Leu variant with 0.5 mM ascorbic acid was $207x10^{-2}$ mM-Az $min^{-1}$ which is ~25 times faster than that of NiR3His-Az ($8.3x10^{-2}$ mM-Az $min^{-1}$) with 0.5 mM ascorbic acid. The absolute reduction rate of NiR3His-Phe114Pro was found to be $2.0x10^{-2}$ mM-Az $min^{-1}$; ~4 times slower than that of NiR3His-Az whereas the NiR3His-Met121Gln was $4.8x10^{-2}$ mM-Az $min^{-1}$; about half the rate of the NiR3His-Az. The reduction rate of NiR3His-Phe15Trp was $8.6x10^{-2}$ mM-Az $min^{-1}$ similar to that of NiR3His-Az under the conditions explained above.

Possible explanations for these trends in rates of reductions can be correlated with the relative reduction potentials of the T1 copper sites in the second generation variants. The NiR3His-Phe15Trp variant has a mutation that doesn't affect the reduction potential of T1 site and hence shows a similar reduction rate to that of NiR3His-Az. The NiR3His-Met121Gln and NiR3His-Phe114Pro mutations lower the reduction potential of the T1 site (see Chapter 1). This results in the slower observed rates of reduction than those of the first generation NiR3His-Az and also 2nd generation NiR3His-Phe15Trp variants as the electron affinity of T1 site decreases with the decrease in reduction potential due to M121Gln and Phe114Pro mutation. The NiR3His-Met121Leu variant has an increased reduction potential at the T1 site, thus causing an increase in the electron affinity of T1 site. This gave a faster reduction of T1 Cu(II) to Cu(I).

### 3.3.2 Re-oxidation rates of second generation variants of NiR3His-Az and NiR-Az:

The $NO_2^-$ re-oxidation assays were run with the second generation single mutant variants of NiR3His-Az and NiR-Az, as well as the double mutant variants of NiR3His-Az. As with the first generation variants, the NiR3His-Az and NiR-Az second

generation, single and double mutant variants re-oxidation assays show a 1st order rate with respect to the azurin (fits not shown here) and an overall pseudo-first order reaction. The pseudo-first order plots of the re-oxidation of T1 Cu(I) to Cu(II) for the single mutant variants of NiR3His-Az and NiR-Az were generated by plotting the initial re-oxidation rates vs the $NO_2^-$ concentrations as shown in Figures 3.19 and 3.20, respectively. The pseudo-first order plots for the re-oxidation of the second generation double mutant variants of NiR3His-Az variants were generated in the same way and are shown in Figure 3.21. Among the double mutant variants of NiR3His-Az, only NiR3His-Phe15Trp/Met121Gln variant showed the re-oxidation upon the addition of $NO_2^-$ (see discussion below).

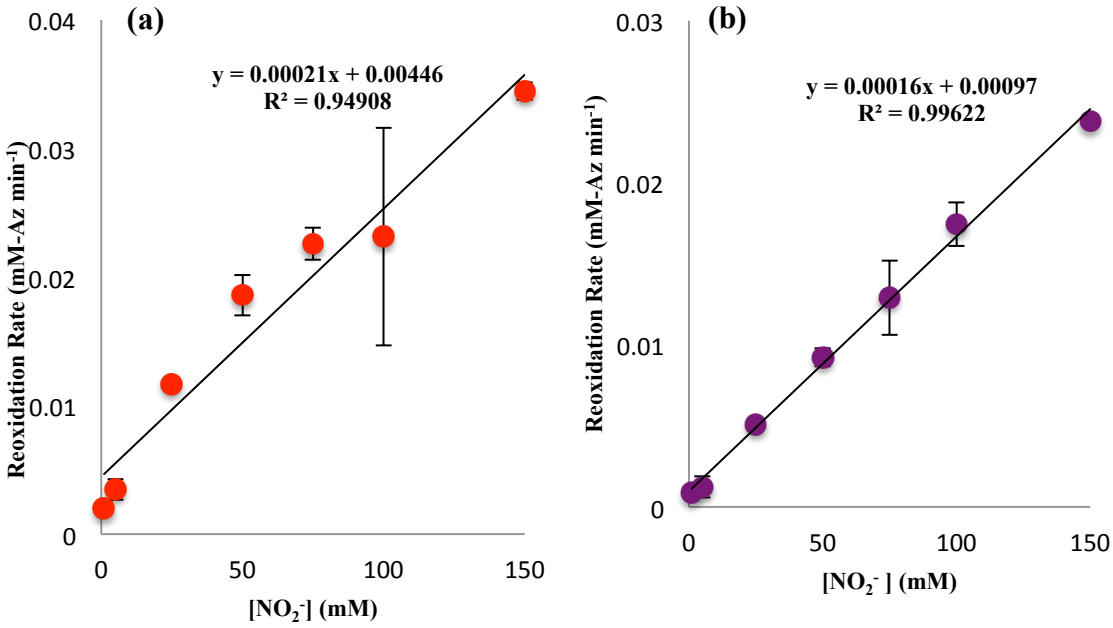


Fig. 3.19: pseudo-first order plots for re-oxidation of NiR3His-Az 2nd generation single mutant variants (a) NiR3HisF15W (b) NiR3HisM121Q. Re-oxidation was not seen in NiR3HisF114P variant.

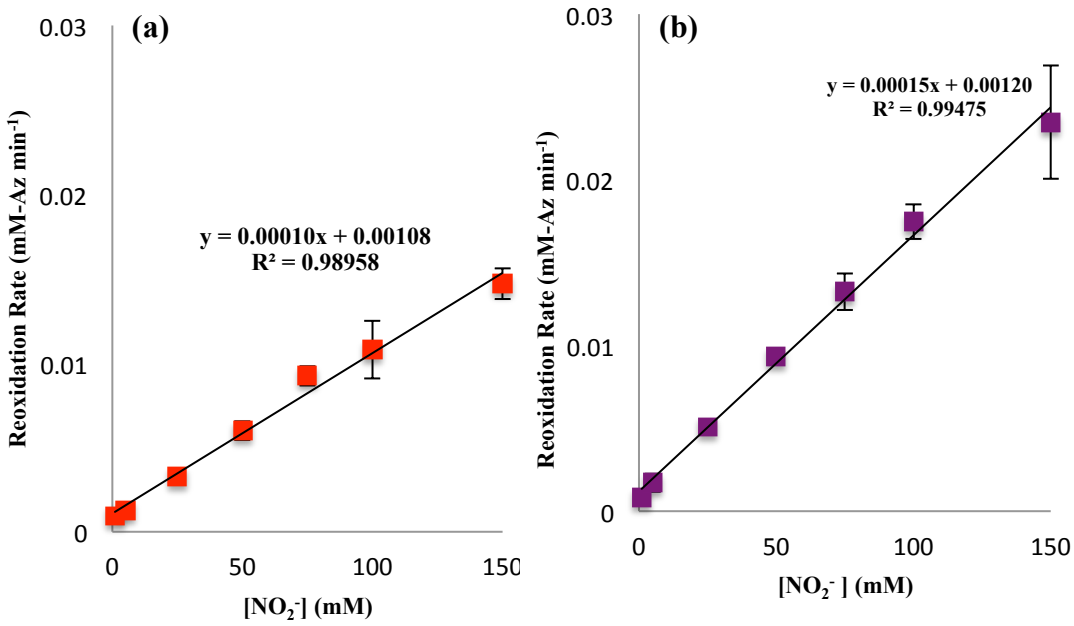


Fig. 3.20: pseudo-first order plots for re-oxidation of NiR-Az second generation single mutant variants (a) NiRF15W (b) NiR-M121Q. Re-oxidation was not seen in NiRF114P variant.

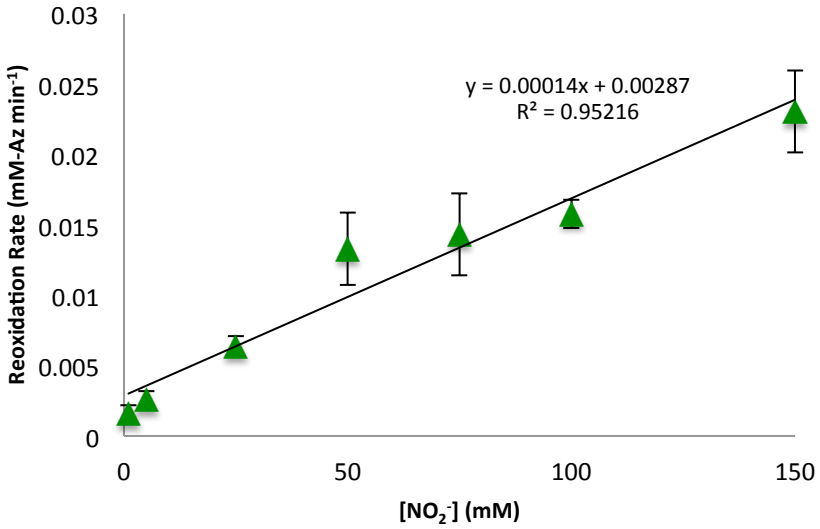


Fig. 3.21: pseudo-first order plot for re-oxidation of second generation double mutant NiR3HisF15W/M121Q variant. The re-oxidation was not observed in F15W/F114P and F114P/M121Q variants.

The rate constants for the re-oxidation of the T1 site of NiR3His-Az and NiR-Az 2nd generation single and double mutant azurin variants with $NO_2^-$ are shown in Table 3.8.

Table 3.8: The rate constants of the re-oxidation with $NO_2^-$ for the second generation variants of NiR3His-Az and NiR-Az.

| Variants | pseudo-first order re-oxidation rate constant (mM-Az $min^{-1}mM^{-1}$-$NO_2^-$) |
|---|---|
| NiR3His-Az | $23x10^{-5} \pm 6.8x10^{-5}$ |
| NiR3His-Phe15Trp | $21x10^{-5} \pm 2.3x10^{-5}$ |
| NiR3His-Met121Gln | $16x10^{-5} \pm 0.21x10^{-5}$ |
| NiR-Az | $15x10^{-5} \pm 3.9x10^{-5}$ |
| NiR-Phe15Trp | $10x10^{-5} \pm 1.0x10^{-5}$ |
| NiR-Met121Gln | $15x10^{-5} \pm 1.6x10^{-5}$ |
| NiR3His-Phe15Trp/Met121Gln | $14\ x10^{-5} \pm 0.57x10^{-5}$ |

Note: The re-oxidation was not seen in NiR3His-Phe114Pro, NiR3His-Phe15TrpPhe114Pro, NiR3His-Phe114ProMet121Gln and NiR-Phe114Pro variants (not shown in the table). The re-oxidation assays of Met121Leu variant is yet to be done.

Among the second generation single mutant variants of NiR3His-Az, the NiR3His-Phe15Trp ($21x10^{-5} \pm 2.3x10^{-5}$ mM-Az $min^{-1}$ $mM^{-1}$-$NO_2^-$**)** had the highest pseudo-1st order re-oxidation rate constant, which was very similar to the parent NiR3His-Az variant. The next fastest re-oxidation was by NiR3His-Met121Gln-Az ($16x10^{-5} \pm 0.21x10^{-5}$ mM-Az $min^{-1}$ $mM^{-1}$-$NO_2^-$**),** whereas the NiR3His-Phe15Trp/Met121Gln ($14\ x10^{-5} \pm 0.57x10^{-5}$ mM-Az $min^{-1}$ $mM^{-1}$-$NO_2^-$) variant shows slightly smaller pseudo-1st order re-oxidation rate constant than both NiR3His-Phe15Trp or NiR3His-Met121Gln variants.

The pseudo-1st order re-oxidation rate constant of fastest NiR3His-Phe15Trp variant was similar to that of NiR3His-Az. This is consistent with the Griess assay results where the second generation single mutant variants show about the same activity. The variants with Met121Gln mutation (i.e. NiR3His-Met121Gln and NiR3His-Phe15Trp/Met121Gln) variants show slightly smaller pseudo-1st order re-oxidation rate constants than the NiR3His-Az and NiR3His-Phe15Trp variants but the difference is not significant. This slight difference in the pseudo-1st order rate constant with Met121Gln

mutation could be caused by the removal of Met121-T1Cu(II) axial interaction, causing a slight decrease in the transfer of the electron between T1 and T2 sites.

For the NiR –Az series, the pseudo-1$^{st}$ order re-oxidation rate constants for the NiR-M121Gln ($15x10^{-5} \pm 1.6x10^{-5}$) was within the error of NiR-Phe15Trp ($10x10^{-5} \pm 1.0x10^{-5}$). Both of these variants show the similar pseudo-1$^{st}$ order rate constant to that of first generation NiR-Az variant ($15x10^{-5} \pm 3.9x10^{-5}$), further supporting findings from Griess assay that shows no improvement in the nitrite reduction activity of the 2$^{nd}$ generation single mutant variants.

Re-oxidation was not observed in the Phe114Pro variants of NiR3His-Az and NiR-Az possibly due to the very slow electron transfer rate between T1 and T2 sites in these Phe114Pro variants of NiR3His-Az and NiR-Az (see Section 3.3.3). It was observed that even in the absence of ascorbic acid, the blue color started to disappear in NiR3His-Phe114Pro variant as soon as $NO_2^-$ is added. In the Phe114Pro mutation, the removal of Phe114-Cys112 hydrogen bond that pushes the Cys112 towards the T1-copper, could as well create the binding pocket for the nitrite near the T1 site, causing further perturbation of T1 site geometry causing the loss of color when the $NO_2$ is added to oxidized Phe114Pro variant. This could potentially prevent the electron transfer to T2 site as well. The absolute re-oxidation rates (not the rate constant) of second generation variants were also compared to the absolute nitrite reduction rates obtained by Michaelis-Menten kinetics analysis by the Griess assay (see the next Section 3.3.3).

### 3.3.3 Rates of re-oxidation of the second generation variants, compared to Michaelis-Menten rates:

The re-oxidation rates of NiR3His-Az single and double mutant and NiR-Az

single mutant variants were compared with the respective Griess assay rates. We hypothesized again that these could be comparable since the rates of reduction by 1 mM ascorbic acid were over 48 times faster than the re-oxidation rates with 1 mM $NO_2^-$, making the reduction of nitrite rate-limiting. For the nitrite reduction with Griess test, 33 mM ascorbic acid was used. For 33 mM ascorbic acid, the estimated rate of reduction is more than 250 times faster than the 1mM $NO_2^-$ re-oxidation rates, as estimated using the equation of best fit from Fig. 3.14. This further supports that the rate-limiting step is not the reduction of the azurin variants. The variants with similar re-oxidation and Michaelis-Menten rates are listed in Table 3.9 whereas the ones that don't have the similar rates are listed in the Table 3.10 (see discussion below for detailed comparison).

Table 3.9: Comparison of the variants with similar absolute re-oxidation rates to Griess rates in phosphate buffer at pH 6.35.

| **Variants with similar re-oxidation rates to Griess assay rates** | **Griess assay rates for 5 mM $NO_2^-$ (mM-$NO_2^-$ $min^{-1}$)** | **Re-oxidation assay rates for 5 mM $NO_2^-$ (mM-Az $min^{-1}$)** |
|---|---|---|
| NiR3His-Az | $38x10^{-4} \pm 5.3x10^{-4}$ | $31x10^{-4} \pm 0.77x10^{-4}$ |
| NiR-Az | $16x10^{-4} \pm 6.7x10^{-4}$ | $11x10^{-4} \pm 2.4x10^{-4}$ |
| PHM-Az | $23x10^{-4} \pm 6.6x10^{-4}$ | $18x10^{-4} \pm 8.3x10^{-4}$ |
| NiR3His-Phe15Trp | $50x10^{-4} \pm 15x10^{-4}$ | $34x10^{-4} \pm 8.0x10^{-4}$ |
| NiR3His-Phe15Trp/Met121Gln | $49x10^{-4} \pm 26x10^{-4}$ | $26x10^{-4} \pm 6.2x10^{-4}$ |
| NiR-Phe15Trp | $25x10^{-4} \pm 13x10^{-4}$ | $13x10^{-4} \pm 8.0x10^{-4}$ |
| NiR-M121Gln | $24x10^{-4} \pm 6.9x10^{-4}$ | $17x10^{-4} \pm 1.0x10^{-4}$ |

Table 3.10: Comparison of the variants with different absolute re-oxidation rates to Griess rates in phosphate buffer at pH 6.35.

| **Variants with different re-oxidation rates to Griess assay rates** | **Griess assay rates for 5 mM $NO_2^-$ (mM-$NO_2^-$ $min^{-1}$)** | **Re-oxidation assay rates for 5 mM $NO_2^-$ (mM-Az $min^{-1}$)** |
|---|---|---|
| PHM3His-Az | $33x10^{-4} \pm 8.9x10^{-4}$ | $14x10^{-4} \pm 3.5x10^{-4}$ |
| NiR3His-Met121Gln | $24x10^{-4} \pm 6.7x10^{-4}$ | $12x10^{-4} \pm 6.7x10^{-4}$ |

As with the parent variants, the rates of re-oxidation were mostly similar and could be correlated to the rates of nitrite reduction. The re-oxidation rates of the NiR3His-Phe15Trp variant in potassium phosphate buffer at pH 6.35 with 5 mM $NO_2^-$ was similar ($34x10^{-4} \pm 8.0x10^{-4}$ mM-Az $min^{-1}$) to that of the Griess assay rates ($50x10^{-4} \pm 15x10^{-4}$ mM $NO_2^-$ $min^{-1}$) in potassium phosphate buffer at pH 6.35 with 5 mM $NO_2^-$. The re-oxidation rates of this NiR3His-Phe15Trp is also comparable to the re-oxidation rates of parent NiR3His-Az ($31x10^{-4} \pm 0.77x10^{-4}$ mM-Az $min^{-1}$, see Table 3.9). This is also consistent with the result from the Griess assay for which NiR3His-Phe15Trp showed no improvement in the turnover number over the first generation variants.

NiR3His-Met121Gln however showed slightly lower re-oxidation rates ($12x10^{-4} \pm 6.7x10^{-4}$ mM-Az $min^{-1}$ for 5 mM $NO_2^-$) as compared to the Griess rates ($24x10^{-4} \pm 6.7x10^{-4}$ mM $NO_2^-$ $min^{-1}$ for 5 mM $NO_2^-$). The re-oxidation rate of NiR3His-Met121Gln is also slightly smaller than that of NiR3His-Az (Table 3.10) further supporting the lack of improvement in the activities on the single mutant variants. The exact reason for the difference in the re-oxidation and Griess rates of NiR3His-Met121Gln variant is not yet understood but a possible explanation could be that electron transfer between T1 and T2 sites in the NiR3His-Met121Gln variant is slower than the rate of nitrite reduction.

Among the second generation double mutant variants of NiR3His-Az, only the Phe15Trp/Met121Gln variant showed the re-oxidation of T1 site. The re-oxidation rate of NiR3His-Phe15Trp/Met121Gln with 5 mM $NO_2^-$ was $26x10^{-4} \pm 6.2x10^{-4}$ mM-Az $min^{-1}$, and is within the error from the $NO_2^-$ reduction rate from the Griess assay. The rate was also comparable to the NiR3His-Az (Table 3.9).

For the NiR-Az variant, similarities between the Griess assay rates and the re-oxidation rates were also observed in the NiR-Phe15Trp variants. The Griess assay rates for 5 mM $NO_2^-$ was $25x10^{-4} \pm 13x10^{-4}$ mM-$NO_2^-$ $min^{-1}$ whereas the re-oxidation rates with 5 mM $NO_2^-$ was $13x10^{-4} \pm 8.0x10^{-4}$ mM-Az $min^{-1}$. These rates are within the error of each other. The Griess assay rate for NiR-Met121Gln ($24x10^{-4} \pm 6.9x10^{-4}$ mM $NO_2^-$ $min^{-1}$ for 5 mM $NO_2^-$) was also comparable to the re-oxidation rate ($17x10^{-4} \pm 1.0x10^{-4}$ mM-Az $min^{-1}$). The re-oxidation rates of NiR-Phe15Trp and NiR-Met121Gln are similar to that of the parent NiR-Az ($11x10^{-4} \pm 2.4x10^{-4}$ mM-Az $min^{-1}$, see Table 3.10) further confirming the similar activities of the first generation and 2nd generation single mutant variant of NiR-Az.

The re-oxidation of T1 site was not seen for any of the variants containing the Phe114Pro mutation. Therefore, the NiR3His-Phe114Pro, NiR3His-Phe15Trp/Phe114Pro, NiR3His-Phe114P/Met121Gln and NiR-Phe114Pro variants didn't have any recovery of blue color. It was observed that even in the absence of ascorbic acid, the blue color started to disappear in NiR3His-Phe114Pro variant as soon as $NO_2^-$ was added. The initial thought was that since the Phe114Pro mutation was intended to remove the hydrogen bond between the Phe114 residue and the Cys112 residue, the T1 Cu(II) could be unstable and fall out when $NO_2^-$ is added due to chelation of $NO_2^-$ by T1 Cu(II). However, the blue color recovered when the NiR3His-Phe114Pro variant sample that lost blue color with $NO_2^-$ addition was oxidized with oxygen outside the glovebox. In addition, the blue color didn't disappear when $NO_2^-$ was added to the other (NiR3His-Phe114/ProMet121Gln and NiR3His-Phe15Trp/Phe114Pro) variants suggesting that copper doesn't fall out of the T1 site. Although the blue color doesn't disappear when

only $NO_2^-$ is added the recovery of blue color with $NO_2^-$ was not observed on the typical timescales with the Phe114Pro variants. The exact reason why the re-oxidation of the T1 copper doesn't occur with $NO_2^-$ in Phe114Pro variants is not yet clear, but the re-oxidation with oxygen suggests that the re-oxidation is possible. Perhaps the weaker oxidizing agent ($NO_2^-$) doesn't have a high enough reduction potential to re-oxidize the T1 site. The Phe114Pro variant of NiR3His-Az decreases the reduction potential of T1 site similar to the Met121Gln variant of NiR3His-Az, thus shifting the equilibrium towards the T2 copper center or towards nitrite. In the Phe114Pro mutation, the removal of Phe114-Cys112 hydrogen bond that pushes the Cys112 towards the T1-copper, could as well create the binding pocket for the nitrite near the T1 site, causing further perturbation of T1 site geometry causing the loss of color when the $NO_2$ is added to oxidized Phe114Pro variant. This could potentially prevent the electron transfer to T2 site as well. It was seen that the re-oxidation rates of NiR3His-Met121Gln variant was slower than the Griess reaction rates. A similar mechanism might be taking place in the NiR3Hishe114Pro variant while decreasing the rate of electron transfer more than the NiR3His-Met121Gln variant.

**3.4: Summary Discussion:**

We have successfully designed and characterized working mimics of NiR using the protein azurin as a scaffold. As the wild type azurin shows minimal to no nitrite reduction, each of our 1st and 2nd generation variants show significant nitrite reduction activities and also show that electron transport takes place from T1 to T2 sites. Our mimic variants show a robust nature and stability that can perform multiple turnovers of nitrite reduction. In addition, the 2nd generation double mutant variants show

improvement in the activity over the 1st generation variants providing evidence that the nitrite reduction activities of these variants can be improved.

The improvement in the nitrite reduction activities for the second generation double mutant variants with Phe15Trp, as observed in the Michealis-Menten derived turnover numbers, was consistent with our hypothesis that a direct electron transport pathway between T1 and T2 sites, along with a decreased reduction potential of T1 site would improve activity. The lack of improvement in the single mutant activity was unexpected. As discussed previously in Section 3.3.3 and also in the Table 3.9 and 3.10, the re-oxidation rates among the second generation variants were fastest in the NiR3His-Phe15Trp variant followed by NiR3His-Met121Gln which re-confirmed the importance of the direct electron transfer pathway between T1 and T2 sites for the faster electron shuttling. Lowering the reduction potential of T1 site alone (in the Phe114Pro or Met121Gln single mutant variants) however doesn't seem to improve the electron transport or the nitrite reduction rates due to the lack of the electron transport pathway between T1 and T2 sites. The similarities between the nitrite reduction rates from Griess assay and the T1 site re-oxidation assays for most of the variants suggest that the nitrite reduction is the rate limiting step. The nitrite reduction could also be affected by the rate of electron transport between T1 and T2 sites, which our data suggest is either equal to or greater than the nitrite reduction rate, depending on the variant.

To understand the mechanism of nitrite reduction in these variants more clearly, the $NO_2^-$ reduction activities from Griess assays as well as the reduction and re-oxidation of T1 site of other variants need to be measured. Comparison of these $NO_2^-$ reduction activities along with the reduction and T1 re-oxidation assays with the single and

double mutant variants of NiR-Az, PHM-Az and PHM3His-Az could give more insight into the role that each mutation plays in the activities of nitrite reduction and re-oxidation of T1 site for the azurin variants. In addition, running EPR spectra of the samples, especially the ones that don't show re-oxidation (such as the variants containing Phe114Pro mutation) after reduction and attempted re-oxidation with $NO_2^-$, could give more insight into the presence as well the function of the T1 and T2 copper sites. The EPR spectra of these Phe114Pro variants could be used to find whether the T1 and T2 Cu(II) remain bound to protein or fall out upon the addition of $NO_2^-$, which could explain why these Phe114Pro variants don't show the re-oxidation. For these purposes, the nitrite reduction assays using the Griess assay along with reduction/re-oxidation assays and the ascorbic acid reduction assays of the second generation variants of PHM3His-Az, NiR-Az, PHM-Az are being done in our lab. Finding the activities of the $2^{nd}$ generation variants of these parent variants could be used to compare the results to the NiR3His-Az $2^{nd}$ generation variants to find the pattern in the mutations for different variants.

In addition, other factors that could affect the rate of nitrite reduction and give insight of the mechanism of our enzymes are being studied in our lab to understand the mechanism better. Recently, we are exploring the possibility of the bidirectional behavior of our variants that could also catalyze the reverse reaction of nitrite reduction (i.e., oxidation of NO to $NO_2^-$) to understand the mechanism of our variants better.

# Chapter 4: Silver(I) and mercury(II) displace Type 1 copper(II) in wild type azurin

## Prologue:

Chapter 1, 2 and 3 of this thesis were focused on the characterization of the engineered azurin variants and comparison of their nitrite reduction activities. While performing the initial reduction assays of wild type azurin with ascorbic acid, we noticed that the reduction rate of T1 copper is about 50x faster in the presence of 1 eq. extra of free Cu(II) than the wild type azurin with no extra Cu(II). This result led us to hypothesize that the reduction of free Cu(II) to Cu(I) takes place in the solution first upon the addition of ascorbic acid. The Cu(I) then rapidly displaces the T1 Cu(II) causing the loss of blue color (or drop of the absorbance peak at 625 nm). This hypothesis was further tested with the Ag(I) and Hg(II) exchange studies presented in this chapter. Written as a stand-alone chapter, some of the materials from Chapters 1.3, and 2.1-2.3 are repeated in sections of this chapter (sections 4.2, 4.3.1 and 4.3.2).

### 4.1: Summary:

Silver (Ag) and mercury (Hg) are well known antimicrobial agents because of their cytotoxic properties. Silver in particular has been used as a disinfectant in human healthcare since ancient times. Although mercury is not as commonly used in human healthcare, it acts as an antimicrobial due to its toxicity. Although silver and mercury are cytotoxic to microorganisms, the exact mechanism of cytotoxicity is not well known. *Pseudomonas aeruginosa* (P.a.) azurin is a mononuclear blue copper protein, containing a copper(II) ion (Cu(II)) binding site, called a Type 1 (T1) copper site. Although the T1 site is primarily a copper binding site, metal ions, such as Ag(I) or Hg(II), can displace the

redox active Cu(II) from the T1 site. In this study, we explore the active site copper ion exchanges with Ag(I) or Hg(II).

## 4.2: Introduction:

*Pseudomonas aeruginosa* (*P.a.)* azurin is a mononuclear blue copper protein in the cupredoxin family, containing a copper ion (Cu(II)) binding site. Amongst the different classes of copper binding sites known in biology, it belongs to the Type 1 (T1) copper binding protein family.[1] *P.a.* azurin has 128 amino acids that fold into the common "cupredoxin" or Greek-key motif composed of eight antiparallel β-strands in a barrel arrangement. The T1 copper binding site functions as the electron transfer site in azurin (Fig. 4.1).[2] The T1 center in azurin is supported by two histidines (His46 & His117) and one cysteine (Cys112) in a trigonal planar geometry. In addition, there are long-range axial interactions with methionine (Met121) and a backbone carbonyl oxygen (Gly45 CO) (Fig. 4.2).[6]

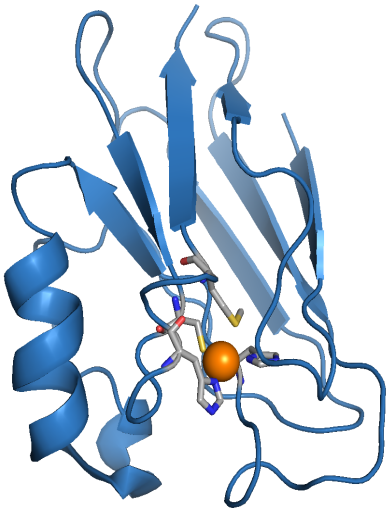

Fig. 4.1: Structure of P.a. azurin (PDB ID: 4AZU).

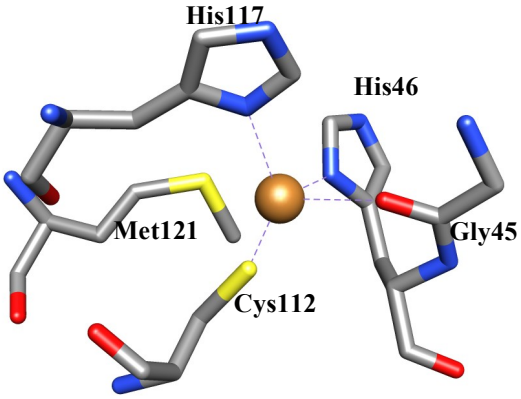


Fig. 4.2: T1 Cu(II) site of P.a. azurin, PDB ID: 4AZU.

Azurin is a well characterized "cupredoxin" family member.[1,4,8,11-13] It is a small, stable protein that can tolerate multiple mutations, which opens the door to its use as a robust mimic system. The oxidized Cu(II) form of azurin has an intense blue color that absorbs at 625 nm due to the charge transfer between $S(\pi)_{Cys}$ and Cu $d_{(x2-y2)}$.[14,15]

One commonly studied aspect of azurin is its electron transfer properties. Azurin is an oxidoreductase protein and is thought to be a redox partner of another copper containing enzyme, nitrite reductase (NiR). In bacteria, *P.a.* azurin is believed to act as an electron shuttle in the denitrification pathway.[1,3] Electron transport proteins play key roles in the electron transport chain, photosynthesis, and many other important biological processes. In addition to electron transfer, *P.a.* azurin has been used extensively for non-native applications, such as a mimic scaffold protein or an anti-cancer agent. Azurin was used as a scaffold in which to engineer artificial amino acids as well as di-copper sites.[11] Azurin was also found to be cytotoxic, blocking breast cancer cell proliferation by inducing apoptosis.[8]

Azurin is believed to be primarily a copper protein in native systems, however, it is also known to bind other metal ions *in vitro*; silver(I), mercury(II), iron(III), zinc(II), nickel(II) and cobalt (II) are reported examples.[10,16-19] Silver (Ag(I)) and mercury (Hg(II)), in particular, have high affinity towards azurin.[10] Ag(I) is not believed to be biologically essential, and there are no known naturally occurring silver binding proteins. Ag(I) is known to be cytotoxic, as is Hg(II). Ag(I) in particular has been known to have antimicrobial activity, commonly used against bacteria, mold, and yeast.[5,7] Silver has been used as a disinfectant in human healthcare and medicine since ancient times. Use of silver nitrate, silver sulfadiazine (SSD) and other silver containing antibiotics for

penicillin and ampicillin resistant bacterial strains, such as *P. aeruginosa* and *S. aereus,* has led to the development of medical grade and bio-available silver based antibiotics.[9] Although, not as commonly used as an antimicrobial due to its high toxicity, Hg(II) is also used as a preservative, such as thiomersal, in human vaccines.[9]

Although the antimicrobial properties of silver salts are well known, the exact mechanism of how silver acts as an antimicrobial agent has been debated.[4] One of the mechanisms suggested is the displacement of metal ions by Ag(I) ions from various proteins. We were interested in studying the activity of Ag(I) and Hg(II) in the displacement of Cu(II) from azurin, to test the feasibility of this hypothesis for silver and mercury toxicity in microorganisms. In this chapter, recent results on metal ion exchange with T1 Cu(II) will be presented.

## 4.3: Materials and Methods:

In this section, the methods for the study of metal exchange properties of T1 site of azurin with Ag(I), Hg(II), Cu(I) and Cu(II) and the results will be discussed. All chemicals used in this work were of reagent grade or higher and used without further purification. All glassware and media used in cell growths were sterilized by autoclaving.

### 4.3.1: Azurin Purification:

The *P.a.* gene for the production of azurin was coded in a pET9a plasmid and the plasmid was transformed into BL21* *E. coli*. The pET9a plasmid also contains a kanamycin resistance gene, hence the BL21* *E. coli* cells were grown on LB-agar plates in the presence of 0.05 g/L kanamycin, which allows the selective growth of the wild type azurin. Once the *E. coli* cells grew in the LB-kanamycin plates, a sterile culture

tube was prepared with ~8 mL volume of LB broth. To the LB broth, ~2 μL of 0.05 g/L kanamycin stock solution was added per mL of LB broth in the sterile culture tube. The cells were incubated at 37 °C for ~6 hours. Four liters of Bacto™tryptone/yeast extract media known as 2xYT was prepared by dissolving 16 g of Bacto™ tryptone, 10 g of yeast extract and 5 g of NaCl per liter of water. All media were sterilized by autoclaving.

About 1 mL each of cells grown in LB-broth was transferred into five flasks containing 0.8 L each of 2xYT media. About 200 mg of solid kanamycin sulfate was dissolved in 5 mL of water and 1 mL each of the kanamycin solution was added to each flask containing the 2xYT media and the cells. The cells were then incubated in a shaker at 30 °C for ~12 hours. After 12 hours of incubation, the gene for the production of azurin was overexpressed for ~3 hours with 3 mM isopropyl-beta-D-thiogalactopyranoside (IPTG). IPTG activates the T7 promoter region of bacteriophage T7 RNA polymerase in the BL21* *E. coli* displacing the repressor on the *lac* operon. When IPTG is added, it results in the overexpression of T7 polymerase, which is able transcribe the pET9a plasmid DNA into RNA. The RNA for azurin is in turn translated to make azurin protein.

To extract the azurin protein from BL21* *E. coli,* the pellets were isolated from the 2xYT media by centrifuging the cells for ~10 minutes at 7000 rpm and 4 °C in Avanti® J-E centrifuge. The cell pellets were then suspended in the 20% sucrose, 1 mM EDTA, 30 mM Tris solution at pH 8.0. The cells were lysed using osmotic shock with pure Millipore water at 4 °C and the azurin was extracted. The protein was purified using a SP-sepharose cation exchange column in 50 mM ammonium acetate buffer at pH 4.10 and Q-sepharose anion exchange column chromatography, in 50 mM ammonium

acetate buffer at pH 6.35. Typical purification yields were about 30 mg azurin per liter of media. The resulting protein was concentrated using Amicon® Millipore stirred ultrafiltration cells. The Amicon® concentrates the protein using a filter membrane, and gas pressure (nitrogen gas in our lab) to filter the buffer while retaining azurin in the cell.

**4.3.2: UV-Vis and EPR sample preparation:**

The concentration of expressed azurin was determined by slowly titrating $CuSO_4$ solution to the apo-protein until the blue color of azurin, which absorbs at $A_{625\ nm}$, reached a maximum. The molar absorptivity of wild type azurin (5000 $M^{-1}cm^{-1}$) was used to determine the final concentration. Once the concentration of protein was determined, holo-azurin was prepared by slowly titrating 5 eq. of $CuSO_4$ with purified apo-azurin with stirring in ice (4 °C). The sample was left on ice for ~20 minutes to ensure the complete equilibration of Cu(II) to the T1 site. As there is only one Cu(II) binding site in wild type azurin, the excess 4 eq. of $CuSO_4$ was removed by running 1 mL aliquots of the samples through the PD-10 size-exclusion desalting column (Sephadex-25 columns from GE Healthcare Life sciences) and collection of the protein fraction. These PD-10 columns were also used to accomplish final buffer exchange to 50 mM ionic strength ammonium acetate buffer (pH 5.1). The sample stocks such prepared were diluted to ~200 μM and UV-Vis absorption spectra were obtained using a Shimadzu UV2401 PC UV-Vis spectrophotometer.

EPR samples were prepared in 50 mM ammonium acetate buffer (pH 5.1) using the stock with the concentration of 500-700 μM. The EPR samples were prepared by slowly titrating 5 eq. of $CuSO_4$ to the apo azurin, stirring over ice, and left to equilibrate

for ~30 minutes. The excess $CuSO_4$ was removed using PD-10 columns as explained above for UV-Vis samples.

EPR spectra were obtained using a Varian E-Line Century Series X-band EPR spectrometer in a liquid nitrogen finger dewar at -196 °C. The microwave frequency was typically 9.27 GHz with a center field of 3000 gauss. A field width of 1600 gauss was scanned over 60 seconds with 2 scans averaged per spectra. A wait time of 10 seconds was set between scans with the modulation amplitude set to 5 Gauss and a time constant of 0.032. Fifteen spectra were obtained for each variant and averaged to yield the final spectrum. Since azurin has T1 Cu(II) site only, EPR spectra showed the signal for T1 Cu(II) only, with no free copper apparent.

Further, the reduction of azurin with ascorbic acid, and the dependence of ascorbic concentration on the rate of reduction of wild type azurin, was studied. The methods for the ascorbic acid reduction assays will be covered in section 4.3.5 and the results will be discussed in section 4.4.2. In addition to the reduction assays, the T1 metal ion exchange properties of azurin were also studied by preparing holo-azurin samples with of either Cu(II), Ag(I) or Hg(II) at the T1 site, and then displacing this T1 metal ion with 1 to 5 eq. of either Ag(I), Hg(II) or Cu(I). The detailed methods of these experiments will be discussed in the section 4.3.5 and the results will be presented in 4.4.2 of this Chapter.

**4.3.3: T1 Cu(II) sample preparation for T1 Cu(II) displacement assays:**

The protein samples were prepared with T1 Cu(II) in potassium phosphate buffer at pH 6.35 to test the displacement of T1 Cu(II) by other metal ions such as Ag(I), Hg(II) and Cu(I). The holo-azurin sample with T1 Cu(II) was prepared by slowly titrating 1

eq. $CuSO_4$ solution with apo-azurin with ~20 min equilibration over ice at 4 °C. Any extra free $CuSO_4$ was removed by passing holo-azurin through PD-10 desalting columns and collecting the blue fraction. These PD-10 columns were also used to accomplish final buffer exchange to 20 mM ionic strength potassium phosphate buffer at pH 6.35. The concentration of T1 Cu(II) holo-azurin stock was determined and azurin stock was diluted to 100 μM to be used for T1 Cu(II) displacement assays (see sections 4.3.5 and 4.4.2) and also for the Electrospray ionization-Mass spectrometry (ESI-MS) experiments (see sections 4.3.6 and 4.4.3)

**4.3.4: T1 Ag(I) and Hg(II) sample preparation for T1 metal ion displacement assays:**

The samples with T1 Ag(I) and T1 Hg(II) were prepared to study the T1 metal ion displacement by Cu(I) (sections 4.3.5 and 4.4.2) and also for the ESI-MS experiments (sections 4.3.6 and 4.4.3). To prepare the azurin sample with T1 Ag(I), the concentration of apo protein stock was determined as described in section 4.3.2. Once the concentration was determined, the Ag(I) substituted azurin was prepared by slowly titrating 5 eq. of freshly prepared silver nitrate ($AgNO_3$) solution with apo-azurin, followed by equilibration for ~30 mins over ice at 4 °C. The $A_{280\ nm}$ was measured for the known protein concentration. To remove any extra free Ag(I), the Ag(I) bound protein was passed through the PD-10 desalting columns and collected in 300 μL fractions. The fractions containing an $A_{280\ nm}$ peak were collected. The the concentration of the protein after removal of excess Ag(I) was estimated based on the ratio of the $A_{280\ nm}$ peak before and after the removal of excess Ag(I). The assay sample was prepared with a final concentration of 100 μM.

The 100 μM azurin sample with T1 Hg(II) was prepared with mercuric chloride ($HgCl_2$) using the same procedure as T1 Ag(I) preparation.

**4.3.5: T1 reduction and Metal ion exchange assay Methods:**

The azurin samples prepared as explained in sections 4.3.3 and 4.3.4 were degassed in a 50 mL falcon tube by bubbling argon gas for 15-20 minutes to minimize dissolved oxygen before bringing them into the glovebox. The samples were incubated at the room temperature in the glovebox for ~20 minutes to equilibrate with the anaerobic conditions.

To study the reaction of azurin variants with ascorbic acid, the initial reduction rate and the dependence of the rate of reduction with various ascorbic acid concentrations were determined. The rate and order of the reaction between ascorbic acid and azurin was analyzed. In a 3 mL cuvette, a 2 mL aliquot of the azurin with T1 Cu(II) was stirred. To the 100 μM azurin sample in 20 mM potassium phosphate buffer at pH 6.35, various concentrations of ascorbic acid (0.05 mM, 0.1 mM, 0.2 mM, 0.5 mM, 0.75 mM and 1 mM, i.e., 0.5 to 10 eq.) were added. The rate of reduction was monitored every 2 seconds during the entire assay by monitoring the rate of loss of the $A_{625\ nm}$ peak with a Genesys-10S UV-Vis spectrophotometer. These initial rates of reduction were plotted against the corresponding ascorbic acid concentrations to find the order of the reaction and the rate constant.

To study the displacement of T1 Cu(II) by Ag(I), 1 to 5 eq. of a freshly prepared $AgNO_3$ solution was added to the holo-Cu(II) azurin sample. The $A_{625\ nm}$ peak was monitored to see if any displacement of T1 Cu(II) occurred. Similarly T1 Cu(II) was displaced from azurin by adding 1 to 5 eq. of $HgCl_2$. The initial rates of Cu(II)

displacement were determined by finding the slope of most linear part of the disappearance of $A_{625\ nm}$.

The displacement of T1 Cu(II), Ag(I) or Hg(II) with 1 to 5 eq. Cu(I) was also tested in the glovebox. Cu(I) was prepared by pre-reducing $CuCl_2$ with 0.5 eq. ascorbic acid, followed by addition to an azurin sample with the appropriate metal ion in T1 site. Since azurin with T1 Ag(I) or Hg(II) doesn't have any color, the rate of displacement couldn't be determined. But, to test the displacement of Ag(I) or Hg(II) with Cu(I), samples were oxidized with oxygen and assayed for blue Cu(II)-azurin. Therefore, the samples were stirred and equilibrated for ~30 min after the addition of Cu(I) and were run through PD-10 columns to remove excess Cu(I) and displaced Ag(I) or Hg(II). The sample was then oxidized with atmospheric oxygen outside the glovebox to see if any blue color appeared. The appearance of blue color confirmed the displacement of T1 Ag(I) or Hg(II) with Cu(I) since the azurin only turns blue when Cu(I) at T1 site oxidizes to Cu(II).

**4.3.6: Electrospray Ionization - Mass Spectrometry (ESI-MS):**

ESI-MS was used to study the metal binding and the displacement of T1 Cu(II), with Ag(I), Hg(II) or Cu(I) as well as the displacement of Ag(I) and Hg(II) with Cu(I). ESI-MS samples were prepared by adding 5 eq. of the intended metal ion to the apo-azurin. Excess metal ions were removed using PD-10 desalting columns in 50 mM ammonium acetate buffer at pH 5.1. The concentration of T1 Cu(II) sample after buffer exchange was determined by measuring $A_{625\ nm}$ and using the molar absorptivity of azurin (5000 $cm^{-1}\,M^{-1}$) whereas the concentrations of T1 Ag(I) and Hg(II) samples were determined using the ratio of $A_{280\ nm}$ peak before and after dilution as explained above

in section 4.3.4. The samples with final concentration of 300-500 μM were prepared. T1 metal displacement assays were carried out in the glovebox as discussed in section 4.3.5. These assay samples, from section 4.3.5 were analyzed using ESI-MS to study the metal loading and metal exchange on T1 site.

The mass spectra were obtained using a Dionex UltiMate 3000 HPLC in combination with a Bruker micrOTOF-Q III mass spectrometer. The electrospray ionization (ESI) method was used to gently ionize the samples. The mass spectra were deconvoluted to the neutral azurin mass from a minimum of three m/z peaks, typically of the +6, +7 and +8 molecular ion peaks.

## 4.4: Results and Discussion:

In this section, the results from the EPR and UV-Vis spectroscopy, ascorbic acid reduction, the metal exchange assays, as well as the ESI-MS will be discussed.

### 4.4.1: UV-Vis absorption and EPR spectra:

The UV-Vis absorption and EPR spectra of copper(II) bound azurin are shown in Figures 4.3 and 4.4. The T1 Cu(II) bound azurin has a characteristic absorption band at 625 nm (Fig. 4.3) due to the charge transfer transition between $S(\pi)_{Cys}$ and Cu $d_{(x2-y2)}$.[14-15] The EPR spectrum of *P.a.* azurin shows four hyperfine peaks on the $g_{//}$ region; a characteristic of Cu(II), with a $g_{//}$ of ~2.26. The Cu(II) hyperfine coupling constant, $A_{//}$, has a value of ~ 55.3 gauss (Fig. 4.4). The *A*- and *g*- values are characteristic of azurin and all T1 Cu(II) proteins.

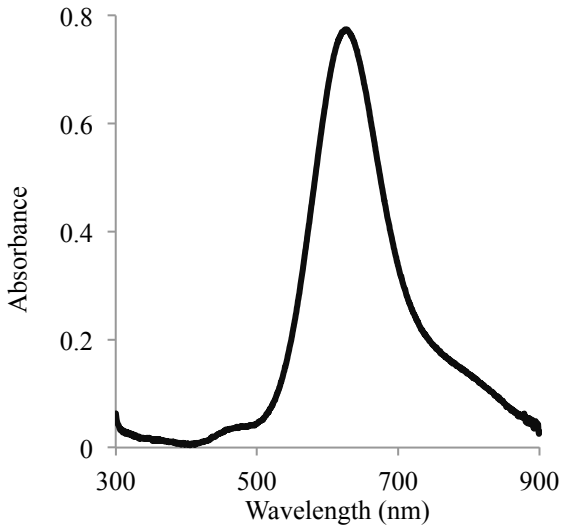


Fig. 4.3: Absorbance spectrum of azurin.

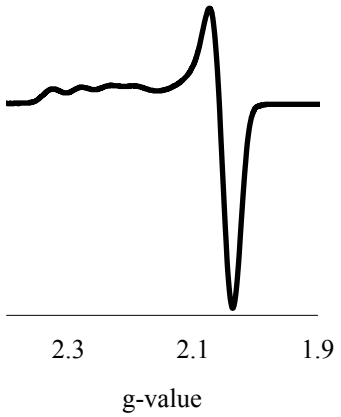


Fig. 4.4: EPR spectrum of azurin.

**4.4.2: Ascorbic acid reduction, and displacement of T1 Cu(II) in Azurin by Ag(I), Hg(II) or Cu(I):**

The absorbance at 625 nm of Cu(II) bound azurin decreases when it is reduced with ascorbic acid in an anaerobic environment. Ascorbic acid is a strong enough reducing agent to reduce T1 copper(II) upon addition of 0.5 equivalents (Fig. 4.5) since each ascorbic acid molecule provides two electrons. Presumably, the disappearance in color is due to reduction of the protein and not loss of copper. This process is reversible, with full recovery of the blue color upon oxygen exposure. The initial rate of reduction of azurin with 0.5 eq. ascorbic acid was found to be 0.0071 mM Az $min^{-1}$ at 100 μM azurin concentration in phosphate buffer at pH 6.35.

The order of reaction of azurin for the reduction with respect to the concentration of ascorbic acid was found to be half order with the rate constant of 0.253 $min^{-1}$ $mM^{-1/2}$ ascorbic acid (Fig. 4.6) at constant azurin concentration of 100 μM.

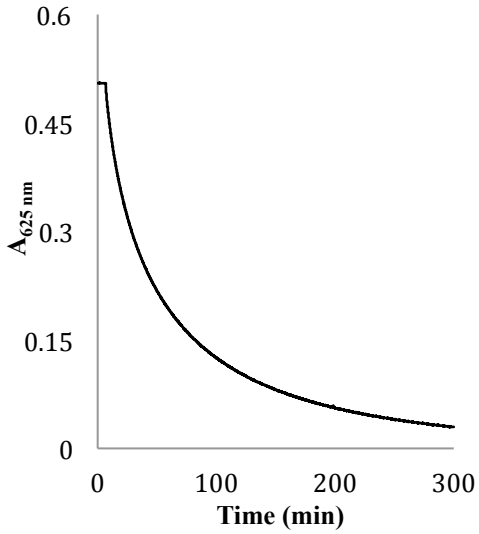


Fig. 4.5: Azurin reduction with 0.5eq ascorbic acid in phosphate buffer at pH 6.35.

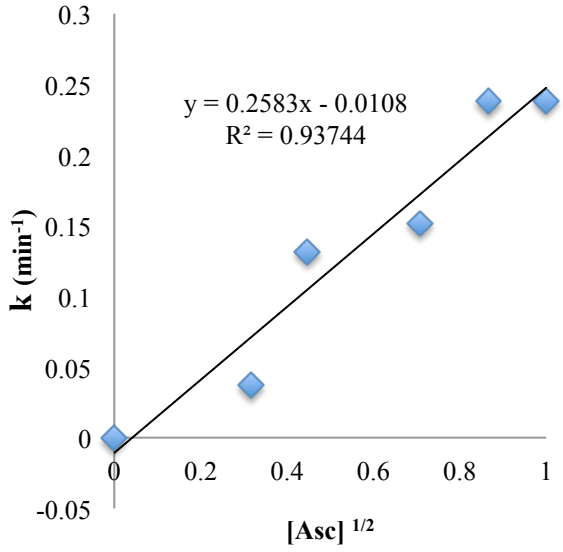


Fig. 4.6: Half-order reaction with respect to ascorbic acid for reduction of azurin.

Interestingly, the rate of reduction of azurin by ascorbic acid increases by an order of magnitude when extra Cu(II) is present in the solution with azurin. When 1 eq. of extra $CuSO_4$ was added to the T1-Cu(II) azurin sample in anaerobic conditions, the initial rate of disappearance of $A_{625\ nm}$ upon the addition of 0.5 eq. of ascorbic acid was 0.3501 mM Az $min^{-1}$ which is ~50 times faster than the rate reduction of Cu(II) azurin alone with 0.5 eq. ascorbic acid (0.00708 mM Az $min^{-1}$) (Fig. 4.7). We hypothesized that free Cu(II) in the solution is first reduced to Cu(I) upon the addition of ascorbic acid by possible rapid inner sphere electron transfer upon ascorbic acid and Cu(II) coordination. The Cu(I) may then rapidly displace the Cu(II) from T1 site. We thus hypothesized that the rapid disappearance of the blue color was due to the exchange of Cu(I) from aqueous solution to the sulfur rich azurin active site with the displacement of Cu(II) from azurin into the solution. There may also be the slower component of direct reduction of Cu(II) azurin by ascorbic acid.

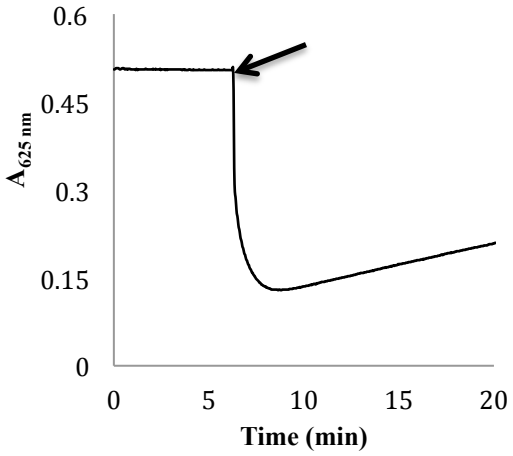


Fig. 4.7: Loss of $A_{625\ nm}$ with 0.5 eq. ascorbic acid in the presence of 1 eq. extra Cu(II). Arrow indicates the point where ascorbic acid was added.

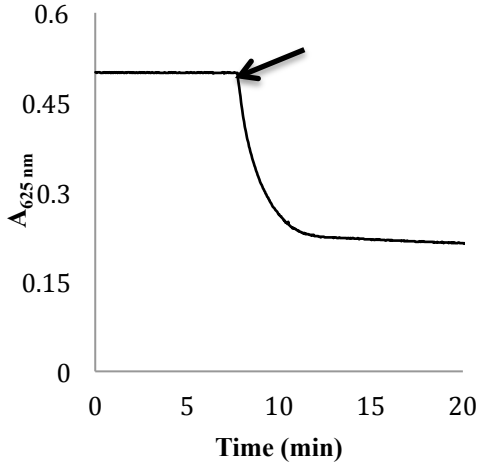


Fig. 4.8: Loss of $A_{625}$ with 1 eq. Cu(I). The arrow indicates the point where 1 eq. extra Cu(I) was added.

To further explore the possible rapid displacement of Cu(II) by Cu(I), 1 eq. of Cu(I) was added to Cu(II) azurin in an inert atmosphere in 20 mM potassium phosphate buffer at pH 6.35. Cu(I) was prepared by pre-incubating 0.5 eq of ascorbic acid with Cu(II) salt. Addition of one equivalent of this Cu(I) solution to Cu(II)-azurin resulted in a similar fast decrease of the $A_{625}$ (Fig. 4.8) at the rate of 0.0510 mM-Az $min^{-1}$. This is ~7 times faster than the reduction of T1 Cu(II) azurin alone with 0.5 eq ascorbic acid, but ~7 times slower than the reduction of Cu(II)-azurin in the presence of excess Cu(II) salt. This rate of loss of blue color with the addition of Cu(I) was intermediate between the rate of reduction by ascorbate and the rate of color loss in the presence of free copper ion. Perhaps this intermediate rate was a result of exclusive metal exchange, with no reduction and little to no excess ascorbic acid present. It should be noted that all samples above return to their full blue ($A_{625\ nm}$) intensity upon exposure to atmospheric oxygen.

An alternate explanation for the more rapid loss of blue copper azurin with the addition of excess Cu(II) is that Cu(I) participates in more rapid outer sphere electron

transfer to Cu(II) azurin than ascorbic acid. This mechanism would require no exchange of metal ions, but only electron transfer. To test this we attempted Cu(II) displacement with other metals.

In titrations similar to those with the addition of Cu(I), addition of one equivalent of $AgNO_3$ (Fig. 4.9) or $HgCl_2$ (Fig. 4.10) in potassium phosphate buffer at pH 6.35, caused a rapid decrease in the absorbance of 625 nm peak. The loss of blue color here is presumably due only to the displacement of Cu(II) from the T1 center by the added metal ion, since neither Ag(I) or Hg(II) could act as reducing agents under these conditions. The rate of disappearance of $A_{625}$ with 1 eq. $AgNO_3$ was 0.102 mMAz $min^{-1}$, which is about ~14 times faster than direct reduction of Cu(II) azurin with 0.5 eq ascorbic acid, and about 2 times faster than the rate of color loss with Cu(I) addition. With 1 eq $HgCl_2$, the rate of disappearance of $A_{625}$ was slower at 0.02 mM-Az $min^{-1}$, which is still ~2.8 times faster than the direct reduction by 0.5 eq. ascorbic acid, and about 2.5 times slower than color loss by Cu(I) (Table 4.1).

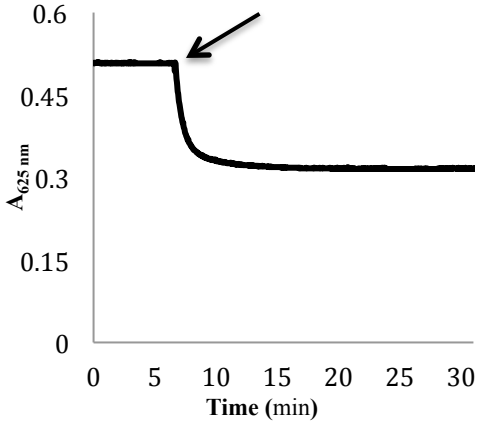


Fig. 4.9: T1 Cu(II) of azurin displaced with 1 eq. $AgNO_3$. The arrow shows the point where $AgNO_3$ was added.

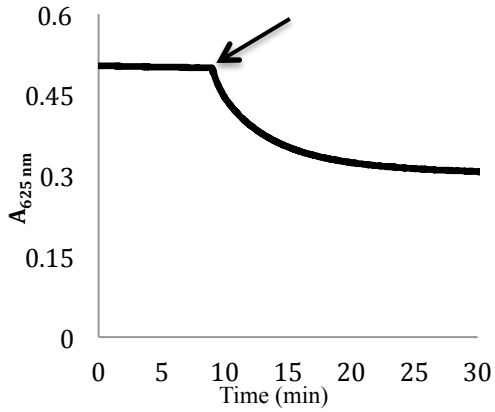


Fig 4.10: T1 Cu(II) of azurin displaced with 1 eq. $HgCl_2$. The arrow shows the point where $HgCl_2$ was added.

Another interesting observation is that the addition of 1 eq. Cu(I) (Fig. 4.8), Ag(I) (Fig. 4.9) or Hg(II) (Fig. 4.10) all resulted in only about a 50% reduction in the blue color. We speculate that either other metal binding sites exist in azurin (vide infra) or that an equilibrium between Cu(II) and added metal ion occurs whereby a mix of species is present (vide infra).

Table 4.1: The reduction/displacement of T1-Cu(II) at various conditions and corresponding initial reduction/T1 Cu(II) displacement rates.

| **T1 Cu(II) reduction/displacement conditions** | **Initial reduction/ Cu(II) displacement rate (mM-Az $min^{-1}$)** |
|---|---|
| T1 Cu(II) reduced with 0.5 eq. ascorbic acid (Fig. 4.5) | 0.0070 |
| T1 Cu(II) with 1 eq. extra Cu(II), reduced with 0.5 eq. ascorbic Acid (Fig. 4.7) | 0.3501 |
| T1 Cu(II) displaced with 1 eq. extra Cu(I) (Fig. 4.8) | 0.0510 |
| T1 Cu(II) displaced with 1eq. $AgNO_3$ (Fig. 4.9) | 0.1018 |
| T1 Cu(II) displaced with 1eq. $HgCl_2$ (Fig. 4.10) | 0.0200 |

We further examined the hypothesis of mercury and silver ion displacement with related displacement studies. Addition of 5 eq. of Ag(I) to Cu(II) azurin in both anaerobic and aerobic conditions resulted in the complete loss of blue color (absorbance at 625 nm) in potassium phosphate buffer at pH 6.35 (Fig. 4.11). Displaced ions were removed with PD-10 desalting columns. Similarly, 5 eq. each of pre-reduced Cu(I) under anaerobic conditions (Fig. 4.12) and 5 eq. of Hg(II) (Figure not shown) were added to Cu(II) azurin samples. The blue color disappeared completely. These samples were then exposed to atmospheric oxygen. The samples in which T1-Cu(II) was displaced with Ag(I) and Hg(II) never returned blue suggesting that the T1 copper was displaced. However, the

sample in which T1-Cu(II) was exchanged with Cu(I) reappeared blue when exposed to oxygen.

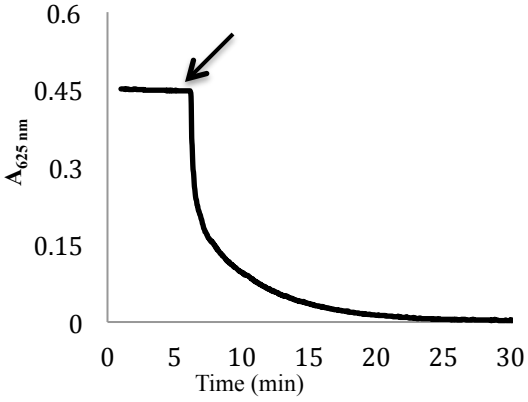


Fig. 4.11: T1 Cu(II) displaced with 5 eq. of Ag(I). The arrow shows the point where Ag(I) was added.

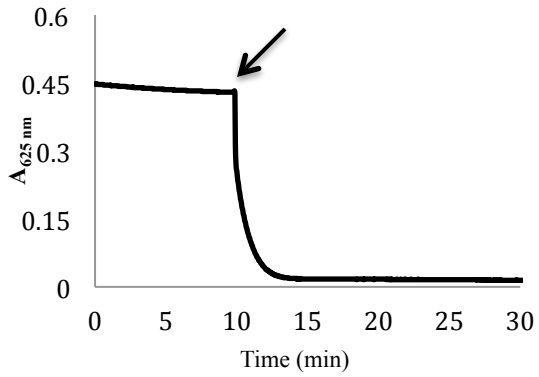


Fig. 4.12: T1 Cu(II) displaced with 5 eq Cu(I). The arrow shows the point where Cu(I) was added.

In further studies, the samples prepared with T1-Ag(I) and T1-Hg(II) were titrated with 5 eq. of Cu(II) in phosphate buffer pH 6.35 and exposed to oxygen. The samples did not result in the return of blue color, even upon days of incubation and addition of further equivalents of Cu(II) ions. However, the titration of T1-Ag(I) and T1-Hg(II) azurin samples with a pre-reduced Cu(I) solution in an anaerobic environment did result in metal ion exchange. After desalting these samples, exposure of the protein solution to the atmospheric oxygen yielded the return of blue color. This indicated that not only does Ag(I), Hg(II), and Cu(I) displace Cu(II) in azurin, but Ag(I) and Hg(II) can also be displaced by Cu(I).

### 4.4.3: ESI-MS results:

ESI mass spectra of the samples used in the assays above were obtained to confirm the metal binding and the mass of azurin (Fig. 4.13). All spectra yielded masses that matched theory with an error of less than 0.03%. In addition, most spectra have adducts corresponding to masses with one $Na^+$, $K^+$, or Cu(II) ion, likely as a result of these residual ions in buffers and/or the instrument.

The theoretical and experimental masses are summarized in Table 4.2.

Table 4.2: List of mass peaks identified in Fig. 4.13:

| **MS Spectra Peaks** | **Experimental Mass (Da)** | **Theoretical Mass (Da)** |
|---|---|---|
| Apo-azurin (Apo-WT) | 13943 | 13943 |
| WT azurin + $Na^+$ | 13964 | 13965 |
| WT azurin + $K^+$ | 13977 | 13981 |
| Cu(II) WT azurin | 14006 | 14006 |
| 2xCu(II) WT azurin | 14066 | 14068 |
| 2xAg(I) WT azurin | 14156 | 14157 |
| 3xAg(I) WT azurin | 14263 | 14266 |
| Ag(I) WT azurin + Cu(I) | 14112 | 14112 |
| Hg(II) WT azurin | 14141 | 14142 |
| Hg(II) WT azurin + Cu(I) | 14203 | 14205 |

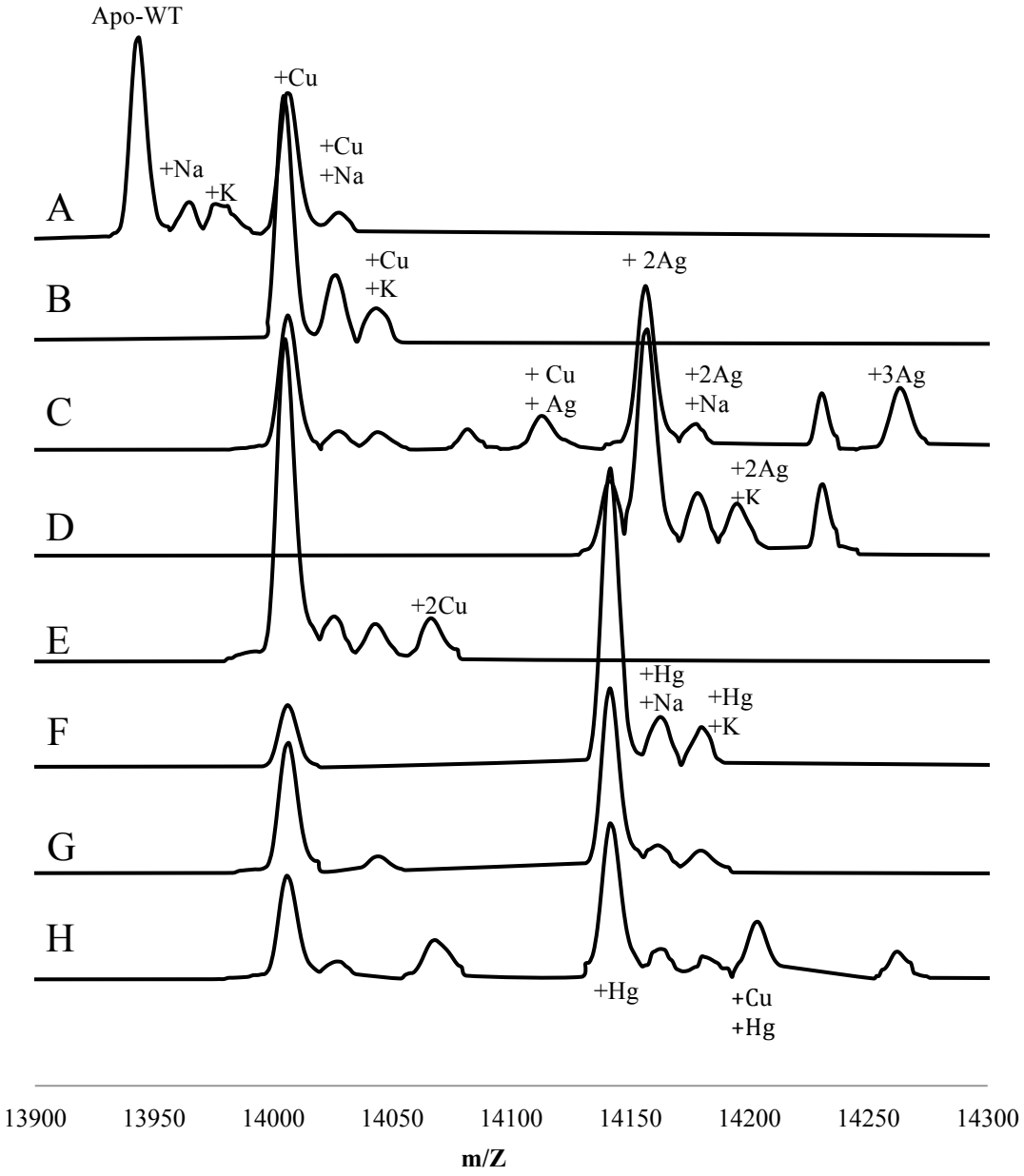


Fig. 4.13: Mass spectra of Azurin: (A): Apo Azurin, (B): T1-Cu(II), (C): T1-Ag(I), (D): T1-Cu(II) displaced by Ag(I), (E): T1-Ag(I) displaced by Cu(I), (F): T1-Hg(II) (G): T1-Cu(II) displaced by Hg(II) (H): T1-Hg(II) displaced by Cu(I).

Apo azurin and Cu(II) azurin yielded masses as expected (Fig. 4.13 A and B). As further controls we prepared samples of pure Hg(II) and Ag(I) substituted azurin (Fig. 4.13 C and F). The prepared Ag(I) azurin sample had peaks corresponding to +2 Ag(I) and +3 Ag(I) ions, in addition to a residual +Cu(II) peak, that must have been a result of the residual copper in the buffer or instruments, since all samples were colorless (Fig. 4.13 C). The mass spectrum of prepared Hg(II) azurin sample indicated a singly bound Hg(II) azurin species, as well as a residual +Cu(II) peak (Fig. 4.13 F) with +Na and +K adducts. The Hg(II) azurin sample prepared by the displacement of T1-Cu(II) with 5 eq. Hg(II), showed the same two peaks in the mass spectrum, but with a larger presence of copper in the sample (Fig. 4.13 G). This was evidence supporting the UV-Vis data, which shows that T1-Cu(II) was not displaced completely by Hg(II) but formed an equilibrium with about half of T1-Cu(II) displaced. This result is also consistent with the mass spectrum of the sample where T1-Hg(II) azurin was displaced by Cu(I), where the resulting sample turned blue upon the exposure to oxygen. The mass spectrum of this sample (Fig. 4.13 H) showed major peaks at m/z of azurin +Cu(II) (~14006), azurin with Hg(II) (~14141) and azurin with both Hg(II) and Cu(II) (~14203). This again confirmed the presence of Cu(II) and Hg(II), and that both Cu(I) and Hg(II) can displace Cu(II) to form an equilibrium .

Unlike the apo-azurin sample titration yielding a single Hg(II) bound protein, the apo-azurin sample titrated with Ag(I) shows major peaks corresponding to azurin with +2Ag(I) (~14156) and azurin with +3Ag(I) (~14263) indicating up to three silver ions bound to azurin (Fig. 13 C). The presence of more than one Ag(II) bound to azurin is also seen in the mass spectrum of the azurin sample generated by displacing the Cu(II) ion

with 5 eq. of Ag(I) ion (Fig 4.13 D). This sample had major peaks with +2 Ag(I) (~14156). The deconvoluted average spectrum of this sample doesn't show any +Cu(II) peak due to the presence of only negligible amount of residual Cu(II) from buffer and the instrument, which was too small to give a visible peak, and was omitted by the deconvolution software. This result indicates that almost all of T1-Cu(II) was displaced by Ag(I) (Fig. 4.13 D). The mass spectrum of the sample where T1-Ag(I) was displaced by Cu(I), and that turned blue upon oxygen exposure, shows the presence of a major peak for the Cu(II) azurin (~14006) and also a minor peak for azurin with +2Cu, but doesn't show any +Ag peak (Fig. 4.13 E), indicating the complete displacement of Ag(I) from T1 site.

It is not clear whether the binding of multiple Ag(I) occurs in the T1 site of azurin as in CuA azurin[12,13] or one of the Ag(I) binds to the surface site of azurin containing sulfur rich amino acid residues. Panzner et al. also observed the Ag(I) metallation of copper-azurin before[4] in which the absorbance of azurin decreased by about 40%, and the mass spectra showed adducts with +2 Ag(I). In addition, the crystal structure of a Hg(II) soaked azurin (PDB Id: 4JKN), shows an additional mercury binding site (Fig. 4.14).[9] Excess Hg(II) ions bound to a surface residue Met56 in azurin with partial occupancy in a methionine rich region of the protein, which caused coordination to another azurin protein in the unit cell creating a binding pocket for the mercury (Fig 4.15).[9] The crystal structure of silver soaked azurin (PDB ID: 3UGE), however, doesn't show any Ag(I) bound to the Met56 or any other cysteine or methionine residues apart from the T1 center.

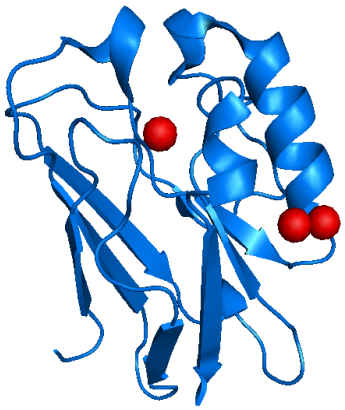

Fig. 4.14: Image of one monomer of Hg(II) bound azurin showing the additional Hg(II) binding site.

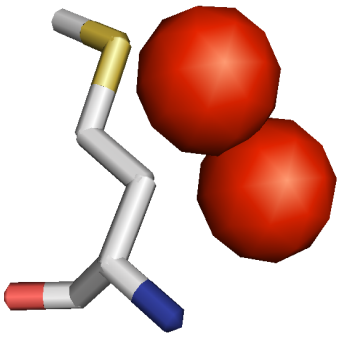

Fig. 4.15: Image of Hg(II) bound with Met56

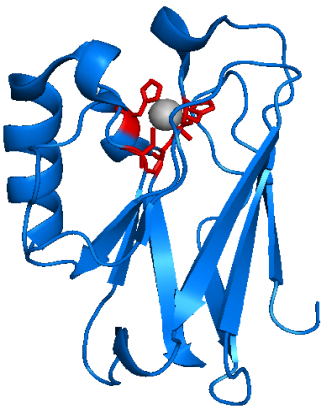

Fig. 4.16: Image of Ag(I) bound azurin

**4.5: Conclusion**:

The T1 site of azurin contains cysteine (Cys 112) and methionine (Met121) residues. Cysteine and methionine are well known Ag(I) and Hg(II) binding amino acids due to presence of soft Lewis base sulfur groups.[9] Our results suggest that the displacement of T1-Cu(II) by Hg(II) or Ag(I) is possible. The displacement of the harder Lewis acid Cu(II) metal ion from the metalloprotein, and hence inhibition of the protein activity by redox inactive ions, could indeed be an contributing factor to the toxicity of silver and mercury.

## Chapter 5: Conclusions and Future Directions:

We were successfully able to create functional mimics of the enzyme NiR using the electron transfer protein azurin as a scaffold. UV-Vis and EPR spectroscopy was used to characterize the variants and results were comparable to the native NiR. The activity assays show the nitrite reductase activity of our variants in addition to showing that the electron transport takes place from T1 to T2 sites. The variants we created were studied using Michaelis-Menten kinetics. Among the first generation variants, NiR3His-Az and PHM3His-Az were the most active, showing the importance of the third histidine residue which helps in better copper(II) binding. Second generation single mutant variants were created as an attempt to improve the activity of first generation variants by lowering the reduction potential of T1 site using Phe114Pro or Met121Gln mutants or by providing a direct electron transport pathway between T1 and T2 sites using the Phe15Trp mutation. The results from the nitrite reduction assays of NiR3His-Az and NiR-Az second generation single mutant variants show about the same activity as their 1$^{st}$ generation variants (NiR3His-Az or NiR-Az). Possible explanations could be that the catalytic T2 Cu(II) site acts independently of T1 Cu(II) site or the reduction of the T1 and T2 Cu(II) sites is not rate limiting. The second generation double mutant variants were created by coupling the mutations done on the first generation variants to either lower the reduction potential of T1 Cu(II) site by 2 fold (Phe114Pro/Met121Gln) or provide the electron transport pathway between T1 and T2 Cu(II) sites while also lowering the reduction potential of T1 Cu(II) site (Phe15Trp/Phe114Pro and Phe15Trp/Met121Gln). The second generation double mutant variants were expected to further improve the activity of the first and second generation single mutant variants. The double mutant variants of the

NiR3His-Az, containing the mutation to provide direct electron transport pathway between T1 and T2 Cu(II) sites along with lowering the reduction potential show the improvement on activity by as much as 3 fold whereas the decreasing the reduction potential by two fold do not show much improvement.

Reduction and re-oxidation of T1 site show the electron transport between T1 and T2 sites and also show difference in the reduction/re-oxidation rates of each variant supporting the rate limiting reduction of nitrite and the faster reduction of azurin. The order of reaction between azurin variants with various concentration of ascorbic acid used for the reduction was found to be $1^{st}$ order with respect to azurin and half order with respect to ascorbic acid. The order of the reaction between azurin and $NO_2^-$ was found to be pseudo $1^{st}$ order. The re-oxidation with nitrite was not seen on the variants involving the Phe114Pro mutations possibly due to the Phe114Pro mutation breaking the hydrogen bond between Phe114 and Cys112 residues and affecting the electron transport between T1 and T2 sites.

The metal exchange properties of wild type azurin were studied. The results show that the T1 Cu(II), can be displaced by either Ag(I), Hg(II) or Cu(I). Furthermore, T1 Ag(I) or Hg(II) can also be displaced by Cu(I). The results from ESI-MS show that more than one Ag(I) bind to azurin whereas Hg(II) forms an equilibrium with T1 Cu(II) while binding with azurin. Whether these have more than one metal ion bound to the T1 active site or to other sulfur rich surface binding sites on azurin is not yet known.

The next steps will be to continue characterizing the remaining second generation single and double mutant variants of NiR-Az, PHM-Az and PHM3His-Az for their $NO_2^-$ reduction activities using Griess assay as well as the electron transport properties

using single turnover of reduction and re-oxidation. These assays will be used to understand the mechanism of nitrite reduction in these variants more clearly. Comparison of these $NO_2^-$ reduction activities along with the reduction and T1 re-oxidation assays with the single and double mutant variants of NiR-Az, PHM-Az and PHM3His-Az could give more insight into the role that each mutation plays in the activities of nitrite reduction and re-oxidation of T1 site of the azurin variants. Finding the activities of the $2^{nd}$ generation variants of these parent variants could be used to compare the results to the NiR3His-Az $2^{nd}$ generation variants to find the pattern of the mutations on different variants.

In addition, other factors that could affect the rate of nitrite reduction and give insight into the mechanism of enzymes are being studied in our lab to understand the mechanism better. Recently, we are exploring the possibility of the bidirectional behavior of our variants that could also catalyze the reverse reaction of nitrite reduction (i.e. oxidation of NO to $NO_2^-$) to understand the mechanism of our variants better.

We will also look to improve the nitrite binding and the nitrite reduction activities by creating third generation variants.

# References

## Chapter 1 References:


1. Smil, V., Scientific American, 1997 (1), 76-81.
2. Canfield, D. E.; Glazer & A. N.; Falkowski, P. G., Science 2010, 330 (6001), 192-196.
3. Jetten Mike, S. M. Environ. Microbiol, 2008, 10 (11), 2903-9.
4. Joo, Y.J., Lee, D. D., Lerman, A., & Aquat Geochem, 2013, 19: 477–500.
5. Suzuki, S., Kataoka, K. & Yamaguchi, K., Acc. Chem. Res, 2000, 33, 728-735.
6. Wagner, S. C.; Nature Education Knowledge, 2011, 3(10):15.
7. Bertini, I.; Gray, H. B.; Lippard, S. J.; & Valentine, J. S., Bioinorganic Chemistry. University Science Books: Sausalito, CA, 1994; p 611.
8. Zumft, W. G., Microbiology and Molecular Biology Reviews **1997,** *61* (4), 533-616.
9. Merkle, A.C. & Lehnert, N., Dalton Trans., 2012, 41, 3355–3368.
10. Morozkina, E. V. & Kurakov, A. V., **2007,** *43* (5), 544-549.
11. Shoun, H., Kano, M., Baba, I., Takaya, N., & Matsuo, M., Journal of Bacteriology, 1998, 180 (17), 4413-4415.
12. Horio, T., Higashi, T., Matsubara, H., Kusai, K., Nakai, M., & Okunuki, K., Biochim. Biophys. Acta, 1958, 29, 297-302.
13. Kuronen, T.& Ellfolk, N., Biochim. Biophys. Acta, 1972, 275, 308-318.
14. Silvestrini, M.C., Citro, G., Colosimo, A., Chersi, A., Zito, R. & Brunori, M., Analytical Biochemistry. 1983, 129, 318-325.
15. Godden, J.W., Turley, S., Teller, D. C., Adman, E. T., Liu, M. Y., Payne, W. J. & LeGall, J., Science, 1991, 253, 438–442.
16. Adman, E.T, Godden J. W., & Turley, S. J. Biol. Chem., 1995, 270, 27458–27474.
17. Nojiri, M., Xie, Y., Inoue, T., Yamamoto, T., Matsumura, H., Kataoka, K., Deligeer, Yamaguchi, K., Kai, Y. & Suzuki, S., Proc. Natl. Acad. Sci. U. S. A., 2007, 104, 4315–4320.
18. Ellis, M. J., Dodd, F. E., Sawers, G., Eady R. R., & Hasnain, S. S. , J. Mol. Biol., 2003, 328, 429–438.
19. Murphy, M. E. P., Turley, S. Kukimoto, M., Nishiyama, M., Horinouchi, S., Sasaki, H., Tanokura, M., & Adman, E. T. , Biochemistry, 1995, 34, 12107–12117.
20. Jacobson, F., Guo, H., Olesen, K., Okvist, M., Neutze, R. & Sjolin, L, Acta Crystallogr., Sect. D, 2005, 61, 1190–1198.
21. Jacobson, F., Pistorius, A., Farkas, D., De Grip, W., Hansson, O., Sjolin, L., &. Neutze, R., J. Biol. Chem., 2007, 282, 6347–6355.
22. Abraham, Z.L., Lowe, D.J. & Smith, B. E., Biochem. J., 1993, 295, 587-593.
23. Nojiri, M., Xie, Y., Inoue, T., Yamamoto, T., Matsumura, H., Kataoka, K., Deligeer, Yamaguchi, K., Kai, Y., & Suzuki, S., 2007, 104, 11, 4315-4320.

24. Fukuda, M., Tse, K. M., Lintuluoto, M., Fukunishi, Y., Mizohata, E., Matsumura, H., Takami, H., Nojiri, M. & Inoue, T.; J. Biochem. 2014;155(2), 123–135.
25. Mizoguchi, T. J.; Di Bilio, A. J.; Gray, H. B. & Richards, J. H., J. Am. Chem. Soc. 1992, 114 (25), 10076-8.
26. LaCroix, L. B.; Shadle, S. E.; Wang, Y.; Averill, B. A.; Hedman, B.; Hodgson, K. O. & Solomon, E. I., J. Am. Chem. Soc., 1996, 118 (33), 7755-68.
27. Sato, K., Firbank, S.J., Li, C., Banfield, M.J., & Dennison, C., Chem. Eur. J, 2008, 14, 5820-5828.
28. Abraham, Z.H.L., Smith, B.E., Howes, B.D., Lowe, D.J., & Eady, R.R, Biochem. J., 1997 324, 511-516.
29. Murphy, M.E.P., Turley, S., & Adman, E.T., J. Biol. Chem. , 1997, 272, 28455-28460.
30. Kataoka, K., Furusawa, H., Takagi, K., Yamaguchi, K., & Suzuki, S., J. Biochem, 2000, 127, 345-350.
31. Boulanger, M.J., Kukimoto, M., Nishiyama, M., Horinouchi, S., & Murphy, M.E. J. Biol. Chem, 2000, 275, 23957-23964.
32. Antonyuk, S.V., Strange, R.W., Sawers, G., Eady, R.R., & Hasnain, S.S., Proc. Natl Acad. Sci. U S A. , 2005, 102, 12041-12046.
33. Averill, B.A., Angew. Chem., Int. Ed., 1994, 33, 2057–2058.
34. Li, Y., Hodak & M., Bernholc, J., Biochemistry, 2015, 54, 1233−1242.
35. Barrett, M.L., Harris, R. L. , Antonyuk, S., Hough, M. A., Ellis, M. J., Sawers, G., R. Eady, R.R., & Hasnain, S.S., Biochemistry, 2004, 43, 16311–16319.
36. Casella, L., Carugo, O., Gullotti, M., Doldi, S., & Frassoni, M. Inorg. Chem., 1996, 35, 1101–1113.
37. Beretta, M., Bouwman, E., Casella, L., Douziech, B., Driessen, W.L., Gutierrez-Soto, L., Monzani E., & Reedijk, J. Inorg. Chim. Acta, 2000, 310, 41–50.
38. Lehnert, N., Cornelissen, U., Neese, F., Ono, T., Noguchi, Y., Okamoto, K., & Fujisawa, K., Inorg. Chem., 2007, 46, 3916–3933.
39. Sutherland, I. W. & Wilkinson, J. F, *J. Gen. Microbiol.* **1963,** *30*, 105-12.
40. Swart, M. and Johansson, M.P. Chemistry & Biodiversity, 2012, 9, 1728-1738.
41. Murphy M.E.P., Lindley, P.F., Adman, E.T.; Protein Sci, 1997, 6: 761–770.
42. Clark, K.M., Yu, Y., Donk, W.A.V.D., Blackburn, N., Lu, Y., Inorg Chem Front. 2014; 1(2): 153–158.
43. Harris, R. L., Eady, R., R., Hasnain, S.S.; Arch Microbiol, (2006), 186: 241–249.
44. Berry, S.M., Gieselman, M.D., Nilges, M.J., Van der Donk, W.A., Lu, Y.J. Am. Chem. Soc. 2002; 124-2084.
45. Berry S.M, Ralle, M., Low, D.W., Blackburn, N.J., Lu Y. J., Am. Chem. Soc. 2003; 125-8760.
46. Punj, V., Bhattacharyya, S., Saint-Dic, D., Vasu, C., Canningham, E.A., Graves, J., Yamada, T., Constantinou, A., Christov, K., White, B., Li, G., Majumdar, D., Chakrabarty, A.M., Das Gupta, T.K.. Oncogene; 2004, 23, 2367-2378.
47. Tegoni, M., Yu, F., Bersellini, M., Penner-Hahn, J.E., &Pecoraro, V.L.; PNAS; 2012, 109(52); 21234-21239.
48. Katarzyna, R.; Chufan, E.; Eipper, B.; Mains, R. & Amzel, M; Handbook of Metalloproteins, 2011, 5, 563-568.
49. De la Lande, A.; Marti, S.; Parisel, O.& Moliner, V; J. Am. Chem. Soc. 2007,

129, 11700-11707.
50. Berry, S.M., Mayers, J. R. & Zehm, J. A., J Biol Inorg Chem; 2009; 14:143–149.
51. Leferink, N. G. H.; Han, C.; Antonyuk, S. V.; Heyes, D. J.; Rigby, S. E. J.; Hough, M. A.; Eady, R. R.; Scrutton, N. S. & Hasnain, S. S., *Biochemistry* **2011,** *50* (19), 4121-4131.
52. Marshall, N. M.; Garner, D. K.; Wilson, T. D.; Gao, Y.-G.; Robinson, H.; Nilges, M. J.; Lu, Y., *Nature* **2009,** *462* (7269), 113-116.
53. Yanagisawa, S.; Banfield, M. J.; Dennison, C.; *Biochemistry,* **2006,** *45* (29), 8812-8822.
54. Lukacs, A., Eker, A.P.M., Byrdin, M., Brettel K., & Vos, M.H. J. AM. CHEM. SOC. 2008, 130, 14394–14395.
55. Nar, H., Messerschmidt, A., Huber, R., Van de Kamp, M., Canters, G. W., J. Mol. Biol., 1991, 221 (3), 765-762.

**Chapter 2 References**:

1. Berry, S.M., Mayers, J. R. & Zehm, J. A., J Biol Inorg Chem; 2009; 14:143–149.
2. Hay, MT.; Ang, MC.; Gamelin, DR.; Solomon, EI.; Antholine, WE.; Ralle, M.; Blackburn, NJ.; Massey, PD.; Wang, X.; Kwon, AH.; Lu, Y. Inorg. Chem. 1998, 37:191-198.
3. Chang, T. K.; Iverson, S. A.; Rodrigues, C. G.; Kiser, C. N.; Lew, A. Y. C.; Germanas, J. P.; Richards, J. H. Proc. Natl. Acad. Sci. U.S.A. 1991, 88, 1325-1329.
4. Nilges, M.J., Matteson, K., Belford, R.L., "SIMPOW6: A software package for the simulation of ESR powder-type spectra" in ESR Spectroscopy in Membrane Biophysics, Biological Magnetic Resonance, Vol. 27, Hemminga, Marcus A., and Berliner, Lawrence Eds. Springer, New York, 2006, pp261-281.
5. Moody, A. J.; Shaw, F. L., Anal. Biochem. 2006, 356 (1), 154-156.
6. Fiddler, R.M.; J. AOAC; 1977, 60, 594–9.
7. Parish, R. V., NMR, NQR, EPR, and Mössbauer Spectroscopy in Inorganic Chemistry. Ellis Horwood Ltd: 2003; p 223.
8. Promega, Griess Reagent System https://www.promega.com/~/media/files/resources/protocols/technical%20bulletins/0/griess%20reagent%20system%20protocol.pdf .May 21, 2015.
9. Prudencio, M.; Eady, R. R.; Sawers, G., J. Bacteriol. 1999, 181 (8), 2323-2329.
10. Griess, P. Ber. Deutsch Chem. Ges. 1879, 12, 426.
11. Sun, J., Jhang, X., Broderick, M., Fein, H., Sensors, 2003, 3, 276-284.

**Chapter 3 References:**

1. Nelson, D.L, Cox, M. M., *Lehninger Principles of Biochemistry,* 5th ed., W.H. Freeman and Company, 2008, pp. 195-198.
2. Wijma, H. J.; Canters, G. W.; de Vries, S.; Verbeet, M. P., Biochemistry, 2004, 43 (32), 10467-10474.
3. Moody, A. J.; Shaw, F. L., Anal. Biochem. 2006, 356 (1), 154-156.

4. Fiddler, R.M.; J. AOAC; 1977, 60, 594–599.
5. Marshall, N. M., Garner, D. K., Wilson, T. D., Gao, Y., Robinson, H., Nilges, M., Lu, Y., Nature, 2009, 462(7269): 113–116.

**Chapter 4 References:**

1. Swart, M. and Johansson, M.P. Chemistry & Biodiversity, 2012, 9, 1728-1738.
2. Murphy M.E.P., Lindley, P.F., Adman, E.T.; Protein Sci, 1997, 6: 761–770.
3. Harris, R. L., Eady, R., R., Hasnain, S.S.; Arch Microbiol, 2006, 186: 241–249.
4. Panzner, M.J., Bilinovioch, S.M., Parker, J.A., Bladholm, E.L., Ziegler, C. J., Berry, S.M., Leeper, T.C.; Journal of Inorganic Biochemistry, 2013, 128, 11–16.
5. Wiegand, C., Abel, M. Ruth, P., J Mater Sci: Mater Med, 2015, 26:18.
6. Clark, K.M., Yu, Y., Donk, W.A.V.D., Blackburn, N., Lu, Y., Inorg Chem Front. 2014, 1(2): 153–158.
7. Melaiye, A. & Youngs, W.J. Expert opin. Ther. Patents, 2005, 15 (2): 125-130.
8. Punj, V., Bhattacharyya, S., Saint-Dic, D., Vasu, C., Canningham, E.A., Graves, J., Yamada, T., Constantinou, A., Christov, K., White, B., Li, G., Majumdar, D., Chakrabarty, A.M., Das Gupta, T.K.. Oncogene, 2004, 23, 2367-2378.
9. Zampino, A.P., Masters, F.M., Bladholm, E.L., Panzner, M.J., Berry, S.M., Leeper, T.C., Ziegler, C.J., Journal of Inorganic Biochemistry, 2014, 141, 152–160.
10. Panzner, M.J., Billinovich, S.M., Parker, Bladholm, E.L , Berry, S.M., Ziegler, C.J., Leeper, T.C., RSCB Protein Data Bank, PDB ID: 3UGE , 2012.
11. Berry, S. M., Mayers, J.R., and Zehm, N.A., J Biol Inorg Chem, 2009, 14:143–149.
12. Hwang, H.J, Lu, Y. Jo Journal of Inorganic Biochemistry, 2004, 98, 797–802.
13. Hay, M.T., Milberg, R.M., Lu, Y., J. Am. Chem. Soc., 1996, 118, 11976-11977.
14. Gewirth, A. A.; Solomon, E. I., J. Am. Chem. Soc. 1988, 110 (12), 3811-9.
15. Hadt, R. G.; Sun, N.; Marshall, N. M.; Hodgson, K. O.; Hedman, B.; Lu, Y.; Solomon, E. I., J. Am. Chem. Soc. 2012, 134 (40), 16701-16.
16. Bonander, N., Vänngård, T., Tsai, L., Langer, V., Nar, H., Sjölin, L., Proteins, 1997, 27, 385-394.
17. Tsai, L.C., Sjölin, L., Langer, V., Bonander, N., Karlsson, B.G., Vänngård, T, Hammann, C., Nar, H., Acta. Crystallogr. D. Biol. Crystallogr., 1995, 51, 711-717.
18. Nar, H., Huber, H., Messerschmidt, A., Filippou, A., Barth, M., Jaquinod, M., Kamp, M., Canters, W., FEBS. J., 1992, 205, 1123-1129.
19. Blackwell, K. A., Anderson, B.F., Baker, E.N., Acta. Crystallogr. D. Biol. Crystallogr., 1994, 50, 263-270.
20. Gewirth, A. A.; Solomon, E. I., J. Am. Chem. Soc. 1988, 110 (12), 3811-3819.